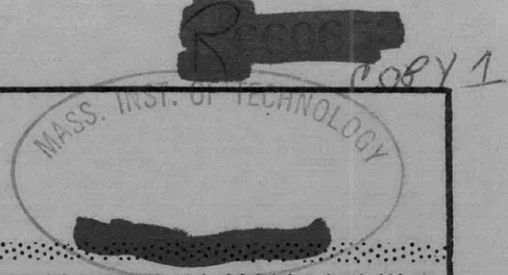


V393
.R46



DEPARTMENT OF THE NAVY



HYDROMECHANICS



AERODYNAMICS



STRUCTURAL
MECHANICS



APPLIED
MATHEMATICS



ACOUSTICS AND
VIBRATION

THREE-DIMENSIONAL
(BEAM-SHELL-SPRUNG BODY)
VIBRATION ANALYSIS
OF
NS SAVANNAH

by

Ralph C. Leibowitz
and
Robert G. Schwendler

Distribution of this document
is unlimited.

ACOUSTICS AND VIBRATION LABORATORY
RESEARCH AND DEVELOPMENT REPORT

April 1965

Report 1728



THREE-DIMENSIONAL
(BEAM-SHELL-SPRUNG BODY)
VIBRATION ANALYSIS
OF
NS SAVANNAH

by

Ralph C. Leibowitz
and
Robert G. Schwendler

**Distribution of this document
is unlimited.**

April 1965

Report 1728

TABLE OF CONTENTS

| | Page |
|---|------|
| ABSTRACT | 1 |
| ADMINISTRATIVE INFORMATION | 1 |
| INTRODUCTION | 2 |
| THEORETICAL ANALYSIS OF THE PROBLEM | 5 |
| RESULTS | 7 |
| VIBRATION MODE SHAPES | 7 |
| AMPLITUDE RESPONSE VERSUS FREQUENCY | 11 |
| DISCUSSION | 13 |
| RECOMMENDATIONS | 23 |
| CONCLUSIONS | 24 |
| ACKNOWLEDGMENTS | 25 |
| APPENDIX A - REPRESENTATION OF NS SAVANNAH AS A BEAM-SHELL-SPRUNG BODY SYSTEM. | 73 |
| APPENDIX B - ANALOG OF STRUCTURAL ELEMENTS OF SHIP | 81 |
| APPENDIX C - SYMMETRIC AND ANTISYMMETRIC ANALYSES | 89 |
| APPENDIX D - SHIP DATA | 94 |
| APPENDIX E - METHOD OF EVALUATING PARAMETERS FOR ANALOG COMPUTATION | 105 |
| APPENDIX F - SCALE FACTORS | 120 |
| APPENDIX G - QUANTITATIVE EVALUATION OF EFFECT OF A MOMENT APPLIED TO PROPELLER. | 122 |

| | Page |
|---|------|
| APPENDIX H - ELECTRICAL ANALOG OF TORQUE BOX. | 124 |
| REFERENCES | 128 |

LIST OF FIGURES

| | Page |
|--|-------|
| Figure 1 - Idealized Model of NS SAVANNAH. | 6 |
| Figure 2 - Vertical Normal-Mode Profiles for NS SAVANNAH | 7 |
| Figure 3 - Panel Points | 12 |
| Figure 4 - Panel Points | 12 |
| Figures 5-136 - Curves of Amplitude Response versus Frequency | 39-71 |
| Figure 137 - Thrust-Coupling Mechanism | 72 |
| Figure 138 - Shell Structure | 78 |
| Figure 139 - Area Lumping for Decks | 78 |
| Figure 140 - Area Lumping for Bulkheads | 79 |
| Figure 141 - Axial Element Analogy | 79 |
| Figure 142 - Beam Analogy. | 79 |
| Figure 143 - Shear Panel Analogy | 80 |
| Figure 144 - Electrical Analogy for a Plate | 80 |
| Figure 145 - Electrical Analogy for a Half Deck | 86 |
| Figure 146 - Interconnection of Decks by Shear Panels | 87 |
| Figure 147 - Interconnection of Beam Analogy and Shell Analogy | 87 |
| Figure 148 - Simplified Antisymmetric Model (Single-Screw). | 93 |

| | |
|---|-----|
| Figure 149 – Inboard Profile and Plan View of NS SAVANNAH | 98 |
| Figure 150 – Data Curves for NS SAVANNAH | 101 |
| Figure 151 – Hull Sections and Corresponding Moments of Inertia | 102 |
| Figure 152 – Circuits for Double Bottom | 126 |
| Figure 153 – Rectangular Torque Box and Its Analog | 127 |

LIST OF TABLES

| | Page |
|--|------|
| Table 1 – Symmetric Vibration Modes | 26 |
| Table 2 – Amplitude Response Data | 30 |
| Table 3 – Principal Characteristics of NS SAVANNAH | 95 |
| Table 4 – Mass and Stiffness Data. | 96 |
| Table 5 – Longitudinal Flexibilities | 110 |
| Table 6 – Lateral Flexibilities | 110 |
| Table 7 – Deck Shear Flexibilities | 111 |
| Table 8 – Double Bottom Beam Flexibilities | 111 |
| Table 9 – Double Bottom Torque Tube Flexibilities | 112 |
| Table 10 – Outer Shell Shear Panel Flexibilities | 112 |
| Table 11 – Bulkhead Shear Panel Flexibilities | 113 |
| Table 12 – Longitudinal Weight Distribution | 114 |
| Table 13 – Vertical Weight Distribution | 115 |
| Table 14 – Lateral Weight Distribution. | 116 |

| | Page |
|---|------|
| Table 15 - Axial and Beam Flexibilities | 117 |
| Table 16 - Weight Distribution | 118 |
| Table 17 - Shaft Axial Flexibility | 119 |
| Table 18 - Shaft Weight Distribution | 119 |

ABSTRACT

The normal modes of coupled vertical, transverse, and longitudinal flexural vibrations and the steady-state damped response were calculated by means of a passive electrical-analog computer for surface ship NS SAVANNAH using a three-dimensional (beam-shell-sprung body) analysis similar to that applied to aircraft. This ship was selected as a case study because of the many test results, data, and calculations available for this ship. Vertical flexural vibrations based upon beam theory were also computed by a digital computer. To demonstrate the techniques involved in making a three-dimensional analysis, the methods and data used in the calculations and the results obtained are presented. Results show that significant reductions in vibration amplitudes can be achieved by such methods as damping or inertia coupling, which directly affect the sharpness of the structural resonance peaks.

ADMINISTRATIVE INFORMATION

This investigation was conceived, planned, and executed by the authors in an attempt to devise a new approach to a complex problem in vibration theory. The work was conducted as a part of the general research program of the Bureau of Ships under the cognizance of the Ship Silencing Branch. This is a final report of the work done

from March 1961 to February 1963. However, further analytical refinements and substantiating efforts, i.e., correlation with test results are recommended.

INTRODUCTION

The normal modes of vertical, transverse, and longitudinal flexural vibration and the steady-state damped response of a particular hull have hitherto been treated by assuming that the hull vibrates as a free-free, continuous, nonuniform beam with equivalent elastic and inertial properties per unit length.^{1, 2} Propellers and their shafting system have been considered as rigid bodies attached to the ship, their combined mass being added to the section of the ship that includes the center of gravity of these structures.

The limitations of this treatment have long been recognized. For when a ship is excited by a vibration generator imposing only (or predominately) a vertical force on the hull, comparisons between experiment and simple beam bending theory show, in general, reasonably good agreement only for the lowest modes. It should also be recognized that when a ship is excited by propeller thrust variations, significant longitudinal vibrations of the shafting system, hull, and other ship components are excited as well as vertical and transverse vibrations. Hence, the coupling between longitudinal, vertical and transverse motions, neglected in beam theory, should be considered in any theoretical analysis for the response of the entire ship system. We require then a theory (or model) which will permit us to advance beyond the limitations of a unidimensional analysis method (i.e., beam theory) with respect to the prediction of ship characteristics and which will make possible a more detailed correlation between

¹References are listed on page 128.

theory and experiment.

In this report, an attempt has been made to more realistically model a ship using a three-dimensional (beam-shell-sprung body) method of analysis similar to that used for aircraft.^{1, 3, 4} In this model the propeller-shafting system is treated as a sprung body¹ attached to a hull that is represented as a beam-shell system. The present study is the first step in a general investigation intended to lead to the development of a three-dimensional method of analysis for ships and to an evaluation of nonuniform beam theory.

The primary and general objective of this report is to demonstrate in detail the methods and techniques involved in performing and displaying the results of such an analysis. For purposes of illustration, a case study was made for surface ship NS SAVANNAH. The choice of this ship is incidental to the above objective. The results of this study should therefore be considered useful only in the sense that they contributed to the development of vibration theory and should not be considered for *immediate application* to design problems. Additional theoretical studies and experimental verification will be necessary before the degree of validity and utility of a three-dimensional theory is established (see Recommendations).

The specific objectives of this case study, which serves to illustrate the use of a three-dimensional (beam-shell-sprung body) theory, are:

1. To apply this type of theory (or model) to SAVANNAH for the purpose of investigating the normal modes and response to sinusoidal thrust pulsations and bending moments applied at the propeller and stern, respectively.
2. To gain some insight into the relative importance of the many parameters

involved in this problem.

3. To study the effect on the ship response of some simple modifications to the shafting system.

4. To investigate the diffusion of the pulsating thrust applied at the thrust block.

The computations made for SAVANNAH in this report represent the first solutions obtained for the vibrations of a full-scale ship using three-dimensional (shell) analysis for the region of interest. This region can, of course, be extended to include the entire ship.

The three-dimensional investigation is limited here to a study of the symmetric response of the ship on a passive analog computer.^{1, 3, 4} For purposes of comparison, a one-dimensional (beam theory) investigation of the vertical response of the ship was made on a digital computer. Only in certain cases will the modes calculated by three-dimensional and beam theories be in reasonable agreement (for a particular mode this may occur, for example, when one component of the coupled vibrations predominates in that mode). The theory may, in general, also be important for obtaining modes of hull vibration beyond the upper limit of those that can be treated meaningfully by beam theory. The present study, however, does not shed adequate light on this aspect because of the limited number of sections or subdivisions used; only comparisons up to the fourth (beam theory) mode should be considered pertinent.*

*Some of the tables and figures of Reference 4 are reproduced here for completeness and ready reference because Reference 4 had only limited distribution.

THEORETICAL ANALYSIS OF THE PROBLEM

An analog computer was used to obtain the normal modes of vertical, transverse, and longitudinal flexural vibration and the steady-state response of NS SAVANNAH. The normal mode analysis for SAVANNAH is based upon the assumption that for the ship to be electrically analogized the propeller-shafting system can be treated as a sprung body attached to a hull representable as a beam-shell system and that small vibration theory is applicable; see Figure 1. The methods given in References 3 and 4 were used as a basis for the analogy, and these methods require evaluation of the inertias and elastic constants of the system. The details of ship structural representation and the derivation of the corresponding electrical analog are given in Appendixes A and B, respectively. Only symmetric motions of the hull are considered in this study and, therefore, only one-half the ship was represented on the computer.* Transverse components of motions of points in the plane of symmetry are zero; discussion of symmetric and antisymmetric motions are presented in Appendix C for completeness. The principal characteristics of NS SAVANNAH and other ship data used in calculating the normal modes and frequencies on the digital computer are given in Appendix D. The method used to evaluate the parameters for analog computation is given in Appendix E. The scale factor used to convert mechanical parameters to

*Symmetry with respect to the vertical centerplane of the ship permits a longitudinal slicing of the ship in this plane so that only the port or starboard side need be considered for analysis; i.e., for the transverse or lateral motion of any point on the port side of the ship there is a corresponding mirror image motion of a point on the starboard side.

electrical parameters are given in Appendix F. A quantitative evaluation of the effects of a moment applied to a propeller is given in Appendix G.

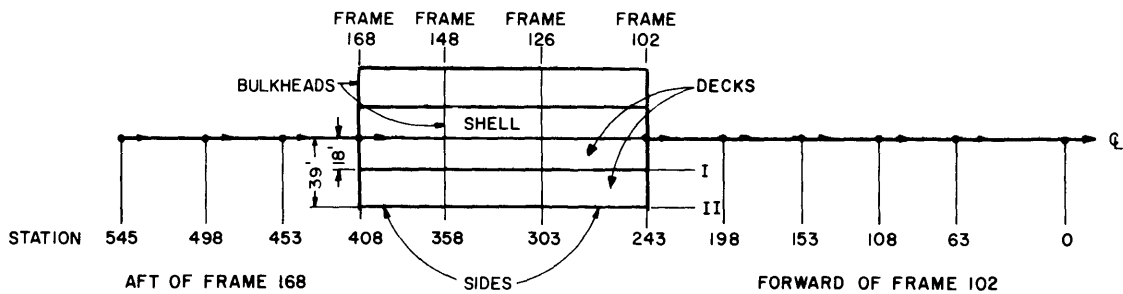


Figure 1a - Longitudinal Representation

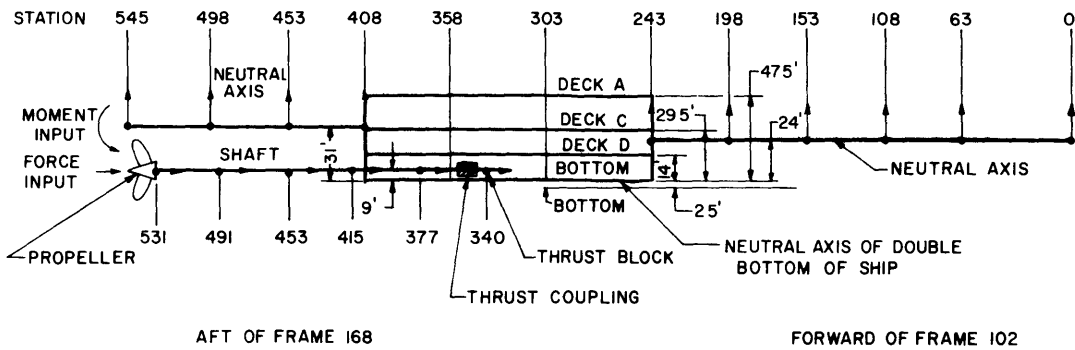


Figure 1b - Vertical Representation and Shaft Representation

Figure 1 - Idealized Model of NS SAVANNAH

RESULTS

VIBRATION MODE SHAPES

The first ten symmetric mode shapes are presented in Table 1.⁴ The fundamental mode has a frequency of 90.7 cpm and is plotted in Figure 2a. The mode deflections were obtained at 83 points on the structure by reading voltages at the corresponding nodes of the electric analogy. Each deflection listed in Table 1 is designated in the column to the extreme left of the table and these points may be geometrically located by means of Figures 1, 3, and 4. Briefly, deflections were obtained at the following stations:

- a. Vertical deflections were obtained at 8 stations forward and aft of the shell structure and at 18 points within the shell.
- b. Longitudinal (y-direction) deflections were obtained at 10 stations forward and aft of the shell structure, at 24 points within the shell, and at 7 points on the propeller shaft.
- c. Transverse deflections were obtained at 16 points within the shell.

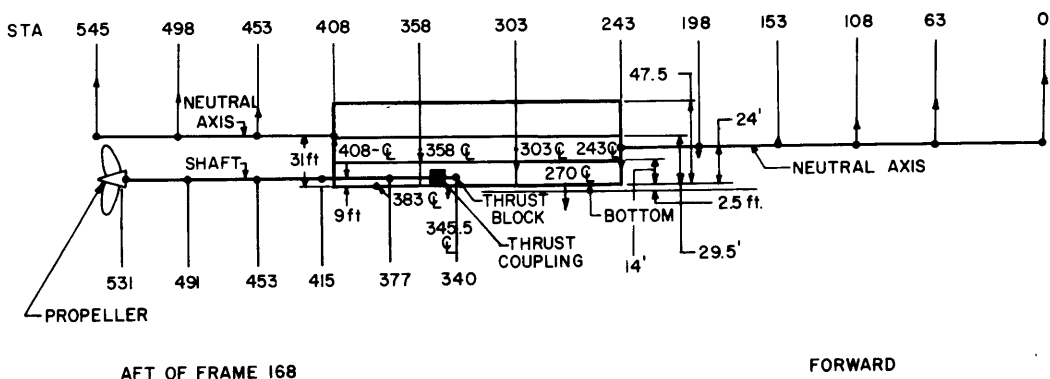
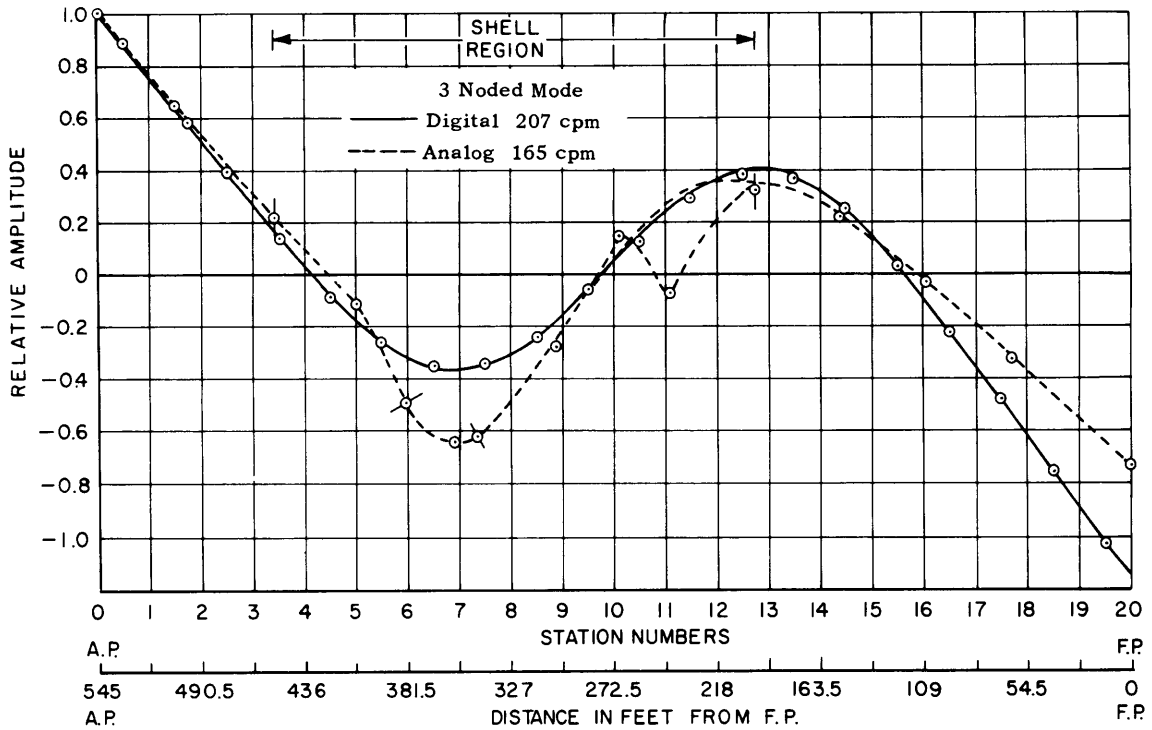
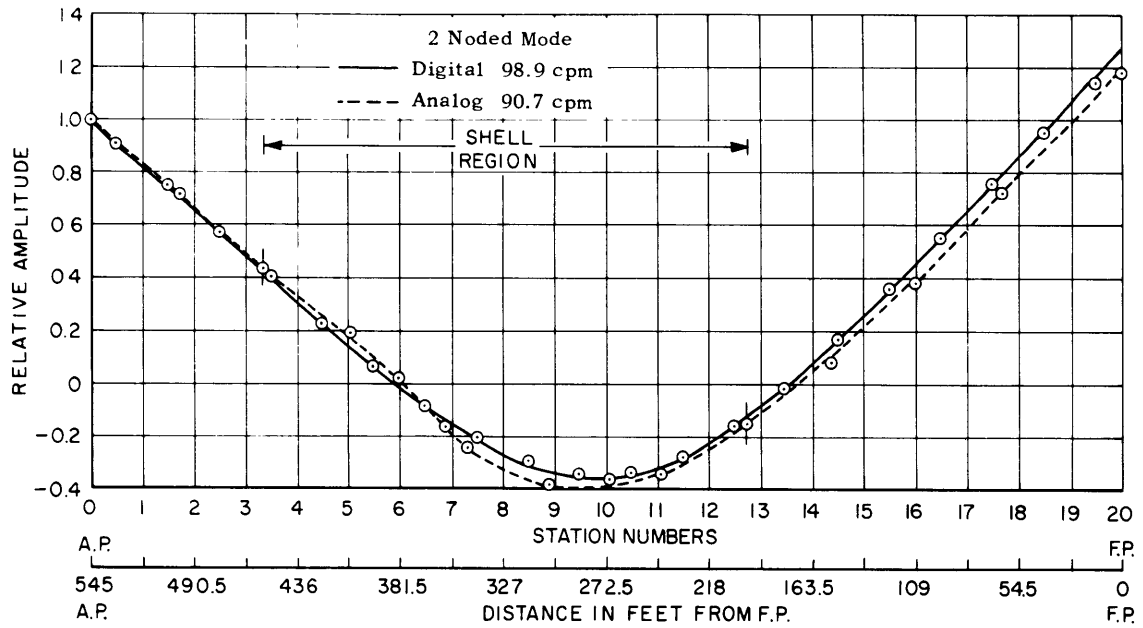


Figure 2a - Fundamental Mode Shape

Figure 2 - Vertical Normal-Mode Profiles for NS SAVANNAH (Sheet 1 of 4)

Figure 2 - Vertical Normal-Mode Profiles for NS SAVANNAH (Sheet 2 of 4)



NOTE: For purpose of comparison, corresponding positions for station numbers used for analog and digital computations are shown.

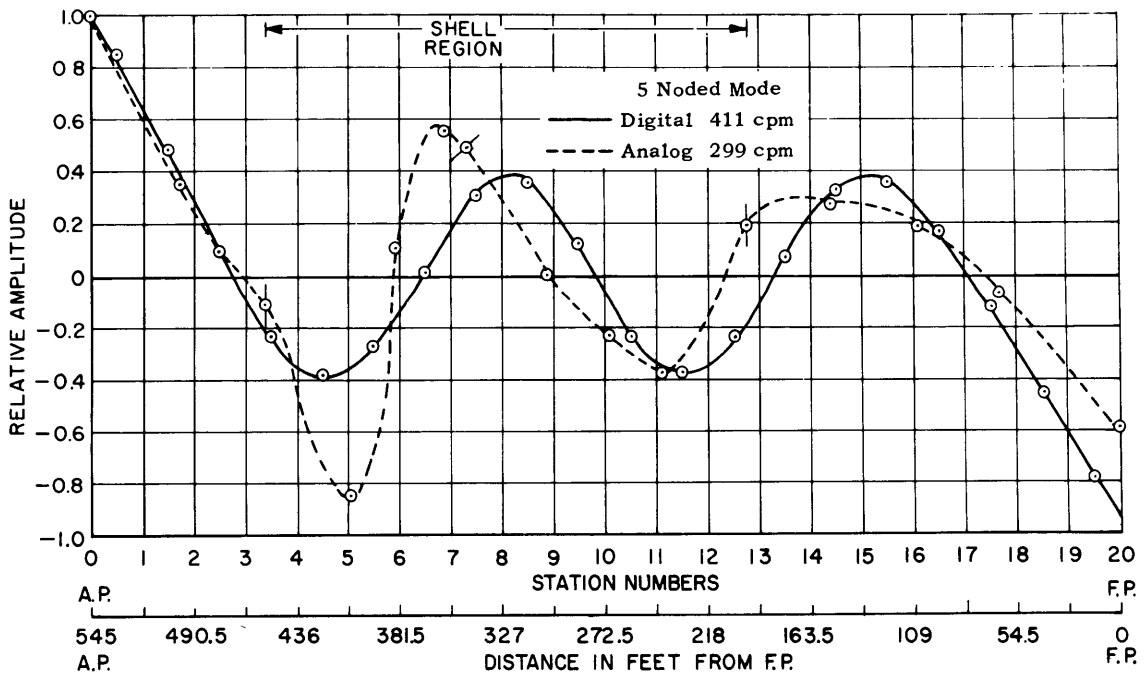
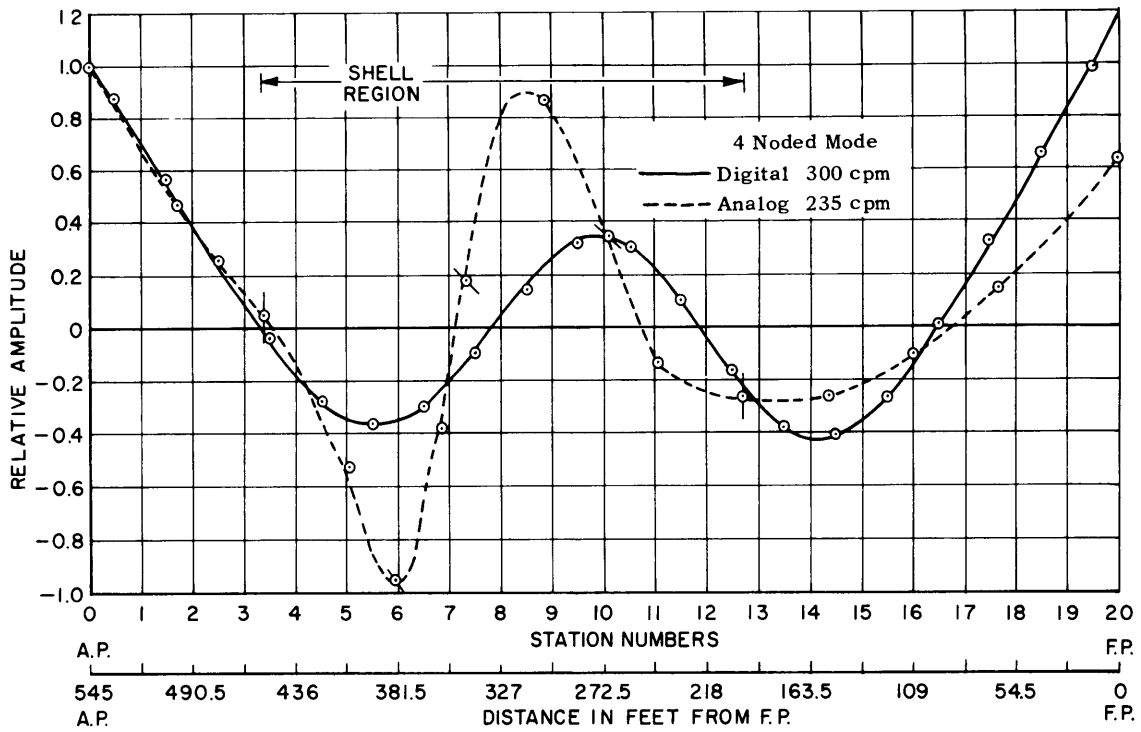


Figure 2 - Vertical Normal-Mode Profiles for NS SAVANNAH (Sheet 3 of 4)

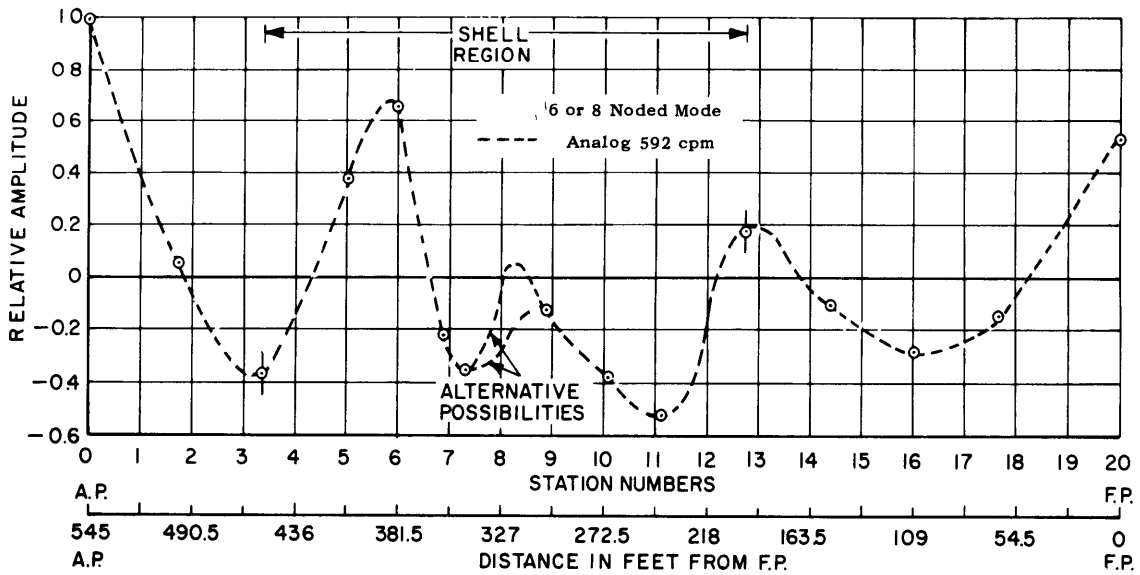
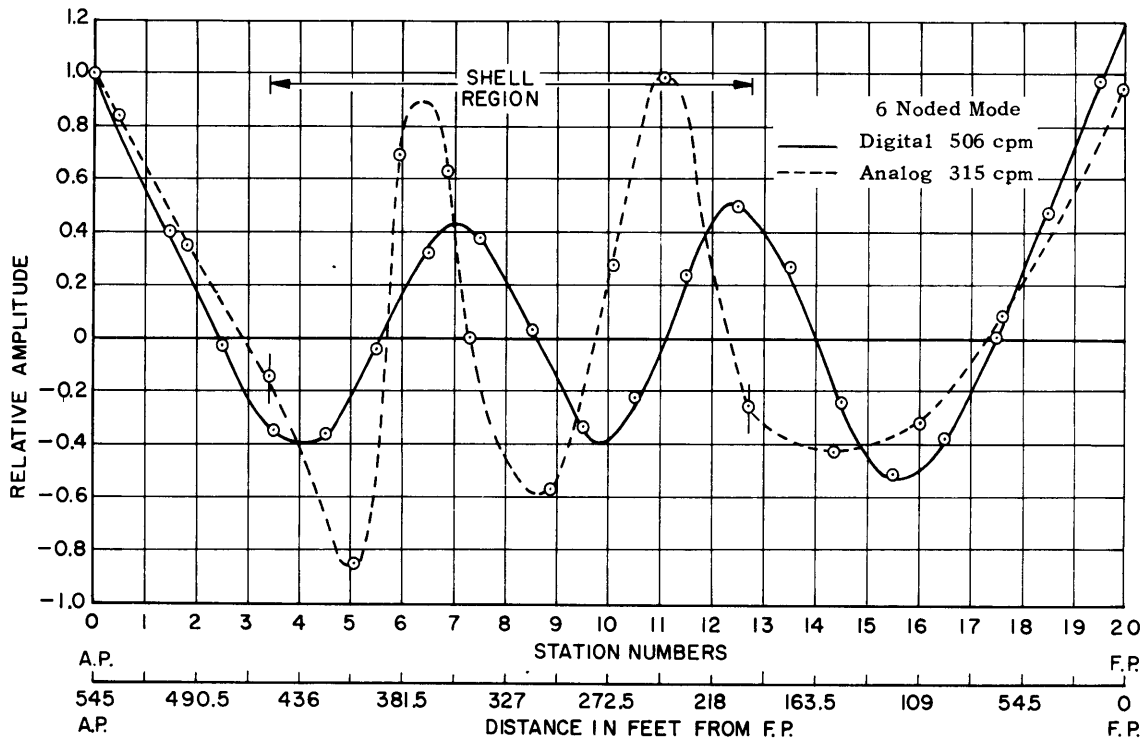


Figure 2 - Vertical Normal-Mode Profiles for NS SAVANNAH (Sheet 4 of 4)

Figures 2b through 2f are plots of the record through six modes of vertical vibration of NS SAVANNAH obtained on the analog and digital computers. Figure 2g is a plot of the 8-noded mode of vertical vibration obtained on the analog computer only. In all cases, the ship was treated as a beam for digital computations. Some of the analog data required normalization for unit amplitude at the aft perpendicular. See Appendix D for ship data used in obtaining digital computer solutions.

AMPLITUDE RESPONSE VERSUS FREQUENCY

The amplitudes of vibration were obtained at 12 coordinates within the hull for input frequencies up to 2500 cpm; see Table 2.⁴ Two types of excitation were employed:

- a. A sinusoidal thrust pulsation applied at the propeller; and
- b. A sinusoidal bending moment applied at the stern (Station 545).

The data obtained are presented in Figures 5 through 136. The ratio of amplitude of response to amplitude of the force or moment producing the motion is plotted versus frequency of the excitation. The value "0 db" in these figures corresponds to the value given in Table 2, which describes the coordinate at which

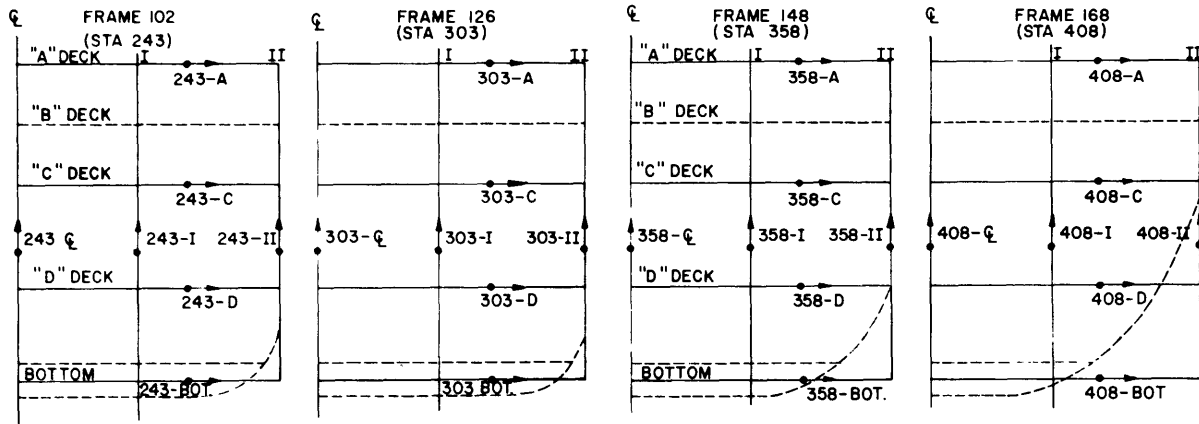


Figure 3 - Panel Points

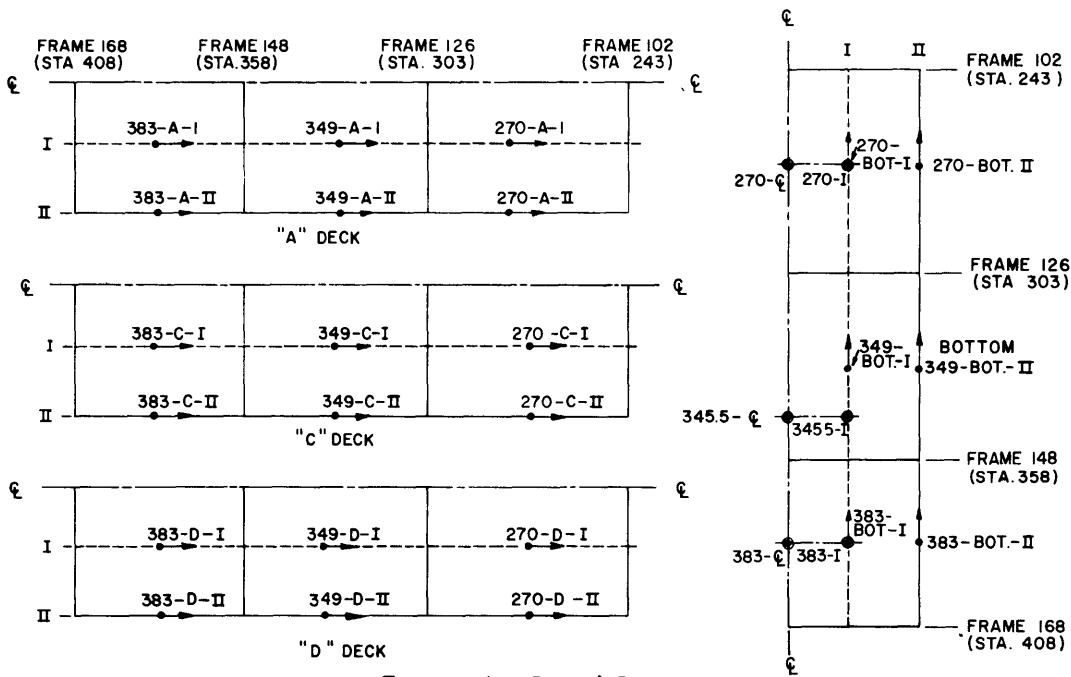


Figure 4 - Panel Points

In Figure 4 the symbol \odot indicates the location of points on the bottom at which inertias to vertical motion were located. These inertias are represented by the capacitors which appear in Figure 152, circuit for out-of-plane motion. The term z-coordinate in this usage does not imply a set of axes with an origin but merely indicates that a motion in the z-direction and the attendant inertia forces are simulated at the points indicated.

the response is plotted. Amplitude response data were taken for 11 different configurations. In comparing these data, note the value of the ratio velocity/force at 0 db of the coordinates under consideration given in Table 2.

DISCUSSION

Before evaluating the results given in the preceding section, it is important to understand the mechanism of "diffusion" of force or energy within the ship.

The hydrodynamic forces of excitation impinge on relatively small areas and are transmitted to the hull of the ship as a whole by "diffusion" through local structural reinforcement and the framing of the hull. Consider, for example, the transmission of propeller thrust. The primary load path includes the propeller shaft, the structure supporting the thrust bearing, the framing of the hull bottom which transmits a vertical couple to the bulkheads, and "shear lag" which transmits longitudinal load components to the hull cross section. The hull itself responds by bending in a vertical plane and stretching longitudinally. Each of the elements in the load path has mass which modifies the transmission characteristics. A proper analysis and evaluation of the results of the problem should include a consideration of each load path element in greater or lesser detail and the corresponding response.

One of the purposes of this study³ was to determine whether or not vibration levels could be drastically reduced by an appropriately chosen thrust coupling mechanism as shown in Figures 1 and 137. To do this required an investigation into the diffusion of the pulsating thrust applied to the thrust block. Hence, the portion of the ship in the vicinity of the thrust block was represented in greater detail than the re-

mainder of the ship.

If the reservoir pressure p is sufficiently high, it will be possible for the thrust coupler to carry the static thrust of the propeller (Figure 137). Also, if the volume of the reservoir is infinite, small motions of the shaft produced by thrust pulsations will not encounter a restoring force (in practice, of course, the reservoir volume will be finite though large, and a small dynamic restoring force will be encountered). A sinusoidal motion of the propeller shaft will be resisted by two forces, (1) the force due to the viscous damper and (2) the inertia force due to the fluid filling the cavity between propeller shaft and thrust block (in practice, the viscous damping might be supplied by frictional losses due to the flow through the orifice). In this initial investigation, the reservoir was assumed infinite in extent, and the two limiting cases of pure viscous damping and pure inertia, respectively, were studied.

Table 1 indicates the character of some of the vibration modes which affect significantly the amplitude response of the structure. Specifically, it is useful to point out here the character of some of the vibration modes which play an important part in the amplitude response of the structure:

a. The lowest mode is a free-free bending mode of the ship with a frequency of 90.7 cpm.

b. The gravest longitudinal mode of the shaft is at 506.4 cpm (9th mode in Table 1).

c. The 8th mode is primarily a longitudinal mode and involves a considerable amount of longitudinal shaft motion. Its frequency is 462 cpm (fairly close to the frequency of the shaft mode).

d. The 2nd and 4th modes are bending modes with frequencies at 165 cpm and 235 cpm, respectively.

e. The 3rd mode is a longitudinal mode which involves a lot of fore-and-aft motion near the front of the ship and some motion of the propeller shaft. Its frequency is 199 cpm.

A discussion of Figures 5 through 136 follows:

a. Figures 5 through 16, basic configuration.

A sinusoidal force was applied at the propeller to analyze the response to thrust pulsations. The ratio of amplitude to force at the propeller shows a pair of sharp maxima at frequencies corresponding to the 8th and 9th modes of the ship. The 9th mode is a "shaft mode" (506 cpm) and the 8th mode (462 cpm) is a longitudinal mode of the ship which involves a considerable amount of shaft motion. Hence, thrust pulsations can excite both these modes strongly if the pulsations have the proper frequency. The 7th mode (315 cpm) also produces a peak in the amplitude response.

b. Figures 17 through 28, thrust coupler composed of a damper (see Appendix A).

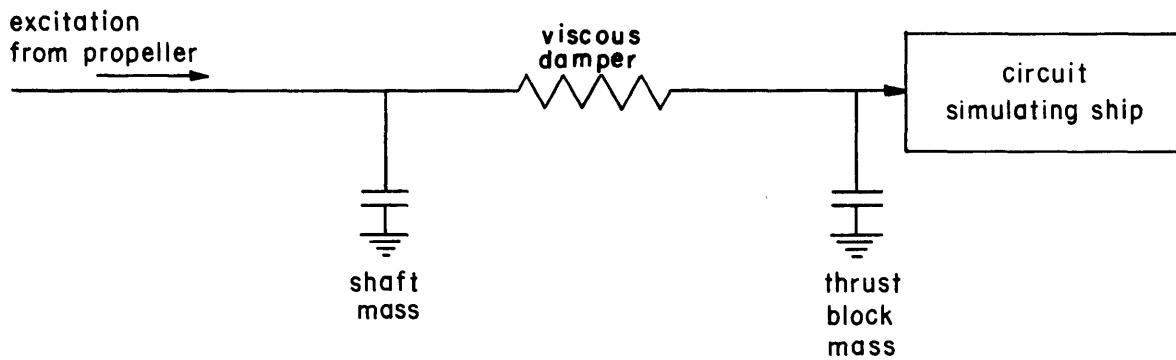
For frequencies between 300 cpm and 600 cpm, the damper resulted in decreased vibration. At the propeller, the reduction of amplitude amounted to about 10 db. Vibration amplitudes at frequencies between 300 cpm and 600 cpm were significantly affected; at other frequencies, however, not much effect was observed. For example, as shown in Figure 19, the amplitude of the peak in the response at 210 cpm is about the same as that shown in Figure 7. (A 10-db shift occurs in 0-db point.) The peaks in the response are rounded because of the presence of damping.

c. Figures 29 through 40, smaller damper employed (see Appendix A).

The effects just noted are even more pronounced when the small damper is employed, since most of the motion produced by the thrust pulsations takes place across the damper and relatively little motion is communicated to the ship. The effects of the damper are noticeable over a broader bandwidth.

With regard to the effects of the incorporation of a viscous damper in the thrust coupling mechanism, the reduction in vibration as the damper is made smaller is not unexpected. It must be remembered that the damper is "large" or "small" according to whether it takes a large or small force per unit relative velocity between the shaft and the thrust block. Since the damper is a series element, all of the force which reaches the thrust block and, hence, causes vibrations of the ship, must be transmitted through the damper. A small damper, in contrast to a large or stiff damper, would require a greater differential velocity between the shaft and the thrust block to transmit an equal force to the ship, giving equal ship vibrations. Obviously, this greater differential velocity could occur only if the shaft underwent larger vibrations itself. But for the same force to be transmitted to the viscous damper with the shaft undergoing larger vibrations (and consequently consuming a greater inertia force itself), it would be necessary for a large excitation force to be applied at the propeller. Thus, for equal excitation force applied at the propeller, we can expect smaller vibration levels in the ship when the small damper is in use.

Perhaps the electrical analogy for this situation points this out more clearly.



In the above analogy, the exciting force from the propeller is represented as a current which flows into the circuit through the lead from the left. When the damper is made smaller, the series resistor which represents it has a greater resistance affecting the diversion of a greater portion of the excitation current into the capacitor representing shaft mass and thereby transmitting a smaller percentage of this current into the circuit representing the thrust block and the remainder of the ship. Thus, as the damper is made smaller the force transmitted to the ship is reduced, and the vibration level is also reduced.

d. Figures 41 through 52, inertia coupler employed (see Appendix A).

The inertia coupler produces a force proportional to the difference in acceleration across the coupler. At very high frequencies, the inertia coupler behaves like a rigid connection and, therefore, produces a negligible effect. At low frequencies, the inertia coupler serves to isolate the ship very effectively from the thrust pulsations. Thus the vibration of the thrust block at 330 cpm is reduced by about 19 db (see Figure 42). At 1000 cpm, however, Figure 42 shows a large response at the thrust block (but not so large as the peak response shown in Figure 6). The inertia coupler simulated would completely isolate the propeller from the ship at low frequency. In

practice, such an inertia coupler could not be built although it could be closely approximated. Thus, in practice, an inertia coupler would also have a large response at some low frequency which could be chosen below the frequency of other structural modes.

e. Figures 53 through 64, a larger inertia coupler employed (see Appendix A).

Here the inertia coupler acts more like a rigid connection and less improvement is noticeable. As a result, the coupling inertia cannot be made too large or a loss of effectiveness becomes evident.

f. Figures 65 through 76, axial flexibility of shaft at coupler increased by a factor of 7.76.

The shaft frequency, originally at 506 cpm, is significantly lowered by the increased flexibility at the coupler. A decrease of vibration amplitude of about 6 db occurs at the propeller. At the thrust block the improvement is only about 3 db.

g. Figures 77 through 88, axial flexibility of shaft at coupler increased by a factor of 17.47.

Because of the decreased frequency of the shaft mode, originally at 506 cpm, three modes are in close proximity to one another. The response at the propeller is somewhat larger than that shown in Figure 65. In general, there is no clear-cut improvement over the results given in Figures 65 through 76; the vibration at some points is more severe and at other points is reduced.

h. Figures 89 through 100, basic configuration, ship excited by a periodic moment applied at Station 545 (stern).

The periodic moment was applied for the purpose of analyzing the response of

the ship to moments originating at the propeller caused by the effect of the free surface above the propeller. The ratio of maximum response to applied moment is about 36 db smaller than that in the corresponding runs where simple longitudinal thrust pulsations were applied. Since the moment originates on the propeller and since the radius of the propeller is about 11 ft, it is reasonable to assume that the moment (in ft-lb) due to the effect of the free surface is only two to six times as large as the force due to thrust pulsations. Therefore, as shown in Appendix G, amplitudes of vibration produced by the moment on the propeller are 33 db to 20 db less than the amplitudes of vibration due to thrust pulsations.

i. Figures 101 through 112, bulkheads rigid in shear.

Frequencies of some of the modes are naturally raised, and amplitudes of vibration are increased at some points. However, levels of vibration are not radically affected. Bulkhead flexibility is a quantitatively significant effect. We infer then that shear lag effects are important for quantitative prediction of vibration amplitudes because shear flexibilities are important for such prediction. However, it is recognized that bending is the major structural contribution to the vibration characteristics of the ship.

j. Figures 113 through 124, bulkheads and decks rigid in shear.

With bulkheads rigid, deck flexibility has a relatively minor effect.

k. Figures 125 through 136, all shear flexibilities zero (beam theory).

The qualitative similarity of these figures with the basic Figures 5 through 16 shows that bending is the most important single mechanism in the prediction of symmetric vibration amplitudes.

Preliminary experimental data for the first four modes show the frequencies to lie within the range of results given in Figures 2b - 2e. Pending additional *experimental* results, discussion of Figures 2b through 2g will be deferred. These curves can serve as a guide for the placement of gages (e.g., accelerometers or velocity pickups) along the longitudinal axis of NS SAVANNAH where the curvatures of the mode patterns of interest are expected to change rapidly. This guide should lead to a better comparison between experimental and theoretical results.

If quantitative estimates regarding the magnitude of hydrodynamic excitation at the propeller are available, the magnitude of vibrations transmitted through the shafting system, at all points in a ship as a function of shaft rpm, can be predicted. Without such estimates, the relative vibration levels in different parts of the ship can still be determined. In addition, the most critical rpm ranges and the effectiveness of various vibration suppression schemes, such as the flexible couplers treated above, can be evaluated. The complete computer measurements and the results of comparative studies can yield significant gains in understanding the mechanisms of ship vibration.

Caution should be exercised in the interpretation of the curves presented in Figure 2 to avoid an improper comparison of analog and digital computer results. First, it will be noted that vertical normal modes for *uncoupled* vibrations obtained on the basis of beam theory, by means of a digital computer, are plotted in Figure 2. Superposed are the most nearly corresponding predominant vertical *components* of modes of *coupled* vibrations, involving vertical, transverse, and longitudinal motions, obtained on the basis of three-dimensional theory by means of an analog computer. Vertical vibration results obtained on the basis of uncoupled and coupled

vibrations cannot, in general, be expected to agree since for any mode the total energy of an uncoupled vibration is unequal to the partial energy associated with the corresponding component of coupled vibrations (unless the energy of the other components is essentially null).

In addition, the beam theory investigation of the symmetric response of the ship made on the digital computer does not permit a description of the relative motions of elements composing a *transverse* section of a ship, whereas the three-dimensional theory investigation by means of an analog computer does lead to such a description. Further, in applying the three-dimensional theory to the present problem, it is seen (Figure 2a) that a shift in the neutral axis occurs in going from the beam to the shell and that in proceeding from Station 408 to Station 243 the points of measurement within the shell vary in the vertical direction.

Finally (see Appendix B), certain constraints, assumptions, and boundary conditions are different for the two methods of analysis.

For these reasons, correlation of beam and three-dimensional theory mode shapes and frequencies in general cannot be expected although good agreement *may* exist for particular modes (see Figure 2b). Comparison between observed and theoretical results for either theory should be made by matching measured quantities with corresponding theoretical quantities at appropriately selected *identical* points in the ship; these points will be different for beam and three-dimensional theory. Thus, comparison between theoretical and observed vertical normal modes for uncoupled vibrations along a longitudinal axis is proper when beam theory is used for computing these modes and when corresponding uncoupled vibrations are experimentally excited. But

comparison of vertical vibrations along a longitudinal axis is improper when three-dimensional theory is used to compute the modes (1) because vertical vibrations are only components of these modes and (2) because corresponding modes of coupled vibrations *are not experimentally excited* by a vibration generator.

Finally, it should be clear that since normal mode frequencies are associated with free vibrations of a system, regardless of whether we are speaking of uncoupled (beam theory) vibrations or coupled (three-dimensional theory) vibrations, the normal mode response should not be expected, in general, to correlate with the amplitude response versus frequency results; see Figures 5 through 136. This is true because the latter results were obtained for a steady-state (sinusoidal) thrust pulsation applied at the propeller or steady-state bending moment applied at the stem. Hence, at a particular location (e.g., stern) the vertical response may be very small compared to the response that would be caused by an equal exciting force acting vertically at the same location as the thrust or bending moments loads, i.e.,

$$\frac{y'_{\text{vertical}}}{F_{\text{thrust}}} \ll \frac{y'_{\text{vertical}}}{F_{\text{vertical}}} \quad \text{where } F_{\text{thrust}} = F_{\text{vertical}}$$

and similarly for the bending moment. On the other hand, if the steady-state thrust pulsation acts at a nodal point the vertical response will also be small, e.g., Table 1 and Figure 5 show that the vertical response at 90.7 cycles is very small because the thrust force is acting at a nodal point (i.e., propeller) for this frequency. Figure 89, however, shows that when a bending moment is applied at the propeller the vertical response at 90.7 cycles is large, as is to be expected.

For ships with a vertical plane of symmetry, the problem may be separated into

an analysis of symmetrical vibrations and an analysis of antisymmetrical vibrations. This separation results in an economy of analog computer components so that greater detail may be included in an analysis with a given computer. The details of the symmetric and antisymmetric analyses are discussed in Appendix C.

RECOMMENDATIONS

To refine the correlation between theory and experiment it is recommended that:

1. The differences between mode shapes and frequencies obtained by beam theory and by three-dimensional theory should be investigated and explained.
2. Future full-scale ship measurements for vibratory response (including the response to slamming forces) should be extended to comprehend the three-dimensional aspects of the beam-shell-sprung body theory presented here. For comparison, subsystems and structures of particular interest such as the propulsion system, nuclear reactor, superstructure, appendages, etc., should be so instrumented and analytically represented as to present greater detailed information of significance. Deformations and corresponding stresses at selected points within a cross section are also of special concern for purposes of design.
3. Digital computer programming for beam-shell-sprung body analysis of a ship should be undertaken. This would permit an independent calculation based on the same theory but obtained by an alternative computational technique; thereby confidence in the accuracy of the theoretical calculations would be established. Moreover, despite the greater flexibility of the electrical-analog computer as compared to the digital computer, the limited number of available electrical components in this

computer sets an upper bound for the degree of structural definition possible in subdividing a ship into its component elements. The memory of the digital computer permits transcendence of this threshold.

4. If after a sufficient number of additional theoretical investigations the theory is considered to be accurate, then design use should be made of beam-shell-sprung body theory by effecting local changes in the axial and/or beam elements and/or plating and/or combinations thereof and by determining the influence of such changes upon the response (to slamming forces in particular) and associated stresses.

CONCLUSIONS

1. The investigation of methods of coupling the shaft to the ship show that significant reduction in vibration amplitudes can be achieved by methods, such as damping or inertia coupling, which directly affect the sharpness of the structural resonant peaks. Methods which merely shift frequency without exerting an effect upon the sharpness of the resonances are not very effective. In particular, changing the position of the thrust block is not likely to produce much reduction in vibration amplitudes. Even if the thrust block is placed upon the node line of one mode, other modes will, in general, be excited more strongly than they would have been otherwise.

2. Vibrations due to propeller moments are relatively unimportant in comparison with vibrations produced by thrust pulsations.

3. Bending modes are of basic importance in the analysis of ship vibrations due to thrust pulsations. The qualitative aspects of the vibration can be predicted from beam theory alone.

4. Shear lag effects are important for the quantitative prediction of vibration amplitudes.

ACKNOWLEDGMENTS

The authors gratefully acknowledge the constructive criticism of Mr. Edward F. Noonan. The authors are also indebted to Mr. Jack Hill of Computer Engineering Associates for his contributions to the present report. The additional data associated with digital computer solutions for the vibrations of NS SAVANNAH submitted by Mr. John Cummings are deeply appreciated. Mr. Basil Nakonechny assisted the authors in furnishing the ship data used in this study for NS SAVANNAH. In particular, the authors wish to thank Dr. Erich Buchmann for various valuable suggestions made during the course of this work.

TABLE 1

Symmetric Vibration Modes

| Panel Point | Mode 1 | Mode 2 | Mode 3 | Mode 4 | Mode 5 | Mode 6 | Mode 7 | Mode 8 | Mode 9 | Mode 10 |
|-----------------|----------|---------|---------|---------|---------|---------|---------|---------|---------|---------|
| Vertical Motion | 90.7 cpm | 165 cpm | 199 cpm | 235 cpm | 271 cpm | 299 cpm | 315 cpm | 462 cpm | 506 cpm | 522 cpm |
| 0 | 1.000 | -0.830 | 0.061 | 0.637 | 0.461 | -0.506 | -0.441 | 0.020 | -0.271 | 0.360 |
| 63 | 0.612 | -0.322 | 0.021 | 0.149 | 0.081 | -0.060 | -0.041 | -0.005 | 0.064 | -0.101 |
| 108 | 0.328 | -0.011 | -0.001 | -0.109 | -0.105 | 0.155 | 0.144 | -0.012 | 0.128 | -0.187 |
| 153 | 0.076 | 0.218 | -0.016 | -0.256 | -0.186 | 0.228 | 0.196 | -0.010 | 0.051 | -0.072 |
| 198 | -0.118 | 0.331 | -0.018 | -0.263 | -0.152 | 0.161 | 0.117 | -0.007 | -0.100 | 0.119 |
| 453 | 0.370 | 0.218 | -0.009 | 0.058 | -0.023 | -0.087 | 0.070 | -0.015 | -0.076 | -0.246 |
| 498 | 0.597 | 0.581 | -0.042 | 0.478 | -0.049 | 0.304 | -0.161 | 0.005 | 0.007 | 0.037 |
| 545 | 0.840 | 1.000 | -0.082 | 1.000 | -0.090 | 0.854 | -0.466 | 0.041 | 0.174 | 0.680 |
| 243- ζ | -0.277 | -0.073 | 0.020 | -0.132 | 0.237 | -0.324 | -0.459 | 0.033 | 0.158 | -0.348 |
| -I | -0.266 | -0.381 | 0.007 | -0.143 | 0.135 | 0.036 | -0.324 | 0.023 | -0.087 | 0.028 |
| -II | -0.236 | 0.326 | -0.008 | -0.173 | -0.049 | 0.037 | -0.007 | -0.017 | -0.223 | 0.226 |
| 270- ζ | -0.294 | 0.154 | -0.014 | 0.350 | 0.133 | -0.199 | -0.131 | 0.041 | 0.250 | -0.254 |
| -I | -0.283 | 0.144 | -0.012 | 0.253 | 0.089 | -0.141 | -0.075 | 0.008 | -0.062 | 0.168 |
| 303- ζ | -0.309 | -0.274 | -0.051 | 0.863 | 0.006 | 0 | 0.264 | 0.030 | 0.249 | -0.085 |
| -I | -0.299 | -0.236 | -0.034 | 0.694 | 0.021 | 0.001 | 0.230 | -0.016 | -0.013 | 0.216 |
| -II | -0.268 | -0.158 | -0.005 | 0.253 | 0.019 | -0.003 | 0.104 | -0.049 | -0.250 | 0.318 |
| 345.5- ζ | -0.200 | -0.626 | 0.002 | 0.182 | -0.023 | 0.420 | -0.002 | 0.006 | 0.195 | -0.235 |
| -I | -0.192 | -0.558 | 0.008 | 0.152 | -0.004 | 0.321 | 0 | -0.038 | -0.029 | -0.188 |
| 358- ζ | -0.127 | -0.640 | 0.038 | -0.372 | 0 | 0.475 | -0.297 | 0.024 | 0.161 | -0.147 |
| -I | -0.121 | -0.571 | 0.039 | -0.348 | 0.010 | 0.356 | -0.227 | -0.018 | -0.069 | -0.138 |
| -II | -0.103 | -0.380 | 0.030 | -0.198 | 0.014 | 0.036 | -0.018 | -0.052 | -0.231 | -0.086 |

TABLE 1

Symmetric Vibration Modes (Continued)

| Panel Point | Mode 1 | Mode 2 | Mode 3 | Mode 4 | Mode 5 | Mode 6 | Mode 7 | Mode 8 | Mode 9 | Mode 10 |
|----------------------|--------|--------|--------|--------|--------|--------|--------|--------|--------|---------|
| 383-G _L | 0.024 | -0.499 | 0.067 | -0.952 | 0.009 | 0.093 | -0.323 | 0.099 | 0.205 | 0.444 |
| -I | 0.029 | -0.440 | 0.067 | -0.906 | 0.017 | 0.001 | -0.263 | 0.051 | -0.061 | 0.422 |
| 408-G _L | 0.170 | -0.118 | 0.031 | -0.521 | -0.022 | -0.727 | 0.392 | 0.036 | 0.226 | 0.262 |
| -I | 0.168 | -0.108 | 0.028 | -0.454 | -0.020 | -0.634 | 0.350 | 0.019 | 0.126 | 0.114 |
| -II | 0.160 | -0.074 | 0.017 | -0.234 | -0.014 | -0.324 | 0.201 | -0.023 | -0.100 | -0.251 |
| Transverse Motion | | | | | | | | | | |
| 243-A | 0 | 0 | 0 | 0 | 0 | 0 | 0 | 0 | 0 | 0 |
| 303-A | -0.004 | -0.012 | -0.004 | 0.057 | 0 | 0.004 | 0.016 | 0.006 | 0.037 | -0.024 |
| 358-A | -0.003 | -0.026 | 0.001 | -0.015 | -0.001 | 0.041 | -0.026 | 0.005 | 0.027 | -0.008 |
| 408-A | 0 | 0 | 0 | 0 | 0 | 0 | 0 | 0 | 0 | 0 |
| 243-C | 0 | 0 | 0 | 0 | 0 | 0 | 0 | 0 | 0 | 0 |
| 303-C | -0.001 | -0.002 | -0.001 | 0.013 | 0.002 | 0 | 0.003 | 0.002 | 0.013 | -0.008 |
| 358-C | -0.001 | -0.006 | 0.001 | -0.005 | 0.001 | 0.009 | -0.005 | 0 | 0.005 | -0.005 |
| 408-C | 0 | 0 | 0 | 0 | 0 | 0 | 0 | 0 | 0 | 0 |
| 243-D | 0 | 0 | 0 | 0 | 0 | 0 | 0 | 0 | 0 | 0 |
| 303-D | 0.001 | 0.007 | 0.002 | -0.024 | 0.004 | -0.003 | -0.008 | -0.001 | -0.007 | 0.006 |
| 358-D | 0 | 0.010 | 0 | 0.003 | 0.002 | -0.019 | 0.013 | -0.004 | -0.014 | -0.002 |
| 408-D | 0 | 0 | 0 | 0 | 0 | 0 | 0 | 0 | 0 | 0 |
| 243-Bot. | 0 | 0 | 0 | 0 | 0 | 0 | 0 | 0 | 0 | 0 |
| 303-Bot. | 0.003 | 0.014 | 0.004 | -0.058 | 0.005 | -0.006 | -0.018 | -0.004 | -0.026 | 0.018 |
| 358-Bot. | 0.002 | 0.025 | 0 | 0.011 | 0.003 | -0.044 | 0.029 | -0.007 | -0.031 | 0.012 |
| 408-Bot. | 0 | 0 | 0 | 0 | 0 | 0 | 0 | 0 | 0 | 0 |

TABLE 1

Symmetric Vibration Modes (Continued)

| Panel Point | Mode 1 | Mode 2 | Mode 3 | Mode 4 | Mode 5 | Mode 6 | Mode 7 | Mode 8 | Mode 9 | Mode 10 |
|---------------------|--------|--------|--------|--------|--------|--------|--------|--------|--------|---------|
| Longitudinal Motion | | | | | | | | | | |
| 0 | -0.016 | 0.153 | 1.000 | 0.176 | 0.123 | 0.312 | 0.365 | 1.000 | -0.267 | -0.173 |
| 63 | -0.016 | 0.135 | 0.842 | 0.138 | 0.088 | 0.198 | 0.302 | 0.091 | 0.020 | 0.025 |
| 108 | -0.015 | 0.119 | 0.682 | 0.102 | 0.056 | 0.105 | 0.195 | -0.336 | 0.134 | 0.092 |
| 153 | -0.014 | 0.097 | 0.471 | 0.356 | 0.016 | -0.004 | 0.053 | -0.556 | 0.155 | 0.091 |
| 198 | -0.013 | 0.068 | 0.227 | 0.003 | -0.024 | -0.104 | -0.092 | -0.466 | 0.077 | 0.030 |
| 243 | -0.012 | 0.042 | 0.019 | -0.039 | -0.051 | -0.166 | -0.185 | -0.168 | -0.031 | -0.039 |
| 408 | 0.042 | 0.112 | -0.156 | -0.135 | 0.109 | 0 | -0.071 | 0.040 | -0.124 | -0.236 |
| 453 | 0.045 | 0.138 | -0.220 | -0.247 | 0.395 | 0.304 | 0.250 | 0.030 | -0.150 | -0.346 |
| 498 | 0.047 | 0.163 | -0.280 | -0.036 | 0.705 | 0.655 | 0.618 | -0.016 | -0.006 | -0.064 |
| 545 | 0.049 | 0.183 | -0.333 | -0.460 | 1.000 | 1.000 | 1.000 | -0.102 | 0.375 | 0.884 |
| 270-A-I | -0.027 | -0.001 | -0.084 | -0.025 | -0.006 | -0.227 | -0.275 | -0.008 | -0.142 | -0.078 |
| -II | -0.027 | -0.040 | -0.087 | 0.012 | -0.015 | -0.221 | -0.252 | -0.004 | -0.121 | -0.077 |
| 349-A-I | 0.048 | 0.051 | -0.103 | -0.076 | -0.022 | -0.172 | -0.260 | 0.022 | -0.117 | -0.196 |
| -II | 0.055 | 0.021 | -0.102 | -0.142 | -0.030 | -0.167 | -0.267 | 0.024 | -0.110 | -0.218 |
| 383-A-I | 0.097 | 0.157 | -0.127 | -0.020 | -0.014 | -0.087 | -0.247 | 0.039 | -0.098 | -0.197 |
| -II | 0.110 | 0.176 | -0.128 | -0.048 | -0.022 | -0.157 | -0.205 | 0.042 | -0.086 | -0.200 |
| 270-C-I | -0.016 | 0.016 | -0.093 | -0.049 | -0.052 | -0.197 | -0.236 | 0.008 | -0.099 | -0.068 |
| -II | -0.015 | 0.014 | -0.094 | -0.047 | -0.050 | -0.196 | -0.234 | 0.010 | -0.095 | -0.076 |
| 349-C-I | 0.016 | 0.054 | -0.111 | -0.086 | -0.038 | -0.172 | -0.234 | 0.031 | -0.100 | -0.139 |
| -II | 0.014 | 0.030 | -0.106 | -0.099 | -0.041 | -0.171 | -0.238 | 0.029 | -0.100 | -0.138 |
| 383-C-I | 0.034 | 0.092 | -0.121 | -0.084 | -0.024 | -0.141 | -0.218 | 0.040 | -0.097 | -0.150 |
| -II | 0.036 | 0.094 | -0.122 | -0.085 | -0.026 | -0.149 | -0.213 | 0.040 | -0.095 | -0.149 |

TABLE 1

Symmetry Vibration Modes (Continued)

| Panel Point | Mode 1 | Mode 2 | Mode 3 | Mode 4 | Mode 5 | Mode 6 | Mode 7 | Mode 8 | Mode 9 | Mode 10 |
|--------------|--------|--------|--------|--------|--------|--------|--------|--------|--------|---------|
| 270-D-I | -0.004 | 0.037 | -0.100 | -0.074 | -0.090 | -0.172 | -0.204 | 0.023 | -0.062 | -0.065 |
| -II | -0.006 | 0.055 | -0.099 | -0.094 | -0.080 | -0.175 | -0.217 | 0.021 | -0.073 | -0.070 |
| 349-D-I | -0.018 | 0.044 | -0.110 | -0.103 | -0.053 | -0.173 | -0.220 | 0.036 | -0.091 | -0.088 |
| -II | -0.018 | 0.051 | -0.111 | -0.086 | -0.054 | -0.175 | -0.217 | 0.035 | -0.090 | -0.081 |
| 383-D-I | -0.024 | 0.031 | -0.116 | -0.135 | -0.031 | -0.179 | -0.198 | 0.040 | -0.100 | -0.111 |
| -II | -0.026 | 0.028 | -0.116 | -0.117 | -0.032 | -0.151 | -0.216 | 0.039 | -0.099 | -0.105 |
| 270-Bot. -I | 0.004 | 0.074 | -0.102 | -0.120 | -0.110 | -0.150 | -0.191 | 0.030 | -0.043 | -0.069 |
| -II | 0.001 | 0.112 | -0.100 | -0.156 | -0.099 | -0.159 | -0.216 | 0.027 | -0.061 | -0.076 |
| 349-Bot. -I | -0.043 | 0.044 | -0.113 | -0.112 | -0.073 | -0.176 | -0.214 | 0.048 | -0.057 | -0.015 |
| -II | -0.050 | 0.069 | -0.115 | -0.056 | -0.065 | -0.180 | -0.200 | 0.041 | -0.079 | -0.014 |
| 483-Bot. -I | -0.079 | -0.028 | -0.112 | -0.164 | -0.037 | -0.184 | -0.198 | 0.040 | -0.100 | -0.070 |
| -II | -0.086 | -0.037 | -0.112 | -0.138 | -0.034 | -0.127 | -0.232 | 0.038 | -0.106 | -0.063 |
| Shaft 340 | 0 | 0.008 | -0.088 | -0.484 | -0.060 | -0.075 | -0.415 | 0.056 | -0.028 | -0.070 |
| 377 | ↓ | 0.010 | -0.094 | -0.538 | -0.070 | -0.088 | -0.526 | 0.153 | 0.333 | 0.342 |
| 415 | ↓ | 0.011 | -0.098 | -0.565 | -0.076 | -0.091 | -0.581 | 0.200 | 0.524 | 0.546 |
| 453 | ↓ | 0.012 | -0.101 | -0.591 | -0.080 | -0.093 | -0.633 | 0.240 | 0.703 | 0.712 |
| 491 | ↓ | 0.012 | -0.103 | -0.612 | -0.085 | -0.094 | -0.678 | 0.265 | 0.862 | 0.884 |
| Propeller | 0 | 0.012 | -0.105 | -0.632 | -0.089 | -0.095 | -0.722 | 0.277 | 1.000 | 1.000 |
| Thrust Coup. | -0.007 | -0.236 | -0.139 | -0.286 | -0.226 | -0.028 | 0.102 | 0.052 | 0.015 | 0.060 |

TABLE 2
Amplitude Response Data

| Figure No. | Excitation | | Coordinate at Which Response was Measured | Velocity/Force at 0 db | Configuration | Remarks |
|----------------------|-------------|---------------|---|------------------------|---|----------|
| | Drive Point | Type of Drive | | (in/sec/lb) | | |
| 5 6 7 8 | Prop. | Thrust | \dot{y} at prop. (Station 531) \dot{y} at thrust block (Station 340) \dot{y} at bow (Station 0) \dot{z} at bow (Station 0) | 4.167×10^{-4} | Basic Configuration | One Page |
| 9 10 11 12 | | | \dot{y} at stern (Station 545) \dot{z} at stern (Station 545) \dot{y} at 349-A-II \dot{y} at 349-C-II | | | |
| 13 14 15 | | | \dot{y} at 349-Bot.-II \dot{y} at cont. vessel \dot{z} at 303 ζ | | | |
| 16 | Prop. | Thrust | \dot{z} at 303 II | 4.167×10^{-4} | Basic Configuration | One Page |
| 17 18 19 20 | Prop. | Thrust | \dot{y} at prop. (Station 531) \dot{y} at thrust block (Station 340) \dot{y} at bow (Station 0) \dot{z} at bow (Station 0) | 1.32×10^{-4} | 30×10^4 lb-sec/in Damper Used for Thrust Coupler | |
| 21 | | | \dot{y} at stern (Station 545) | | | |

TABLE 2

Amplitude Response Data (Continued)

| Figure No. | Excitation | | Coordinate at Which Response was Measured | Velocity/Force at 0 db | Configuration | Remarks |
|----------------------------------|-------------|---------------|--|------------------------|---|----------|
| | Drive Point | Type of Drive | | (in/sec/lb) | | |
| 22 | Prop. | Thrust | \dot{z} at stern (Station 545) | 1.32×10^{-4} | 30 x 10 ⁴ lb-sec/in Damper Used for Thrust Coupler | One Page |
| 23 24 | ↓ | ↓ | \dot{y} at 349-A-II \dot{y} at 349-C-II | ↓ | | |
| 25 26 27 28 | Prop. | Thrust | \dot{y} at 349-Bot.-II \dot{y} at cont. vessel \dot{z} at 303 C \dot{z} at 303 II | 1.32×10^{-4} | 30 x 10 ⁴ lb-sec/in Damper Used for Thrust Coupler | One Page |
| 29 | Prop. | Thrust | \dot{y} at prop. (Station 531) | 1.32×10^{-4} | | |
| 30 31 32 33 34 35 | ↓ | ↓ | \dot{y} at thrust block (Station 340) \dot{y} at bow (Station 0) \dot{z} at bow (Station 0) \dot{y} at stern (Station 545) \dot{z} at stern (Station 545) \dot{y} at 349-A-II | ↓ | 6 x 10 ⁴ lb-sec/in Damper Used for Thrust Coupler | One Page |

TABLE 2

Amplitude Response Data (Continued)

| Figure No. | Excitation | | Coordinate at Which Response was Measured | Velocity/Force at 0 db (in/sec/lb) | Configuration | Remarks |
|------------|-------------|---------------|---|------------------------------------|--|----------|
| | Drive Point | Type of Drive | | | | |
| 36 | Prop. | Thrust | \dot{y} at 349-C-II | 1.32×10^{-4} | 6×10^4 lb-sec/in Damper Used for Thrust Coupler | One Page |
| 37 | ↓ | ↓ | \dot{y} at 349-Bot.-II | ↓ | ↓ | One Page |
| 38 | | | \dot{y} at cont. vessel | | | |
| 39 | | | \dot{z} at 303 \bar{C} | | | |
| 40 | | | \dot{z} at 303 II | | | |
| 41 | Prop. | Thrust | \dot{y} at prop. (Station 531) | 4.167×10^{-4} | 31 ton Inertia Coupler | One Page |
| 42 | ↓ | ↓ | \dot{y} at thrust block (Station 340) | 4.167×10^{-5} | | |
| 43 | | | \dot{y} at bow (Station 0) | | | |
| 44 | | | \dot{z} at bow (Station 0) | | | |
| 45 | | | \dot{y} at stern (Station 545) | | | |
| 46 | | | \dot{z} at stern (Station 545) | | | |
| 47 | | | \dot{y} at 349-A-II | | | |
| 48 | | | \dot{y} at 349-C-II | | | |
| 49 | | | \dot{y} at 349-Bot.-II | | | |
| 50 | | | \dot{y} at cont. vessel | | | |
| 51 | | | \dot{z} at 303 \bar{C} | | | |

32

TABLE 2

Amplitude Response Data (Continued)

| Figure No. | Excitation | | Coordinate at Which Response was Measured | Velocity/Force at 0 db (in/sec/lb) | Configuration | Remarks |
|------------|---------------------------|---------------|---|------------------------------------|---|----------|
| | Drive Point | Type of Drive | | | | |
| 52 | Prop. | Thrust | \dot{z} at 303 II | 4.167×10^{-5} | 31-Ton Inertia Coupler 310-Ton Inertia Coupler | One Page |
| 53 | Prop. | Thrust | \dot{y} at prop. (Station 531) | 4.167×10^{-4} | | One Page |
| 54 | ↓ | ↓ | \dot{y} at thrust block (Station 340) | 1.32×10^{-4} | | |
| 55 | | | \dot{y} at bow (Station 0) | 1.32×10^{-4} | | |
| 56 | | | \dot{z} at bow (Station 0) | 1.32×10^{-4} | | |
| 57 | | | \dot{y} at stern (Station 545) | 4.167×10^{-4} | | |
| 58 | | | \dot{z} at stern (Station 545) | 1.32×10^{-4} | | |
| 59 | | | \dot{y} at 349-A-II | ↓ | | |
| 60 | | | \dot{y} at 349-C-II | | | |
| 61 | | | \dot{y} at 349-Bot.-II | | | |
| 62 | \dot{y} at cont. vessel | | | | | |
| 63 | Prop. | Thrust | \dot{z} at 303 \mathcal{C} | 1.32×10^{-4} | 310-Ton Inertia Coupler | One Page |
| 64 | Prop. | Thrust | \dot{z} at 303 II | | | |
| 65 | Prop. | Thrust | \dot{y} at prop. (Station 531) | 4.167×10^{-4} | Axial Flexibility of Shaft between Stations 377 and 340 Increased by a Factor of 7.76 | One Page |
| 66 | ↓ | ↓ | \dot{y} at thrust block (Station 340) | 1.32×10^{-4} | | |

TABLE 2

Amplitude Response Data (Continued)

| Figure No. | Excitation | | Coordinate at Which Response was Measured | Velocity/Force at 0 db (in/sec/lb) | Configuration | Remarks |
|------------|-------------|---------------|---|------------------------------------|---|----------|
| | Drive Point | Type of Drive | | | | |
| 67 | Prop. | Thrust | \dot{y} at bow (Station 0) | 1.32×10^{-4} | Axial Flexibility of Shaft between Stations 377 and 340 Increased by a Factor of 7.76 | One Page |
| 68 | ↓ | ↓ | \dot{z} at bow (Station 0) | ↓ | | |
| 69 | | | \dot{y} at stern (Station 545) | | | |
| 70 | | | \dot{z} at stern (Station 545) | | | |
| 71 | | | \dot{y} at 349-A-II | | | |
| 72 | | | \dot{y} at 349-C-II | | | |
| 73 | | | \dot{y} at 349-Bot.-II | | | |
| 74 | | | \dot{y} at cont. vessel | | | |
| 75 | | | \dot{z} at 303 ϕ | | | |
| 76 | Prop. | Thrust | \dot{z} at 303 II | 1.32×10^{-4} | Axial Flexibility of Shaft between Stations 377 and 340 Increased by a Factor of 7.76 | One Page |
| | ↓ | ↓ | | ↓ | | |

TABLE 2

Amplitude Response Data (Continued)

| Figure No. | Excitation | | Coordinate at Which Response was Measured | Velocity/Force at 0 db (in/sec/lb) | Configuration | Remarks |
|------------|--------------------|---------------|---|------------------------------------|--|--|
| | Drive Point | Type of Drive | | | | |
| 77 | Prop. | Thrust | \dot{y} at prop. (Station 531) | 4.167×10^{-4} | Axial Flexibility of Shaft between Stations 377 and 340 Increased by a Factor of 17.47 | One Page |
| 78 | ↓ | ↓ | \dot{y} at thrust block (Station 340) | 1.32×10^{-4} | | |
| 79 | | | \dot{y} at bow (Station 0) | 4.167×10^{-4} | | |
| 80 | | | \dot{z} at bow (Station 0) | 1.32×10^{-4} | | |
| 81 | | | \dot{y} at stern (Station 545) | ↓ | | |
| 82 | | | \dot{z} at stern (Station 545) | | | |
| 83 | | | \dot{y} at 349-A-II | | | |
| 84 | | | \dot{y} at 349-C-II | | | |
| 85 | | | \dot{y} at 349-Bot.-II | | | |
| 86 | | | \dot{y} at cont. vessel | | | |
| 87 | \dot{z} at 303 C | | | | | |
| 88 | Prop | Thrust | \dot{z} at 303 II | | 1.32×10^{-4} | Axial Flexibility of Shaft between Stations 377 and 340 Increased by a Factor of 17.47 |
| | ↓ | ↓ | | | ↓ | |

35

TABLE 2

Amplitude Response Data (Continued)

| Figure No. | Excitation | | Coordinate at Which Response was Measured | Velocity/Force at 0 db (in/sec/lb) | Configuration | Remarks |
|------------|------------------|-------------------------|---|---------------------------------------|----------------------|----------|
| | Drive Point | Type of Drive | | | | |
| 89 | Stern (Sta. 545) | Moment in Plane of Sym. | \dot{y} at prop. (Station 531) | 0.596×10^{-5} (in/sec/ft-lb) | Basic Configuration | One Page |
| 90 | ↓ | ↓ | \dot{y} at thrust block (Station 340) | ↓ | ↓ | |
| 91 | | | \dot{y} at bow (Station 0) | | | |
| 92 | | | \dot{z} at bow (Station 0) | | | |
| 93 | | | \dot{y} at stern (Station 545) | | | |
| 94 | | | \dot{z} at stern (Station 545) | | | |
| 95 | | | \dot{y} at 349-A-II | | | |
| 96 | | | \dot{y} at 349-C-II | | | |
| 97 | | | \dot{y} at 349-Bot.-II | | | |
| 98 | | | \dot{y} at cont. vessel | | | |
| 99 | | | \dot{z} at 303 C | | | |
| 100 | Stern (Sta. 545) | Moment in Plane of Sym. | \dot{z} at 303 II | 0.596×10^{-5} (in/sec/ft-lb) | Basic Configuration | One Page |
| 101 | ↓ | ↓ | \dot{y} at prop. (Station 531) | 4.167×10^{-4} | Bulkheads Made Rigid | One Page |
| 102 | | | \dot{y} at thrust block (Station 340) | 1.32×10^{-4} | | |
| 103 | | | \dot{y} at bow (Station 0) | 4.167×10^{-4} | | |
| 104 | | | \dot{z} at bow (Station 0) | 1.32×10^{-4} | | |

36

TABLE 2

Amplitude Response Data (Continued)

| Figure No. | Excitation | | Coordinate at Which Response was Measured | Velocity/Force at 0 db (in/sec/lb) | Configuration | Remarks |
|------------|-------------|---------------|---|------------------------------------|---------------------------|----------|
| | Drive Point | Type of Drive | | | | |
| 105 | Prop. | Thrust | \dot{y} at stern (Station 545) | 4.167×10^{-4} | Bulkheads Made Rigid | One Page |
| 106 | | | \dot{z} at stern (Station 545) | 1.32×10^{-4} | | |
| 107 | | | \dot{y} at 349-A-II | | | |
| 108 | | | \dot{y} at 349-C-II | | | |
| 109 | | | \dot{y} at 349-Bot.-II | | | |
| 110 | | | \dot{y} at cont. vessel | | | |
| 111 | | | \dot{z} at 303 ζ | | | |
| 112 | Prop. | Thrust | \dot{z} at 303 II | 1.32×10^{-4} | Bulkheads Made Rigid | One Page |
| 113 | Prop. | Thrust | \dot{y} at prop. (Station 531) | 4.167×10^{-4} | Bulkheads and Decks Rigid | One Page |
| 114 | | | \dot{y} at thrust block (Station 340) | 1.32×10^{-4} | | |
| 115 | | | \dot{y} at bow (Station 0) | 4.167×10^{-4} | | |
| 116 | | | \dot{z} at bow (Station 0) | 1.32×10^{-4} | | |
| 117 | | | \dot{y} at stern (Station 545) | 4.167×10^{-4} | | |
| 118 | | | \dot{z} at stern (Station 545) | 1.32×10^{-4} | | |
| 119 | | | \dot{y} at 349-A-II | | | |
| 120 | | | \dot{y} at 349-C-II | | | |
| 121 | | | \dot{y} at 349-Bot.-II | | | |
| 122 | | | \dot{y} at cont. vessel | | | |
| 123 | | | Prop. | Thrust | | |

TABLE 2

Amplitude Response Data (Continued)

| Figure No. | Excitation | | Coordinate at Which Response was Measured | Velocity/Force at 0 db (in/sec/lb) | Configuration | Remarks |
|------------|-------------|---------------|---|------------------------------------|---|----------|
| | Drive Point | Type of Drive | | | | |
| 124 | Prop. | Thrust | \dot{z} at 303 II | 1.32×10^{-4} | Bulkheads and Decks Rigid Bulkheads, Decks, and Side Plating Rigid (Rigid Shell) | One Page |
| 125 | Prop. | Thrust | \dot{y} at prop. (Station 531) | 4.167×10^{-4} | | One Page |
| 126 | ↓ | ↓ | \dot{y} at thrust block (Station 340) | 1.32×10^{-4} | | |
| 127 | | | \dot{y} at bow (Station 0) | 4.167×10^{-4} | | |
| 128 | | | \dot{z} at bow (Station 0) | 1.32×10^{-4} | | |
| 129 | | | \dot{y} at stern (Station 545) | 4.167×10^{-4} | | |
| 130 | | | \dot{z} at stern (Station 545) | 1.32×10^{-4} | | |
| 131 | | | \dot{y} at 349-A-II | ↓ | | |
| 132 | | | \dot{y} at 349-C-II | | | |
| 133 | | | \dot{y} at 349-Bot. -II | | | |
| 134 | | | \dot{y} at cont. vessel | | | |
| 135 | ↓ | ↓ | \dot{z} at 303 C | ↓ | Bulkheads, Decks, and Side Plating Rigid (Rigid Shell) | |
| 136 | Prop. | Thrust | \dot{z} at 303 II | 1.32×10^{-4} | | One Page |

Figures 5 through 136 - Curves of Amplitude Response versus Frequency

These figures correspond to data given in Table 2

39

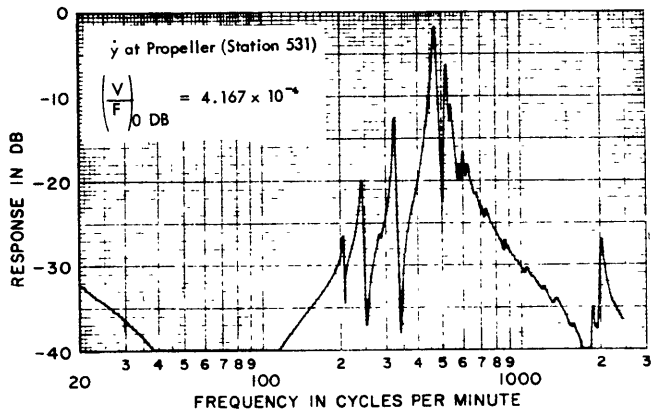


Figure 5

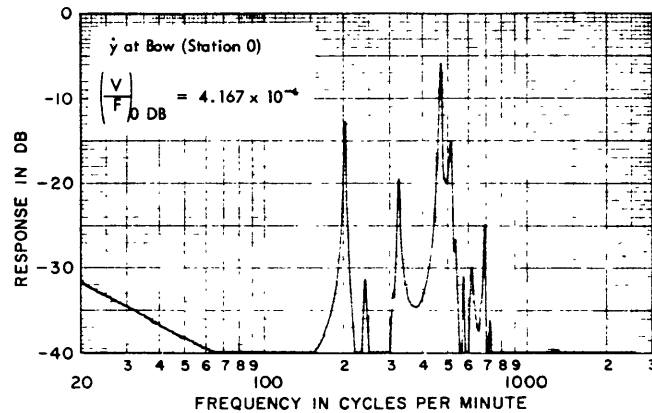


Figure 7

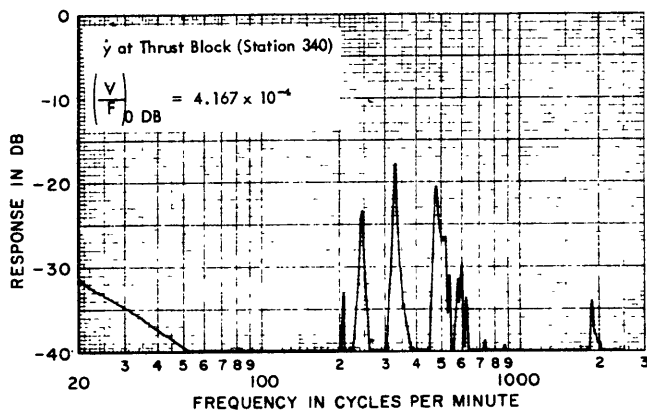


Figure 6

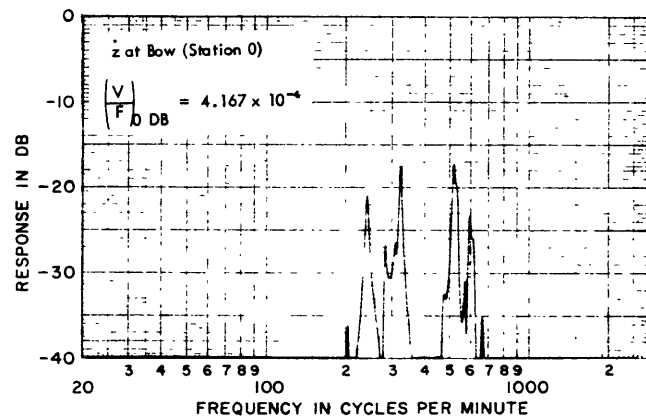


Figure 8

Excitation { Drive Point - Propeller
Type of Drive - Thrust

Configuration-Basic

Coordinate at which response was measured is shown on each figure. The value of the velocity/force at 0 DB (in/sec/lb) is shown by $\left(\frac{V}{F}\right)_{0 \text{ DB}} =$

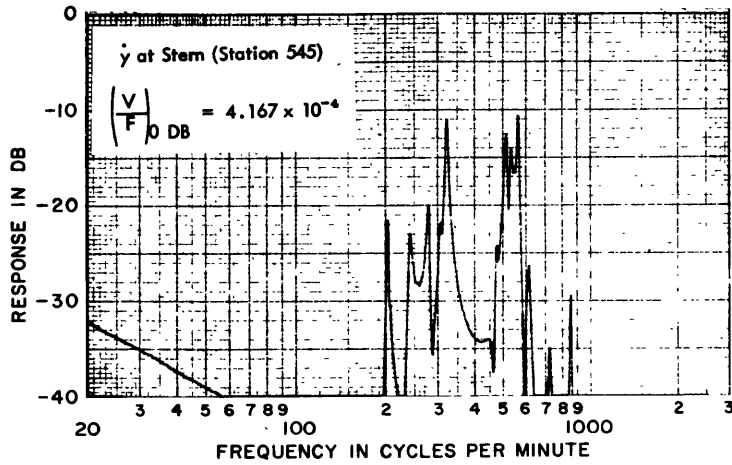


Figure 9

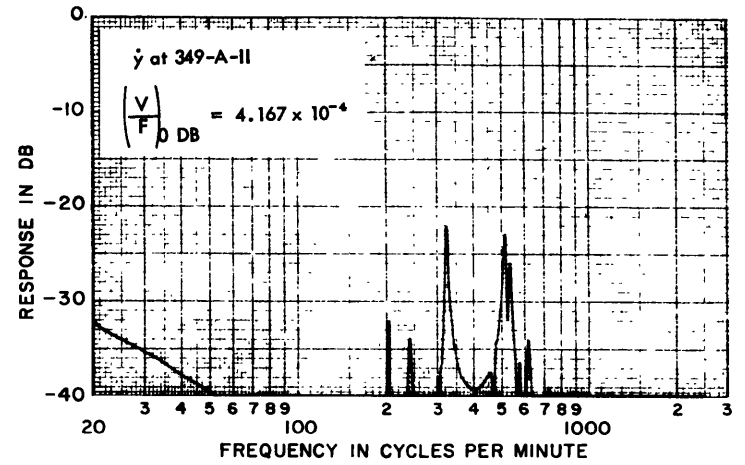


Figure 11

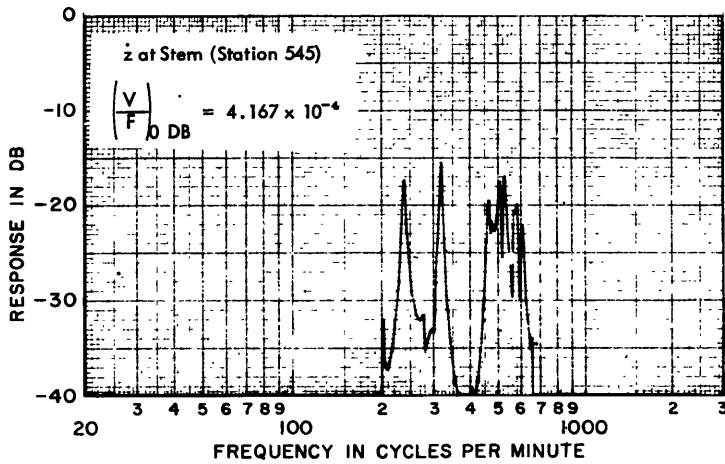


Figure 10

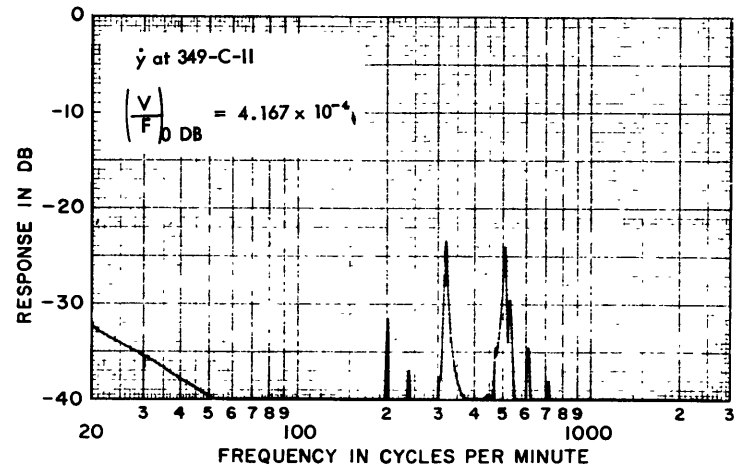


Figure 12

40

Excitation { Drive Point - Propeller
 Type of Drive - Thrust

Configuration-Basic

Coordinate at which response was measured is shown on each figure. The value of the velocity/force at 0 DB (in/sec/lb) is shown by $\left(\frac{V}{F}\right)_{0 \text{ DB}} =$

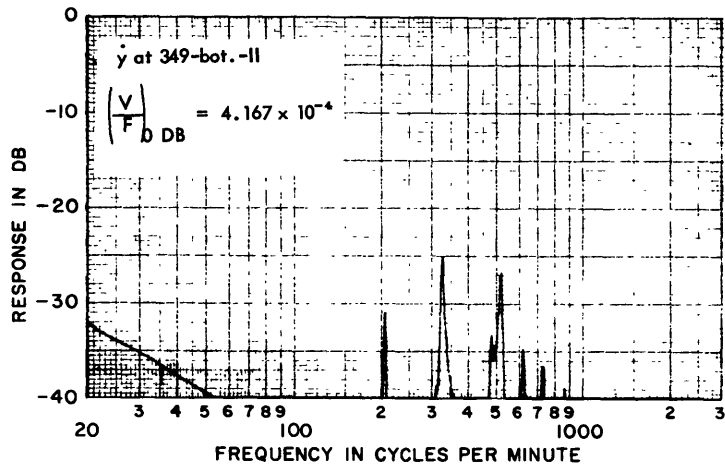


Figure 13

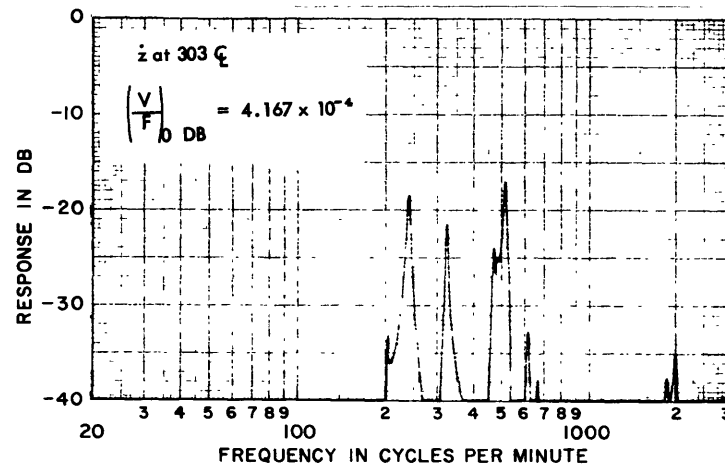


Figure 15

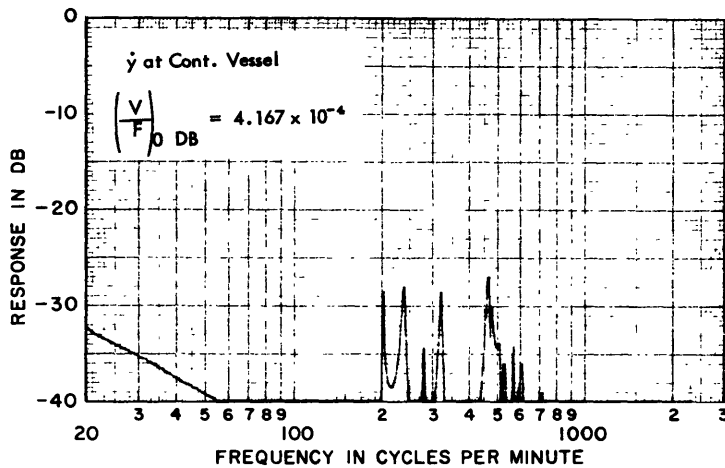


Figure 14

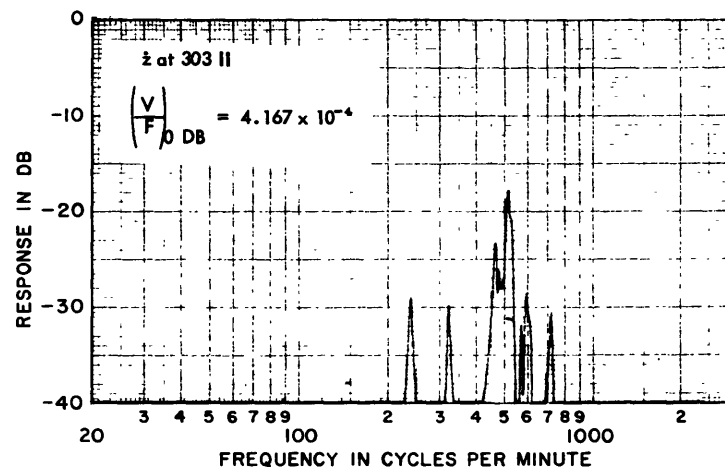


Figure 16

41

Excitation { Drive Point - Propeller
 Type of Drive - Thrust

Configuration-Basic

Coordinate at which response was measured is shown on each figure. The value of the velocity/force at 0 DB (in/sec/lb) is shown by $\left(\frac{V}{F}\right)_{0 \text{ DB}} =$

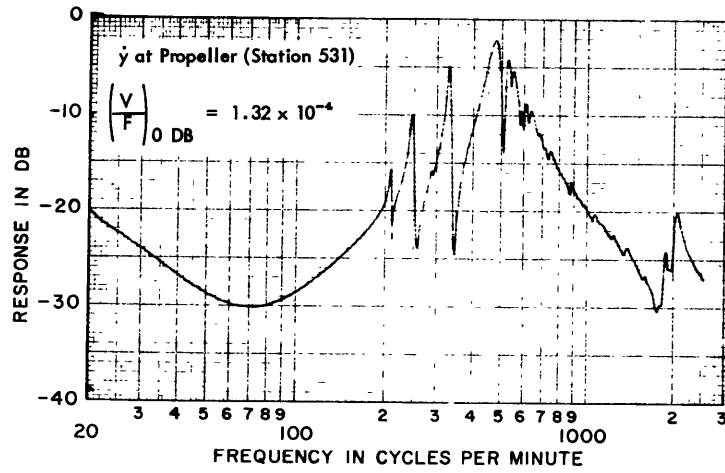


Figure 17

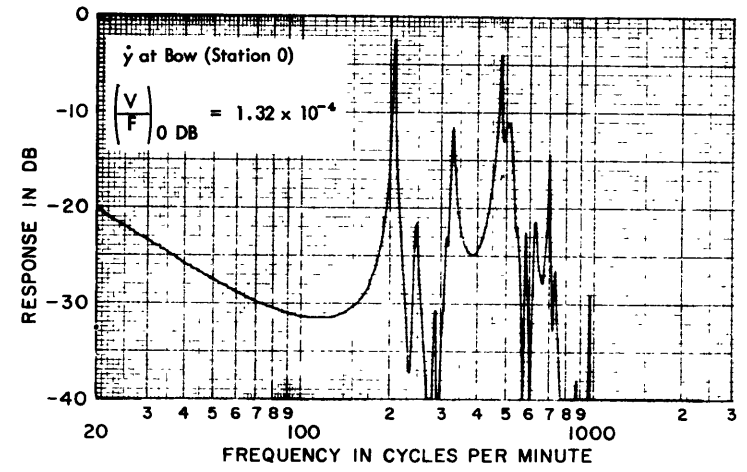


Figure 19

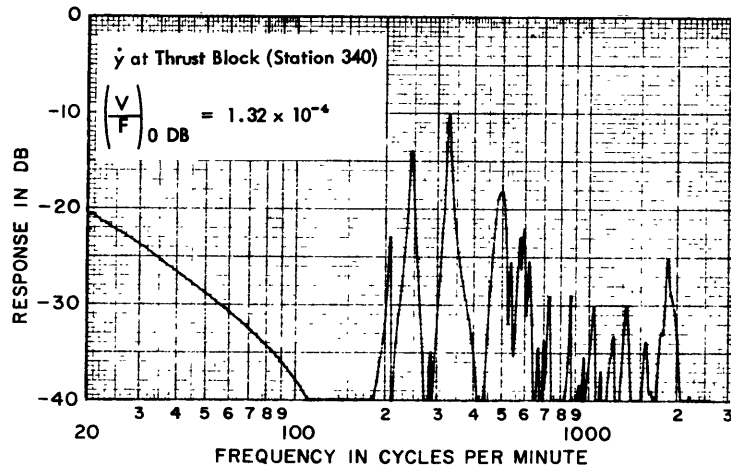


Figure 18

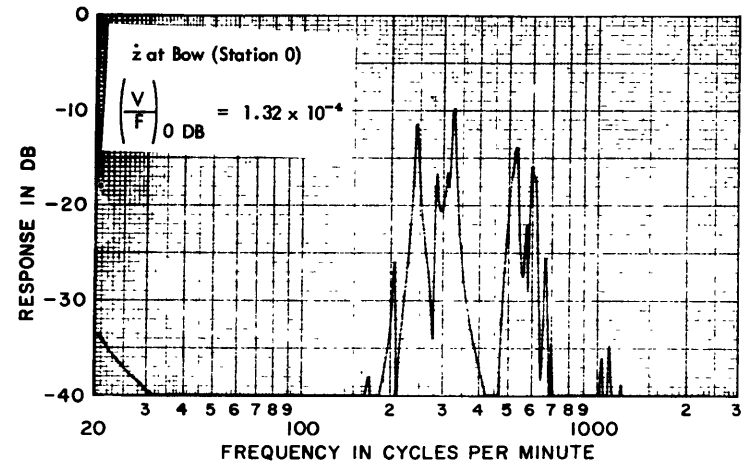


Figure 20

42

Excitation $\left\{ \begin{array}{l} \text{Drive Point - Propeller} \\ \text{Type of Drive - Thrust} \end{array} \right.$

Configuration - 30×10^4 lb-sec/in. Damper
Used for Thrust Coupler

Coordinate at which response was measured is shown on each figure. The value of the velocity/force at 0 DB (in/sec/lb) is shown by $\left(\frac{V}{F}\right)_{0 \text{ DB}} =$

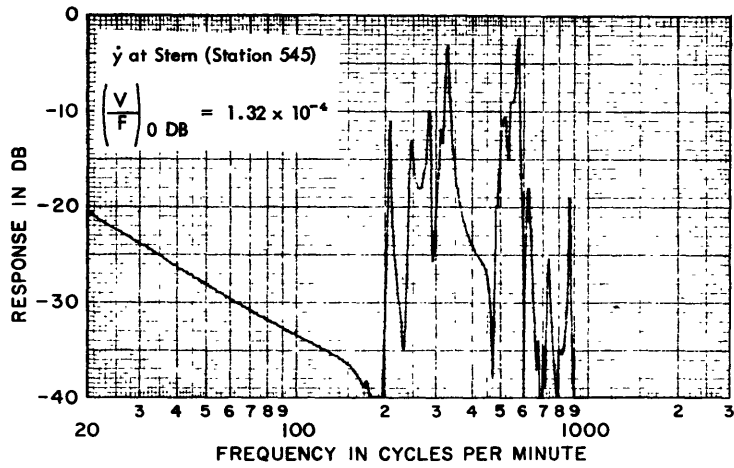


Figure 21

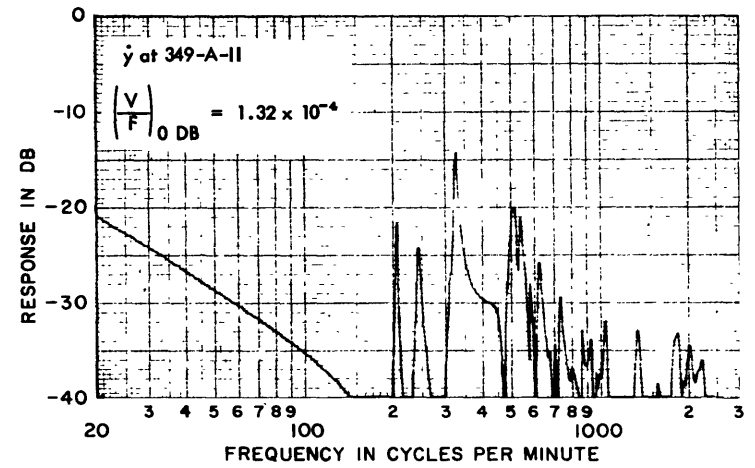


Figure 23

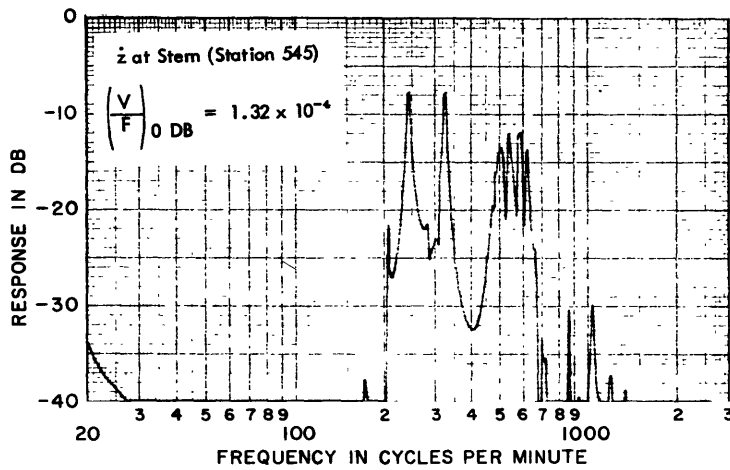


Figure 22

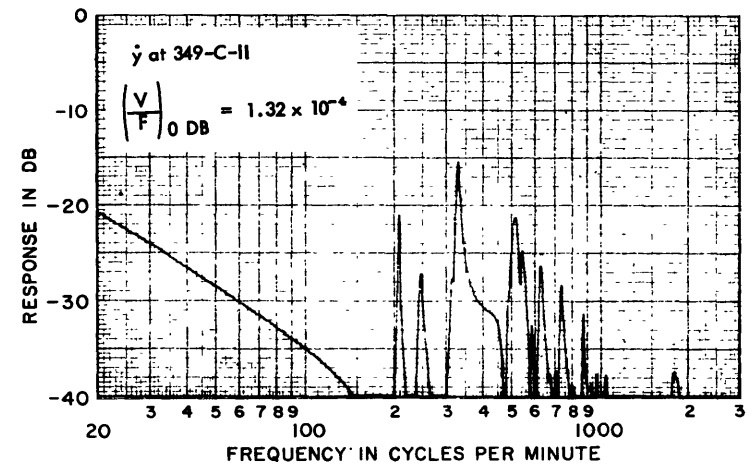


Figure 24

43

Excitation { Drive Point - Propeller
Type of Drive - Thrust

Configuration - 30×10^4 lb-sec/in. Damper
Used for Thrust Coupler

Coordinate at which response was measured is shown on each figure. The value of the velocity/force

at 0 DB (in/sec/lb) is shown by $\left(\frac{V}{F}\right)_{0 \text{ DB}} =$

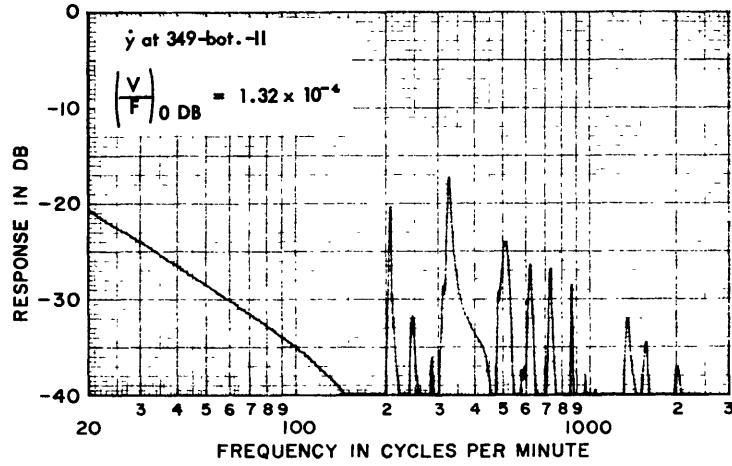


Figure 25

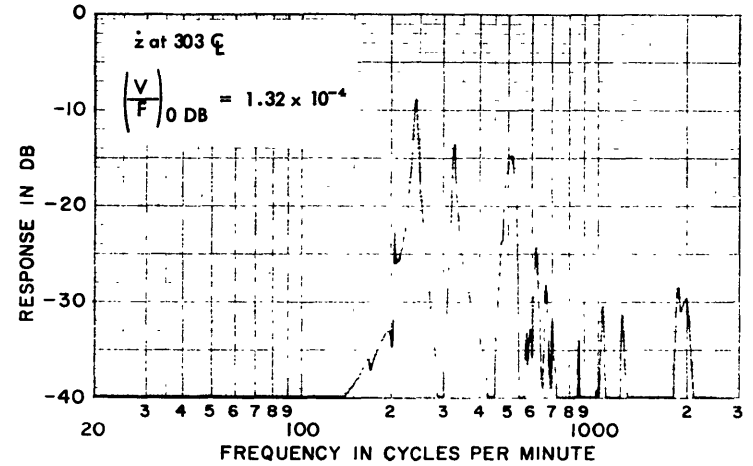


Figure 27

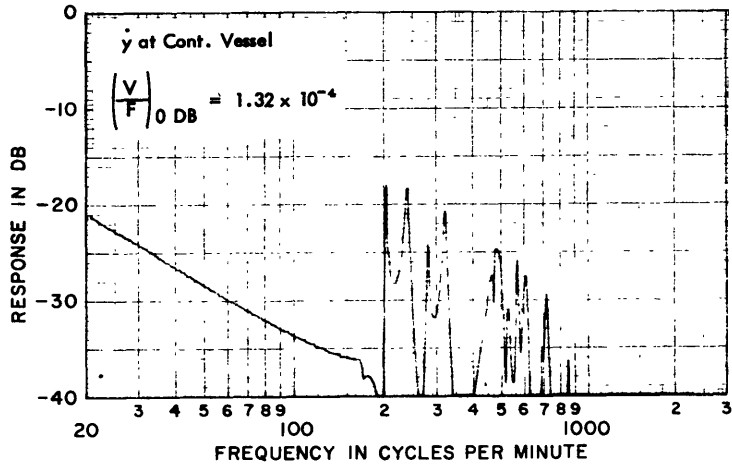


Figure 26

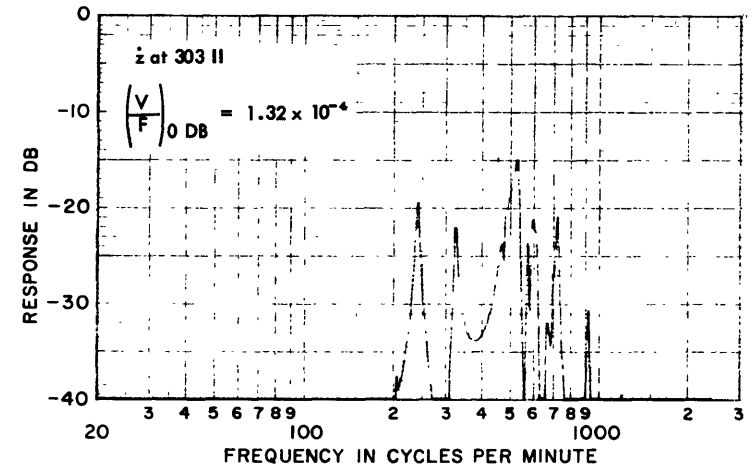


Figure 28

Excitation { Drive Point - Propeller
Type of Drive - Thrust

Configuration - 30 x 10^4 lb-sec/in. Damper
Used for Thrust Coupler

Coordinate at which response was measured is shown on each figure. The value of the velocity/force at 0 DB (in/sec/lb) is shown by $\left(\frac{V}{F}\right)_{0\text{ DB}} =$

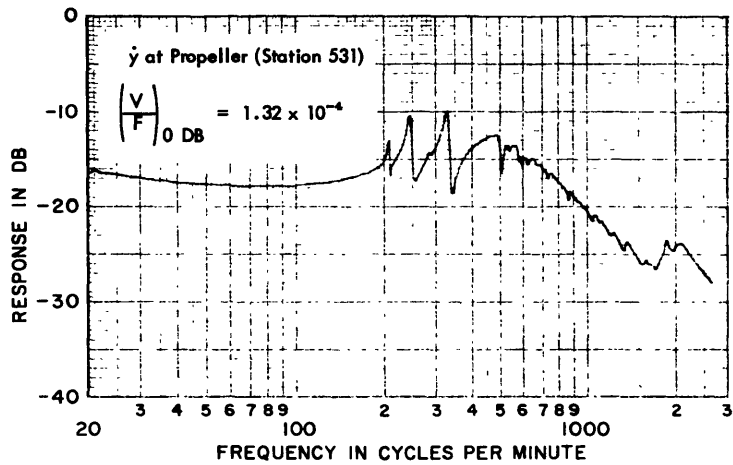


Figure 29

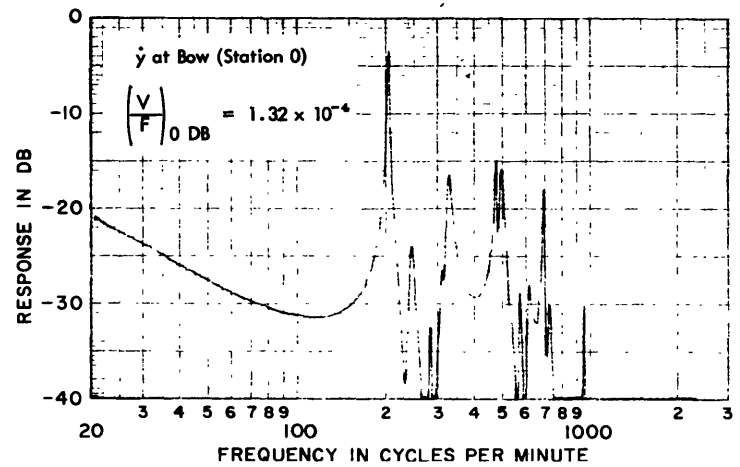


Figure 31

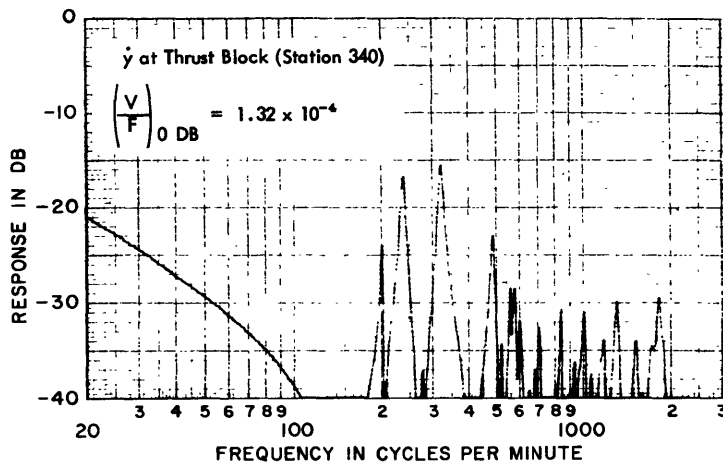


Figure 30

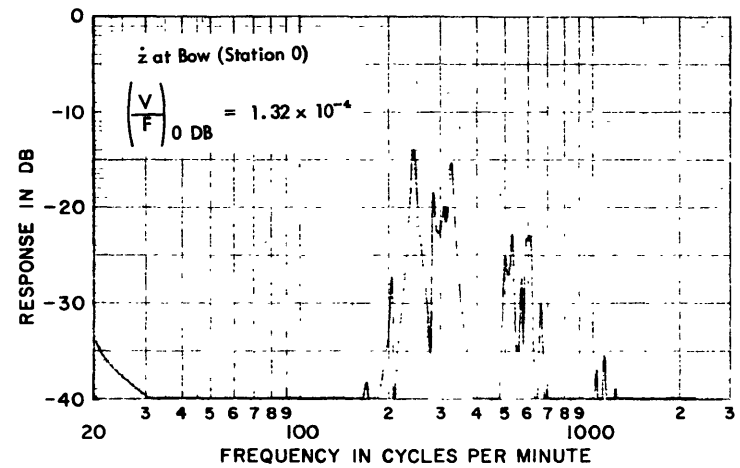


Figure 32

45

Excitation { Drive Point - Propeller
Type of Drive - Thrust

Configuration - 6×10^4 lb-sec/in Damper
Used for Thrust Coupler

Coordinate at which response was measured is shown on each figure. The value of the velocity/force at 0 DB (in/sec/lb) is shown by $\left(\frac{V}{F}\right)_{0 \text{ DB}} =$

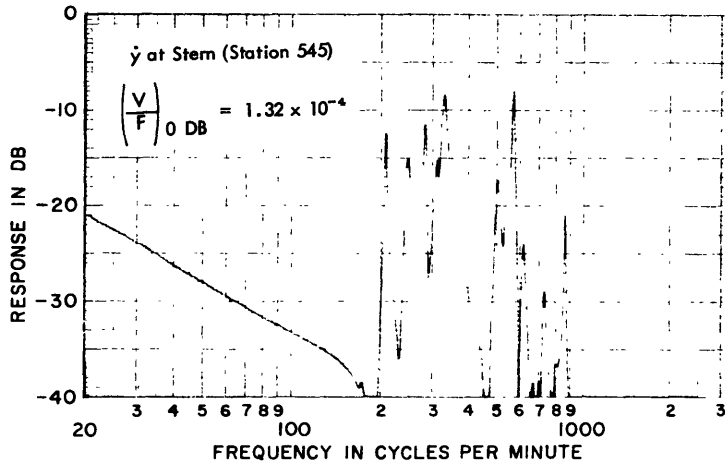


Figure 33

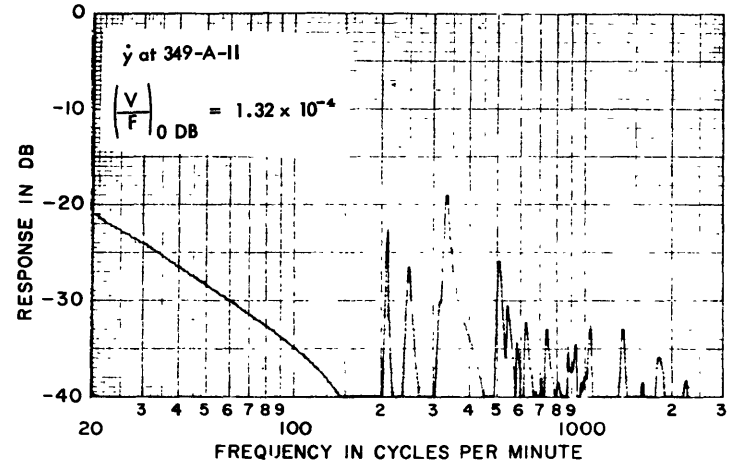


Figure 35

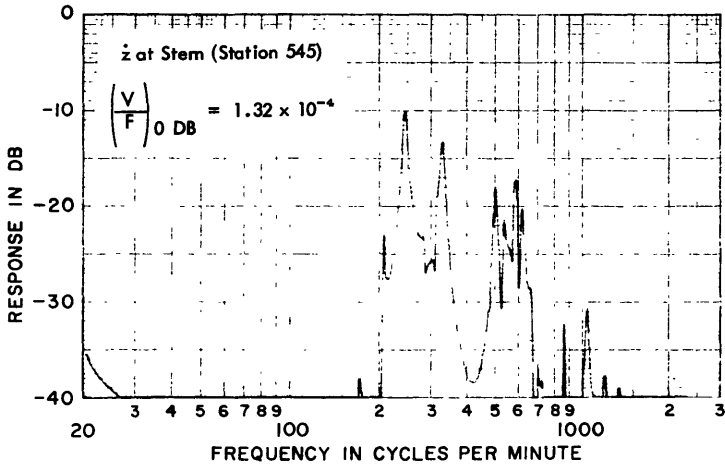


Figure 34

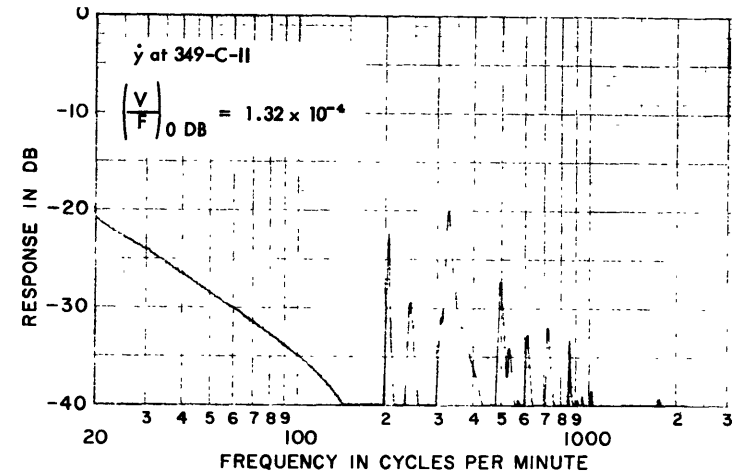


Figure 36

46

Excitation $\left\{ \begin{array}{l} \text{Drive Point - Propeller} \\ \text{Type of Drive - Thrust} \end{array} \right.$

Configuration - 6×10^4 lb-sec/in Damper
 Used for Thrust Coupler

Coordinate at which response was measured is shown on each figure. The value of the velocity/force at 0 DB (in/sec/lb) is shown by $\left(\frac{V}{F}\right)_{0 \text{ DB}} =$

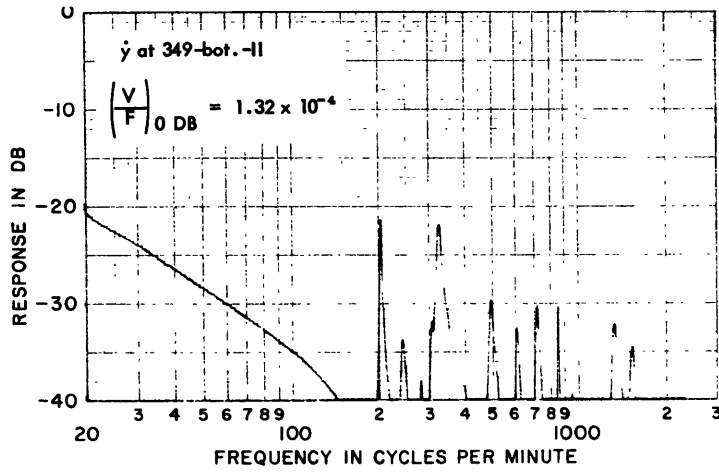


Figure 37

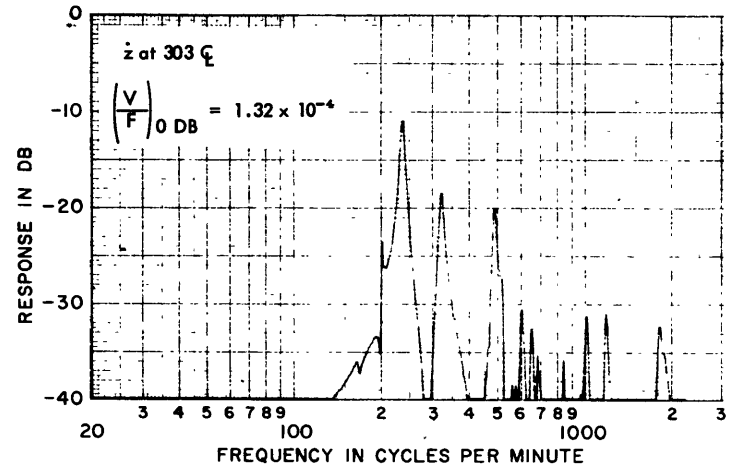


Figure 39

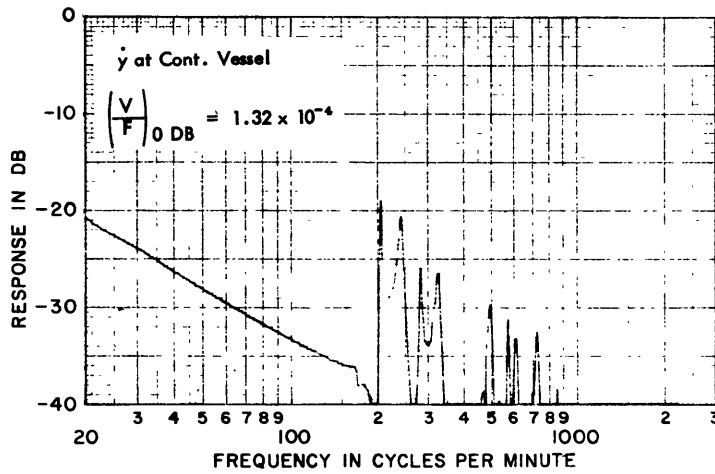


Figure 38

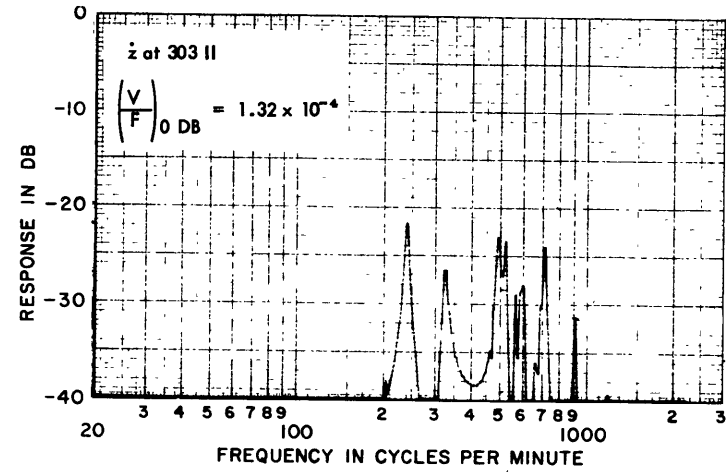


Figure 40

47

Excitation { Drive Point - Propeller
Type of Drive - Thrust

Configuration - 6×10^4 lb-sec/in Damper
Used for Thrust Coupler

Coordinate at which response was measured is shown on each figure. The value of the velocity/force at 0 DB (in/sec/lb) is shown by $\left(\frac{V}{F}\right)_{0 \text{ DB}} =$

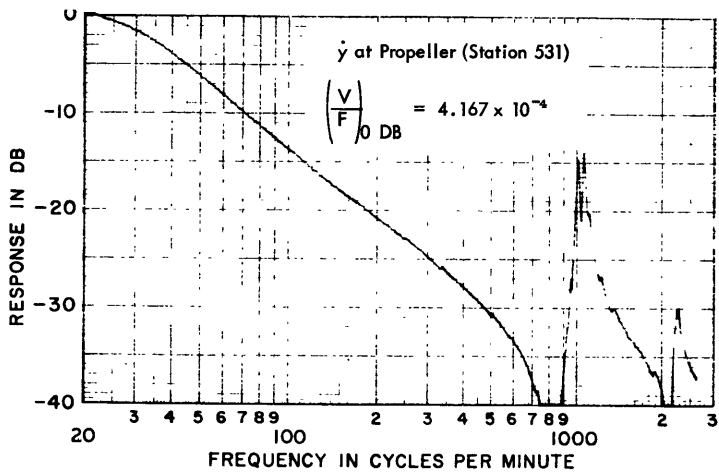


Figure 41

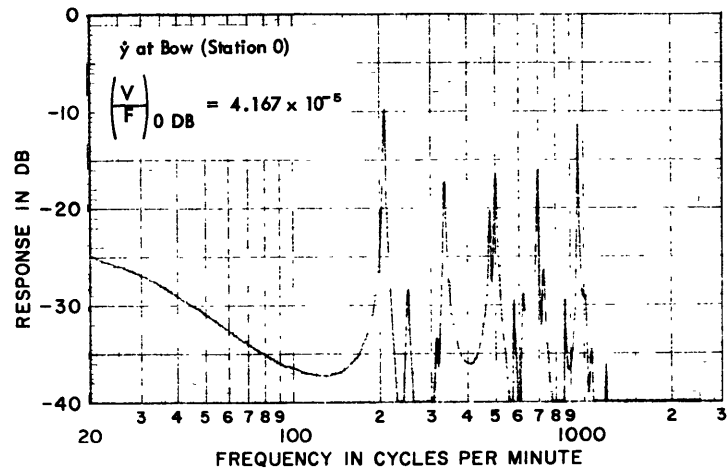


Figure 43

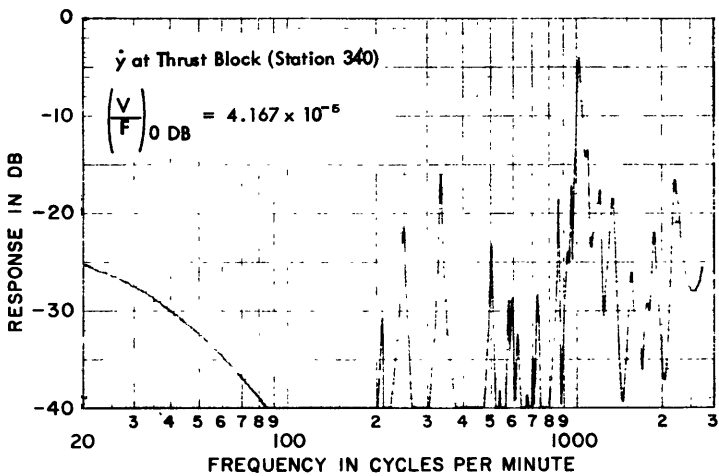


Figure 42

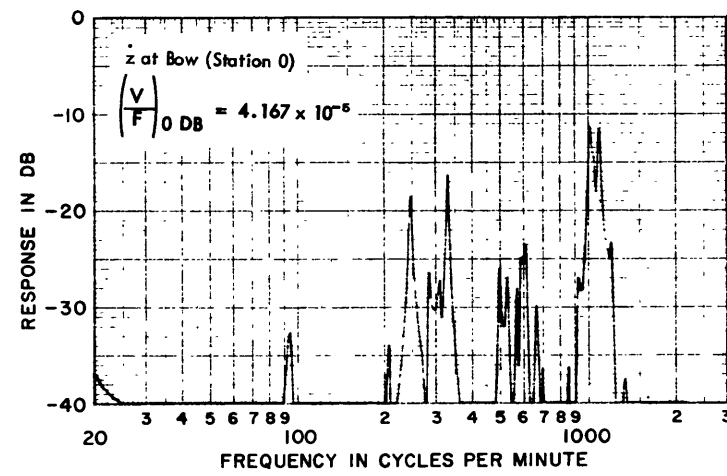


Figure 44

48

Excitation { Drive Point - Propeller
Type of Drive - Thrust

Configuration - 31-Ton Inertia Coupler

Coordinate at which response was measured is shown on each figure. The value of the velocity/force at 0 DB (in/sec/lb) is shown by $\left(\frac{V}{F}\right)_{0 \text{ DB}} =$

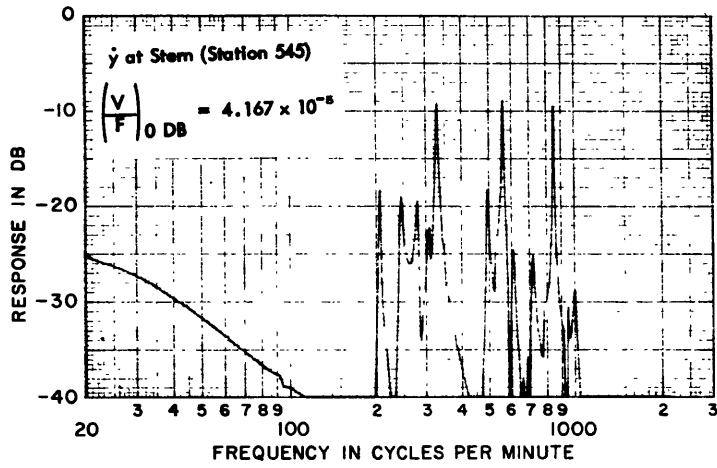


Figure 45

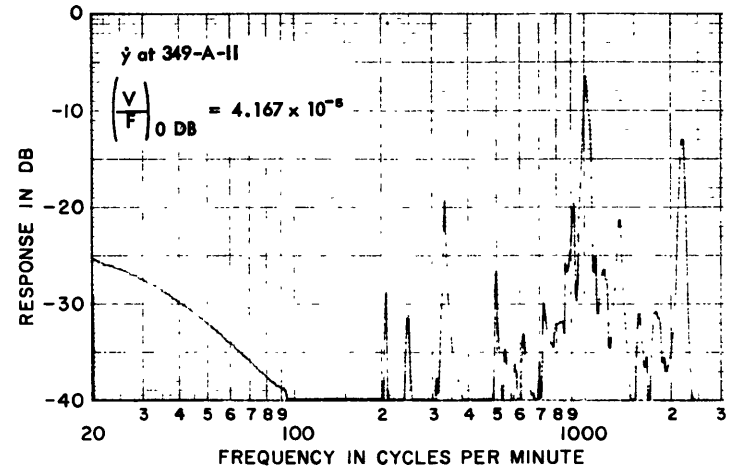


Figure 47

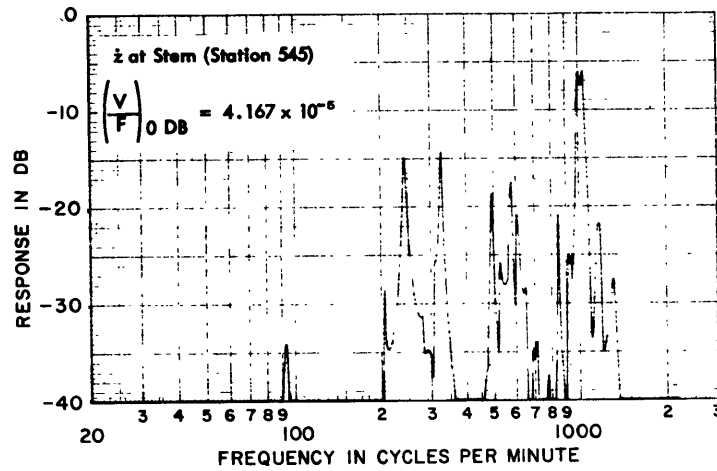


Figure 46

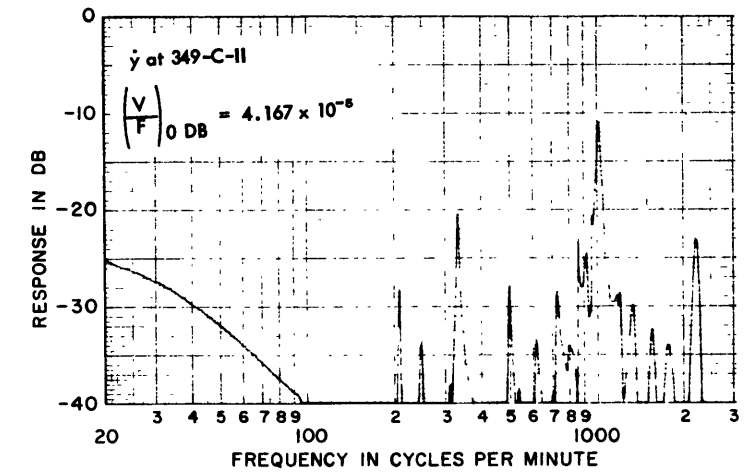


Figure 48

64

Excitation { Drive Point - Propeller
Type of Drive - Thrust

Configuration-31-Ton Inertia Coupler

Coordinate at which response was measured is shown on each figure. The value of the velocity/force at 0 DB (in/sec/lb) is shown by $\left(\frac{V}{F}\right)_{0\text{ DB}} =$

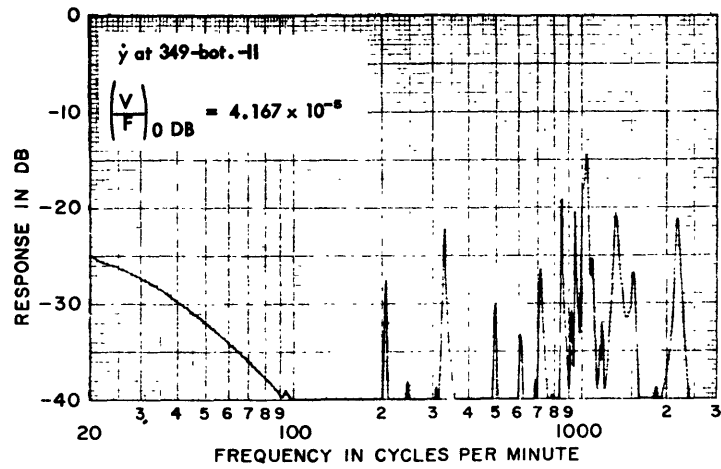


Figure 49

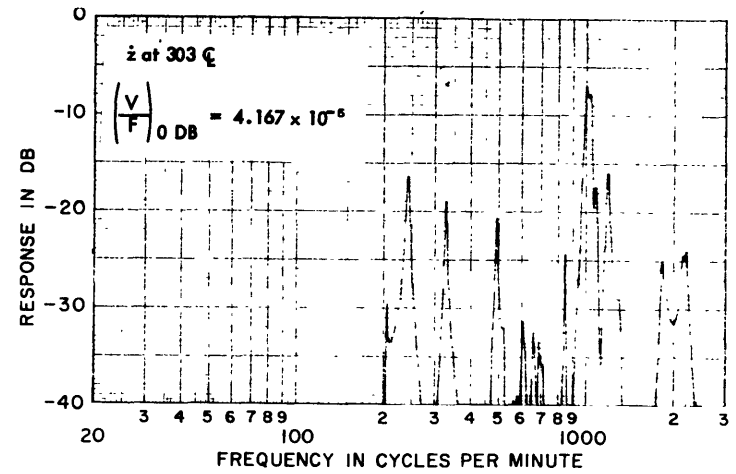


Figure 51

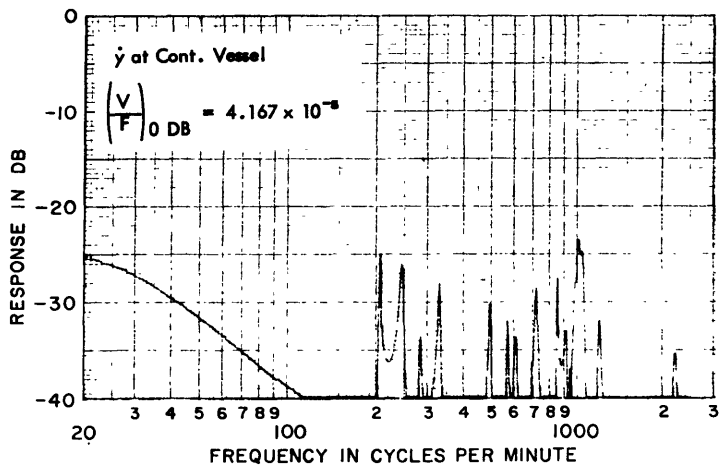


Figure 50

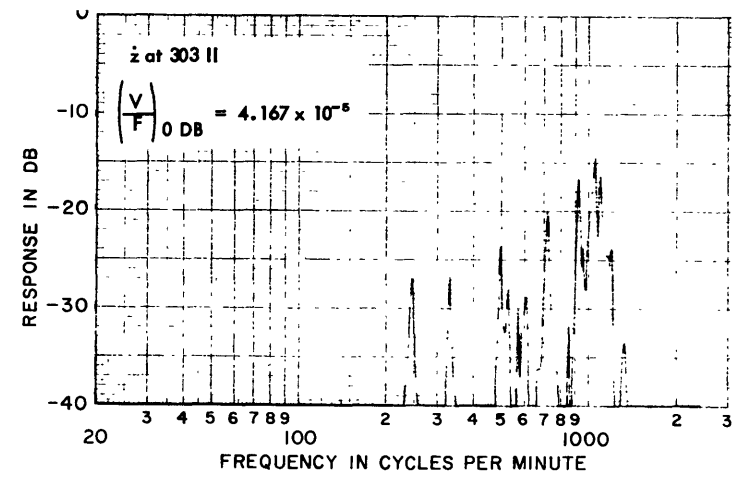


Figure 52

50

Excitation { Drive Point - Propeller
Type of Drive - Thrust

Configuration - 31-Ton Inertia Coupler

Coordinate at which response was measured is shown on each figure. The value of the velocity/force at 0 DB (in/sec/lb) is shown by $\left(\frac{V}{F}\right)_{0 \text{ DB}} =$

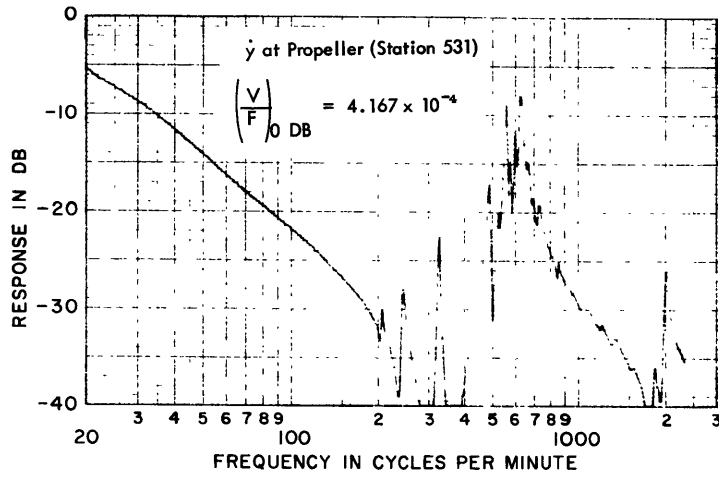


Figure 53

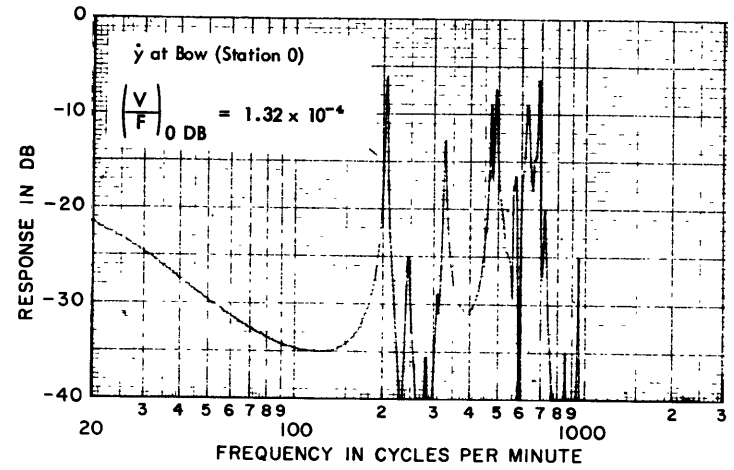


Figure 55

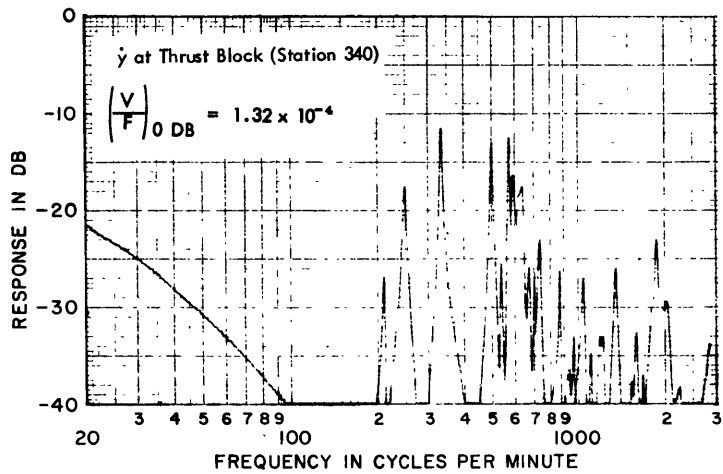


Figure 54

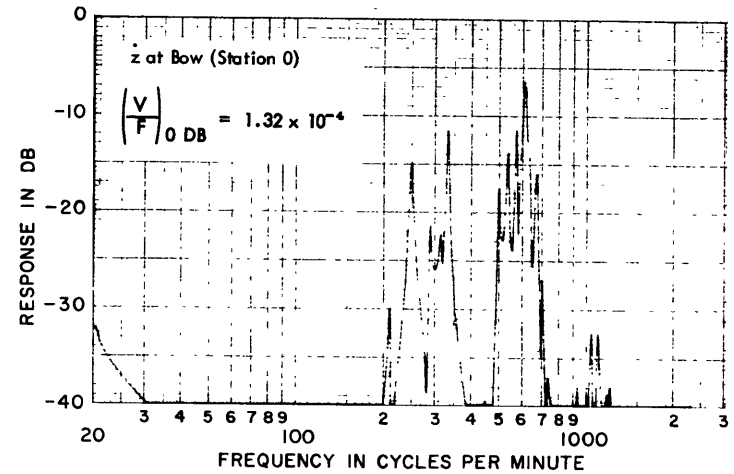


Figure 56

51

Excitation { Drive Point - Propeller
Type of Drive - Thrust

Configuration - 310-Ton Inertia Coupler

Coordinate at which response was measured is shown on each figure. The value of the velocity/force

at 0 DB (in/sec/lb) is shown by $\left(\frac{V}{F}\right)_{0 \text{ DB}} =$

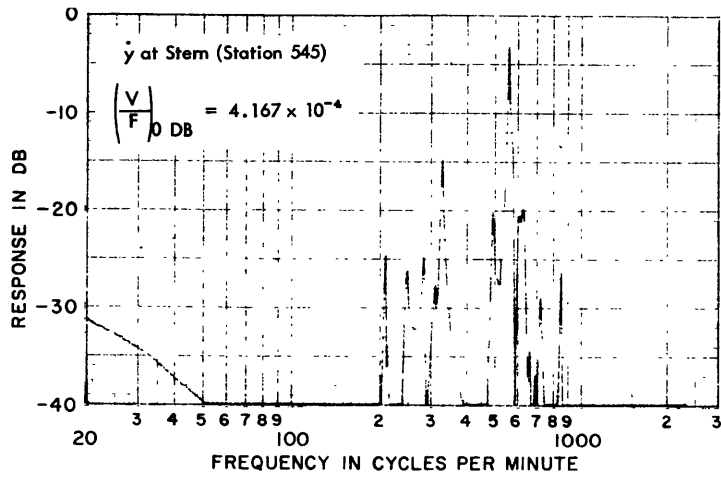


Figure 57

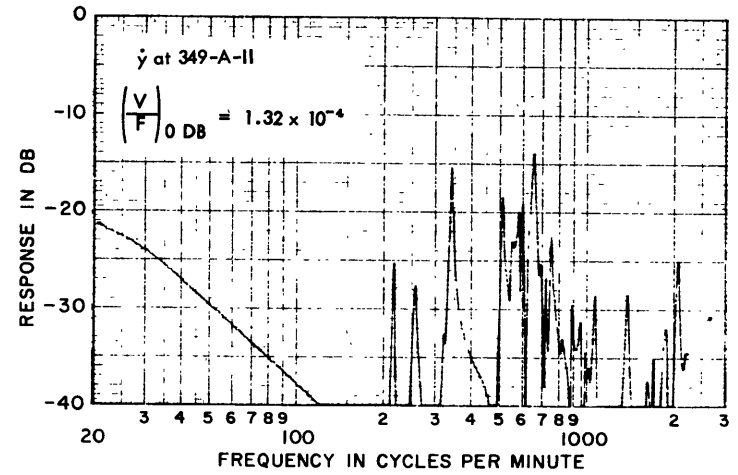


Figure 59

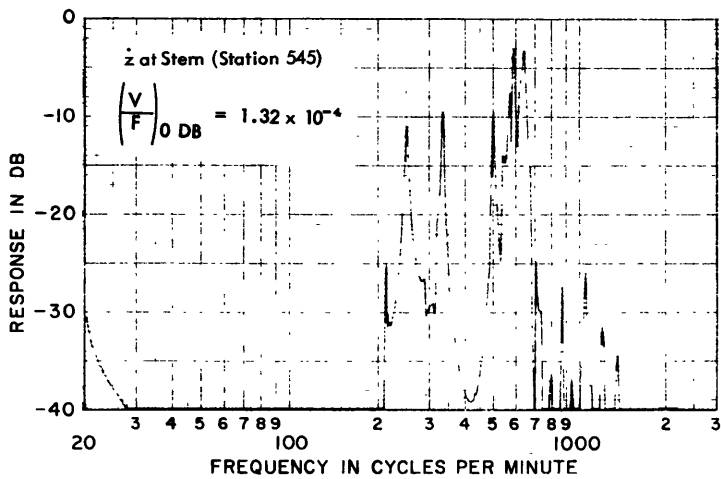


Figure 58

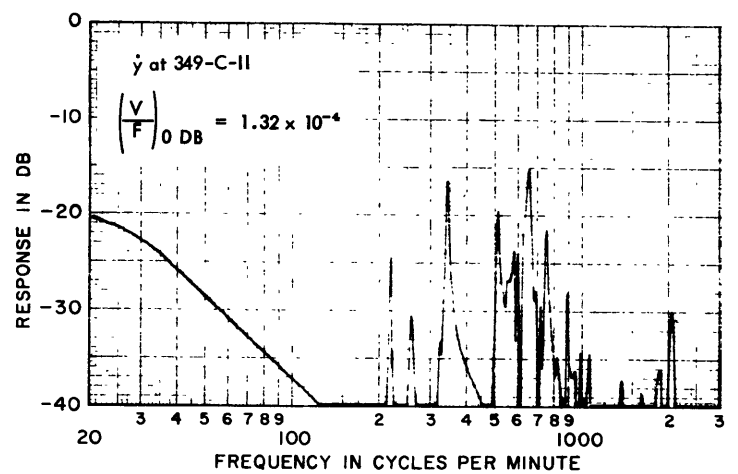


Figure 60

52

Excitation { Drive Point - Propeller
Type of Drive - Thrust

Configuration - 310-Ton Inertia Coupler

Coordinate at which response was measured is shown on each figure. The value of the velocity/force

at 0 DB (in/sec/lb) is shown by $\left(\frac{V}{F}\right)_{0\text{ DB}} =$

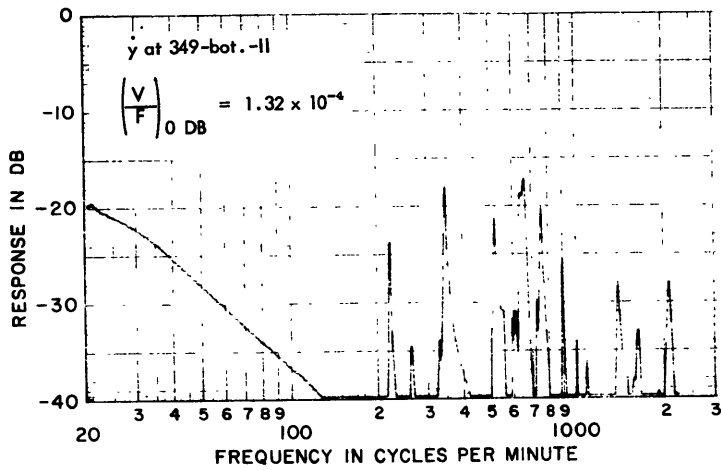


Figure 61

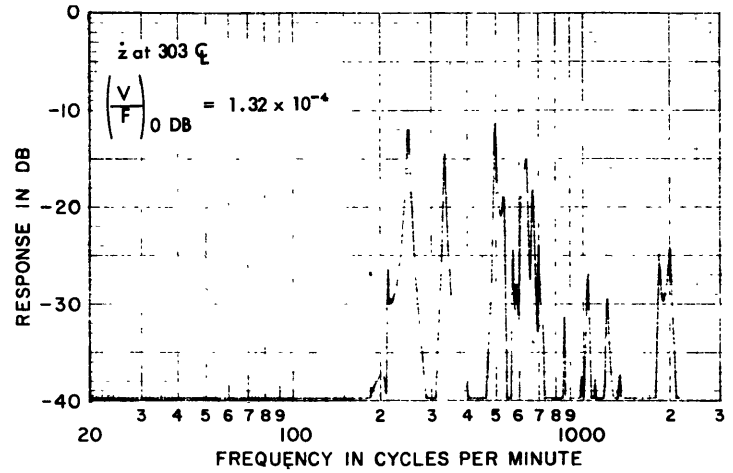


Figure 63

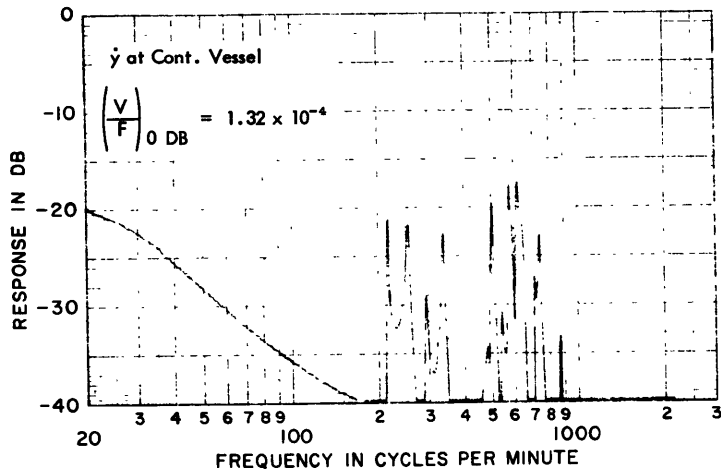


Figure 62

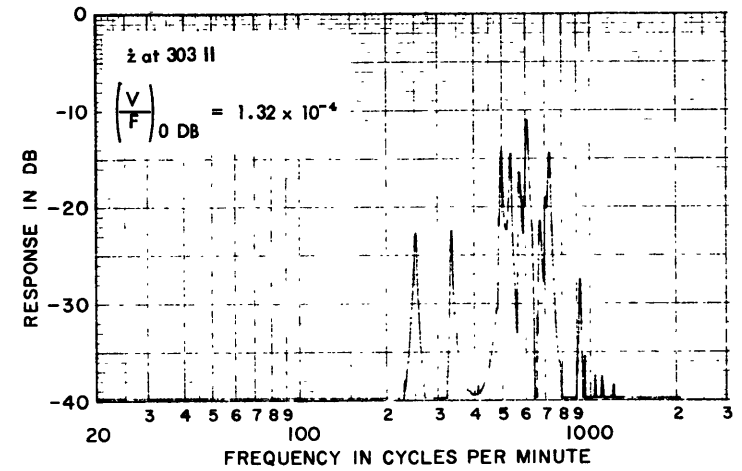


Figure 64

Excitation $\left\{ \begin{array}{l} \text{Drive Point - Propeller} \\ \text{Type of Drive - Thrust} \end{array} \right.$

Configuration- 310-Ton Inertia Coupler

Coordinate at which response was measured is shown on each figure. The value of the velocity/force at 0 DB (in/sec/lb) is shown by $\left(\frac{V}{F}\right)_{0 \text{ DB}} =$

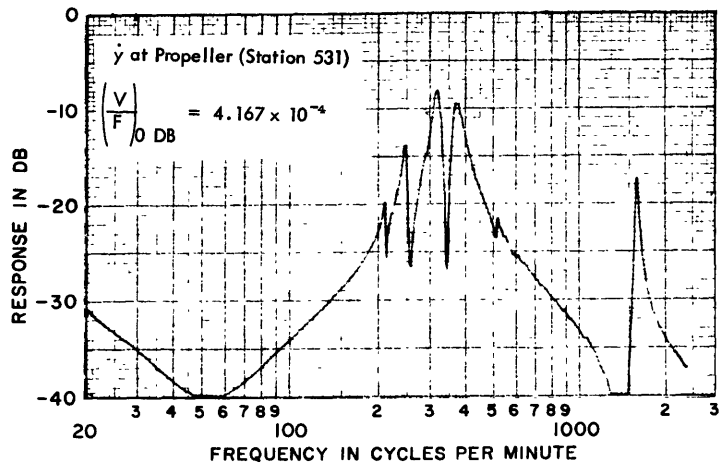


Figure 65

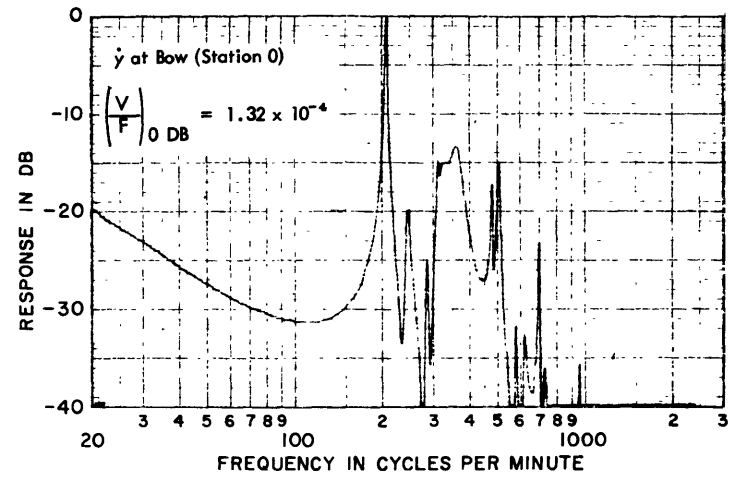


Figure 67

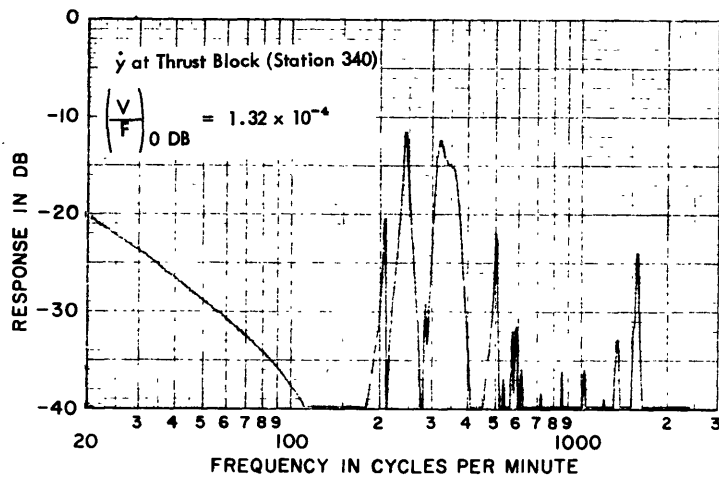


Figure 66

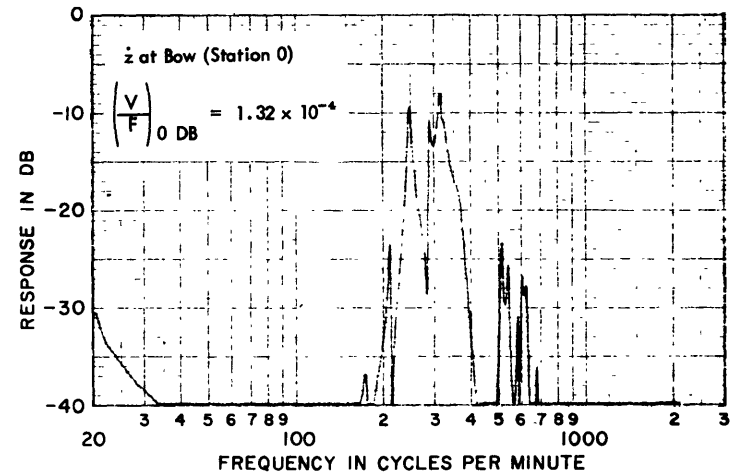


Figure 68

54

Excitation { Drive Point - Propeller
Type of Drive - Thrust

Configuration - Axial Flexibility of Shaft
between Stations 377 and
340 Increased by a Factor
of 7.76

Coordinate at which response was measured is shown on each figure. The value of the velocity/force at 0 DB (in/sec/lb) is shown by $\left(\frac{V}{F}\right)_{0 \text{ DB}} =$

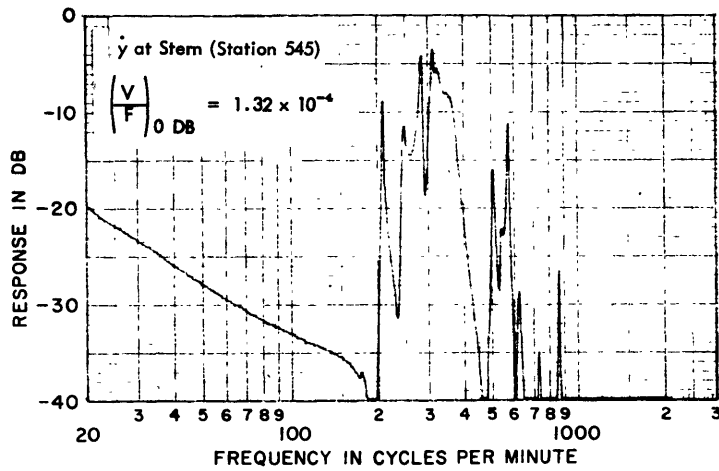


Figure 69

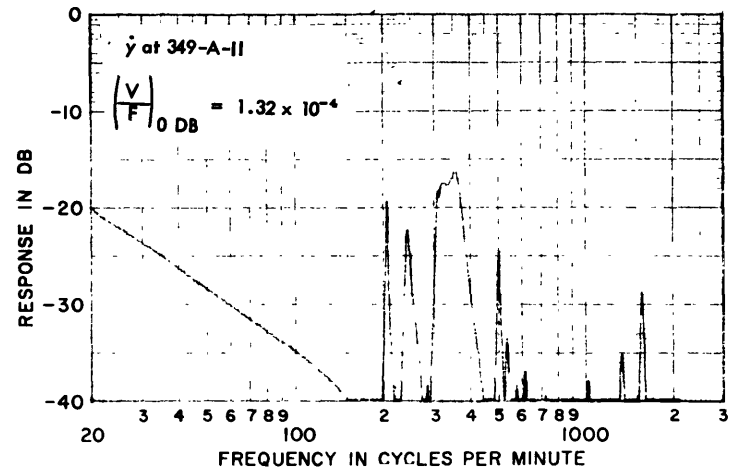


Figure 71

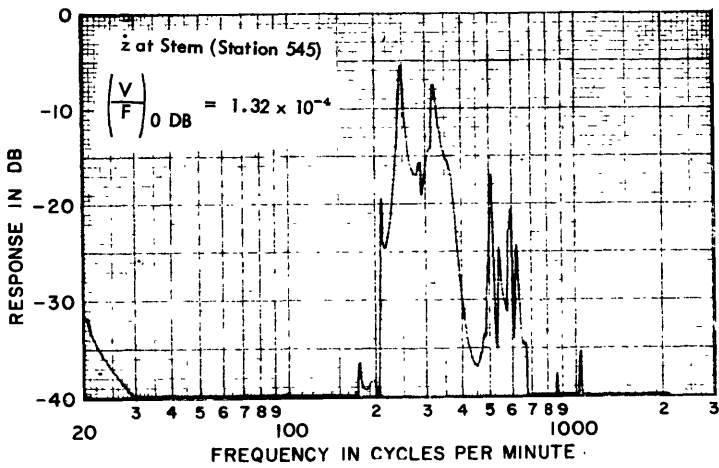


Figure 70

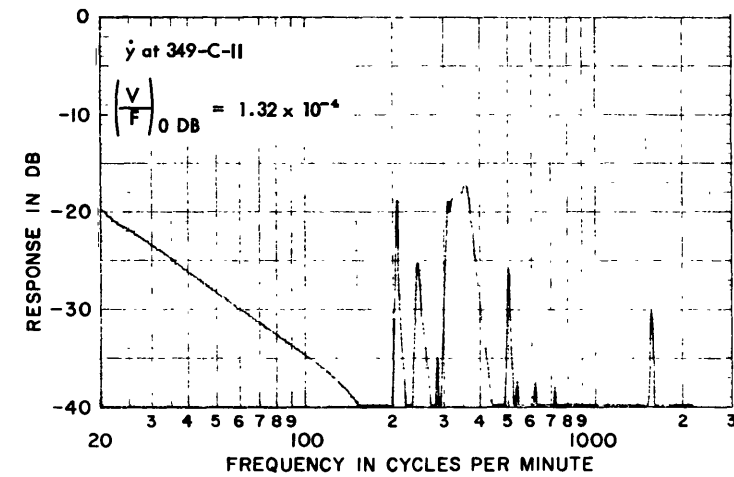


Figure 72

Excitation { Drive Point - Propeller
Type of Drive - Thrust

Axial Flexibility of Shaft
between Stations 377 and
340 Increased by a Factor
of 7.76

Coordinate at which response was measured is shown on each figure. The value of the velocity/force

at 0 DB (in/sec/lb) is shown by $\left(\frac{V}{F}\right)_{0\text{ DB}} =$

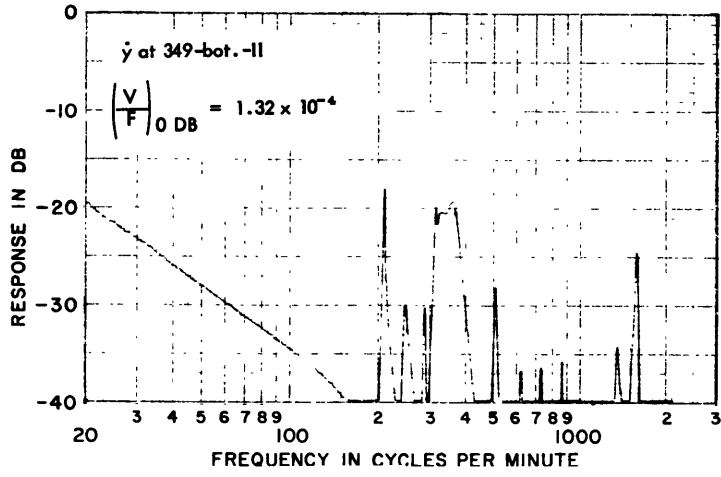


Figure 73

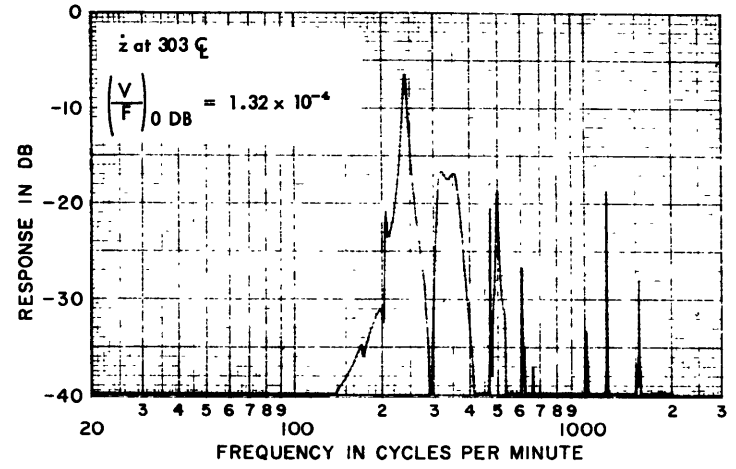


Figure 75

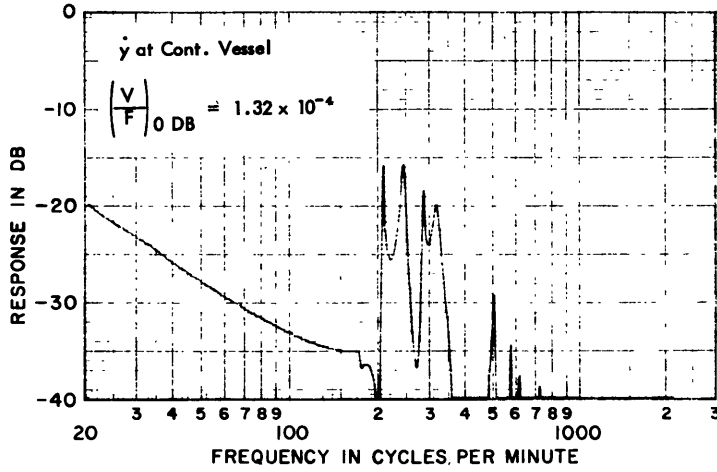


Figure 74

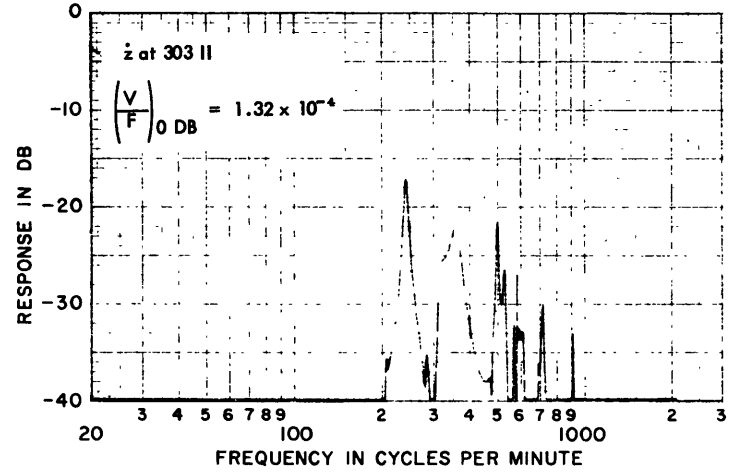


Figure 76

Excitation { Drive Point - Propeller
 Type of Drive - Thrust

Configuration - Axial Flexibility of Shaft between Stations 377 and 340 Increased by a Factor of 7.76

Coordinate at which response was measured is shown on each figure. The value of the velocity/force at 0 DB (in/sec/lb) is shown by $\left(\frac{V}{F}\right)_{0\text{ DB}} =$

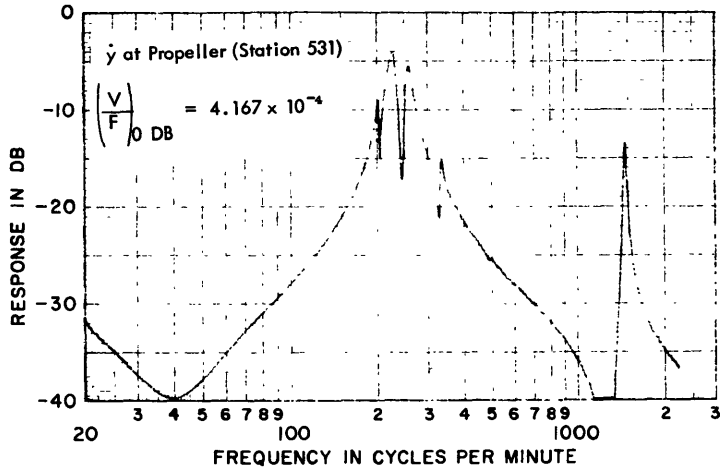


Figure 77

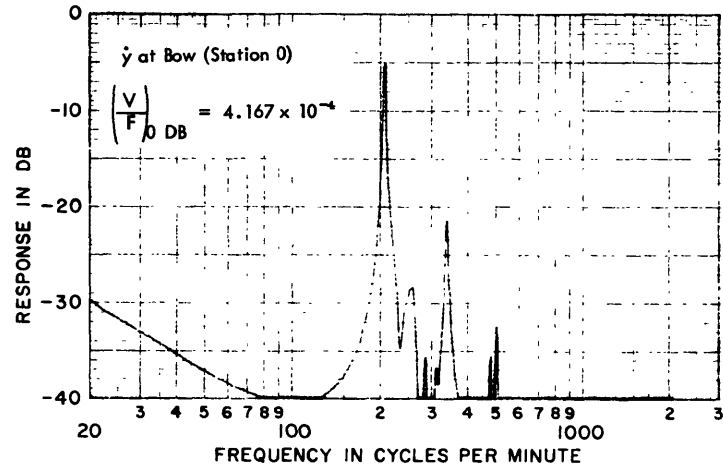


Figure 79

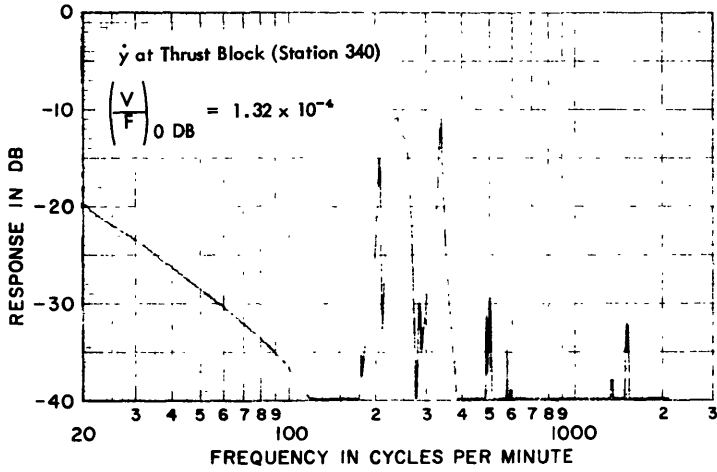


Figure 78

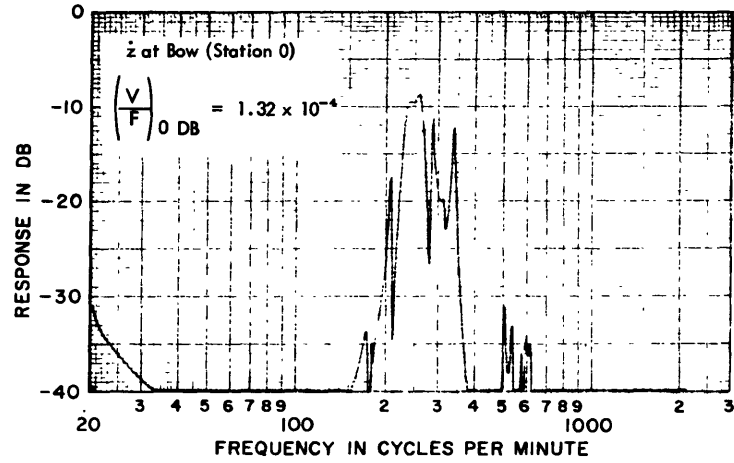


Figure 80

Excitation { Drive Point - Propeller
 Type of Drive - Thrust

Configuration - Axial Flexibility of Shaft
 between Stations 377 and
 340 Increased by a Factor
 of 17.47

Coordinate at which response was measured is shown on each figure. The value of the velocity/force at 0 DB (in/sec/lb) is shown by $\left(\frac{V}{F}\right)_{0 \text{ DB}} =$

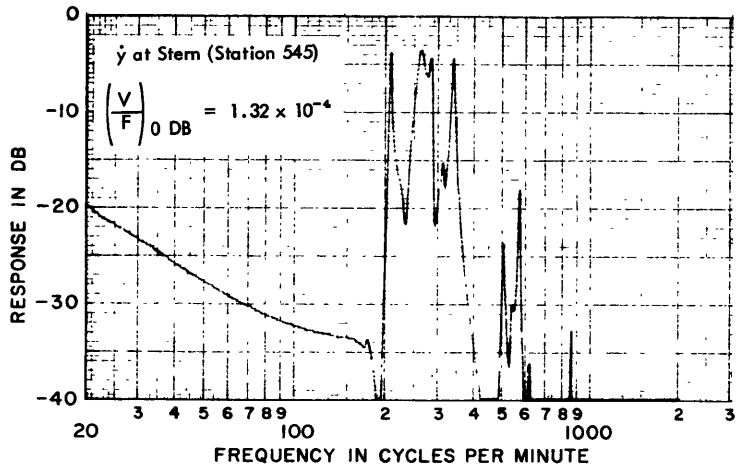


Figure 81

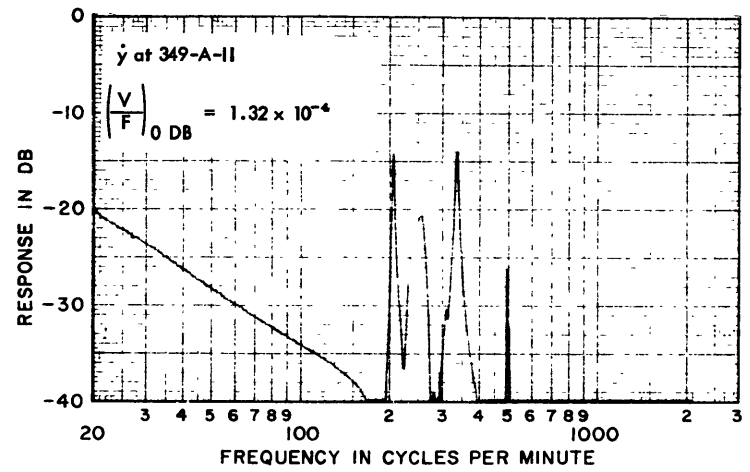


Figure 83

88

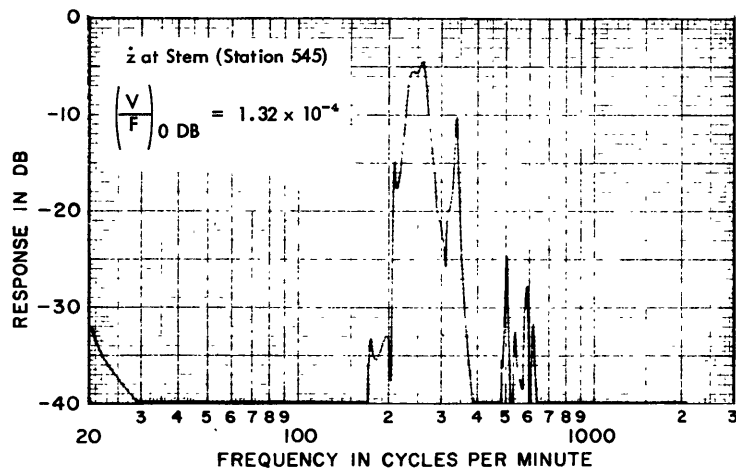


Figure 82

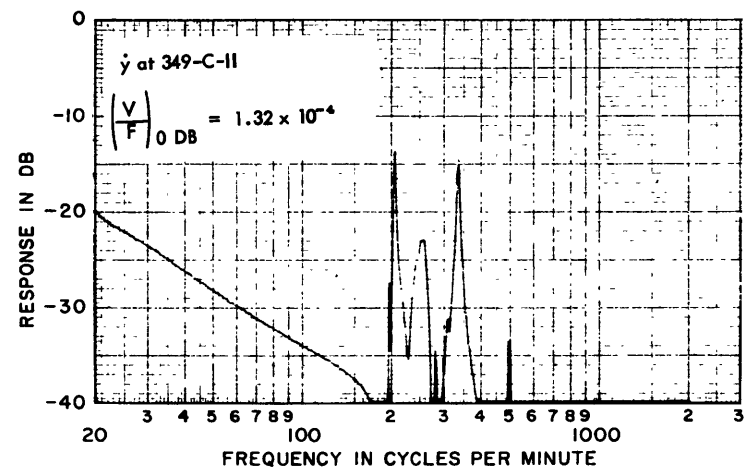


Figure 84

Excitation { Drive Point - Propeller
Type of Drive - Thrust

Configuration - Basic
Axial Flexibility of Shaft
between Stations 377 and
340 Increased by a Factor
of 17.47

Coordinate at which response was measured is shown on each figure. The value of the velocity/force at 0 DB (in/sec/lb) is shown by $\left(\frac{V}{F}\right)_{0\text{ DB}} =$

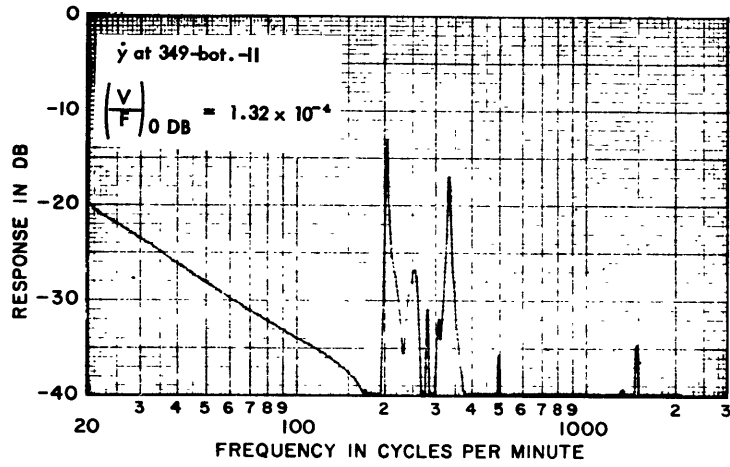


Figure 85

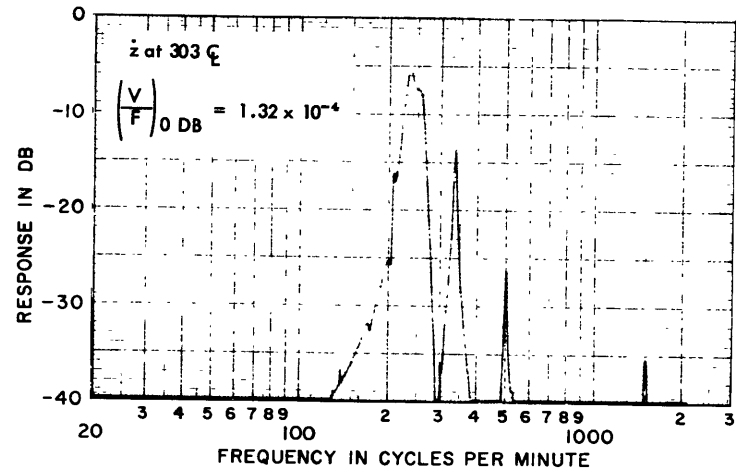


Figure 87

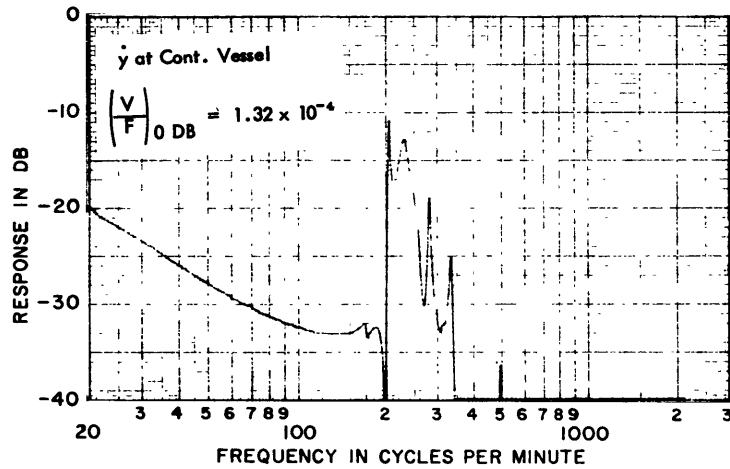


Figure 86

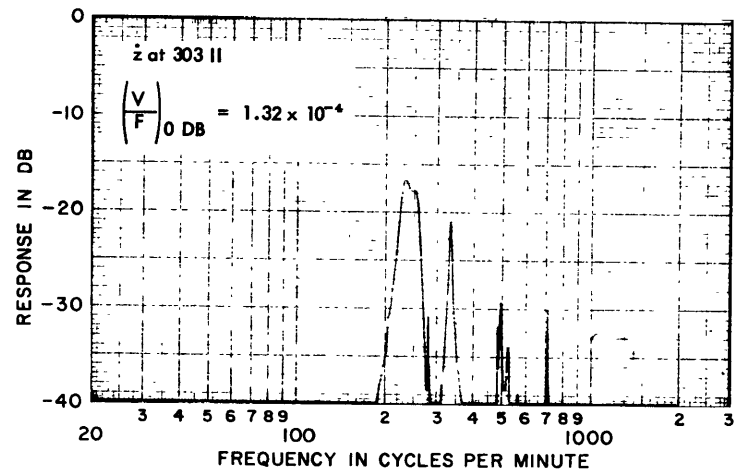


Figure 88

59

Excitation { Drive Point - Propeller
Type of Drive - Thrust

Axial Flexibility of Shaft
between Stations 377 and
Configuration - 340 Increased by a Factor
of 17.47

Coordinate at which response was measured is shown on each figure. The value of the velocity/force at 0 DB (in/sec/lb) is shown by $\left(\frac{V}{F}\right)_{0 \text{ DB}} =$

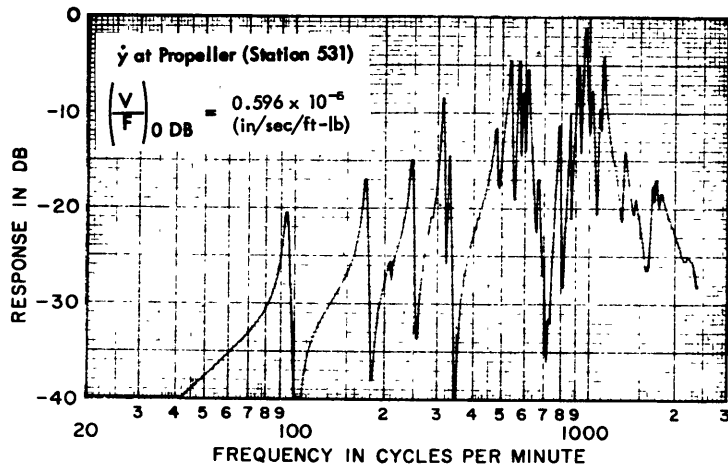


Figure 89

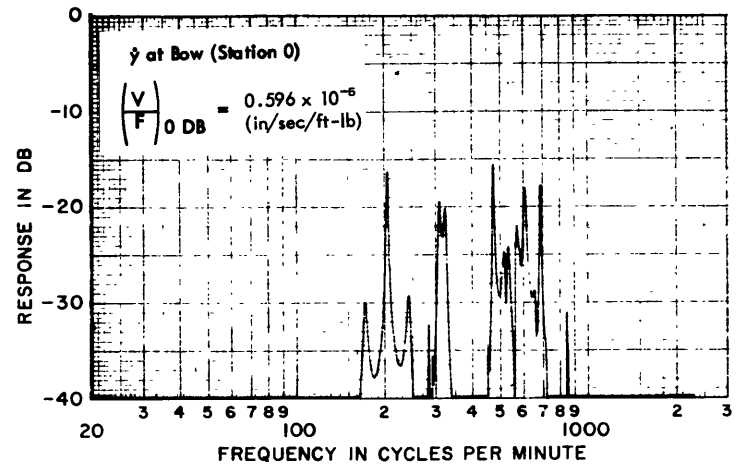


Figure 91

09

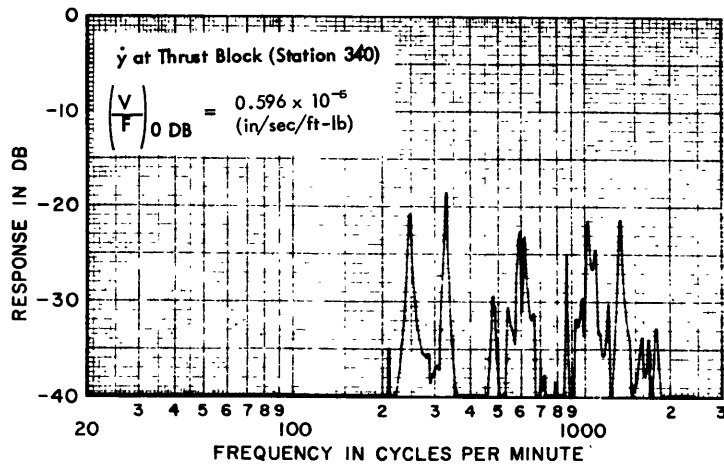


Figure 90

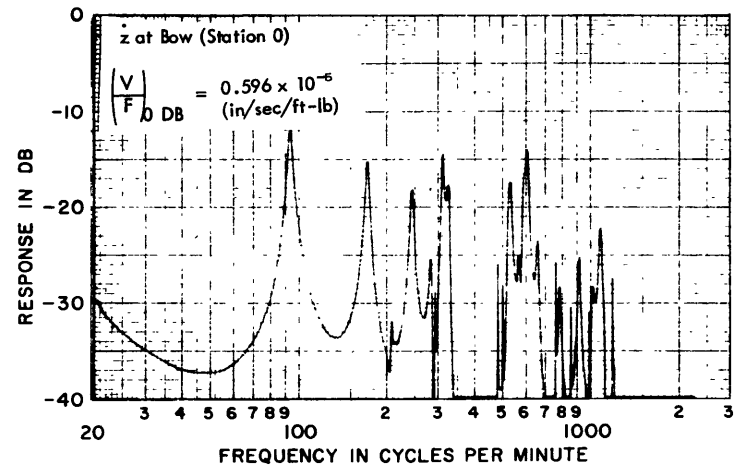


Figure 92

Excitation { Drive Point - Stem
 (Sta. 545)
 Type of Drive - Moment in Plane of Sym. Configuration-Basic

Coordinate at which response was measured is shown on each figure. The value of the velocity/force at 0 DB (in/sec/lb) is shown by $\left(\frac{V}{F}\right)_{0 \text{ DB}} =$

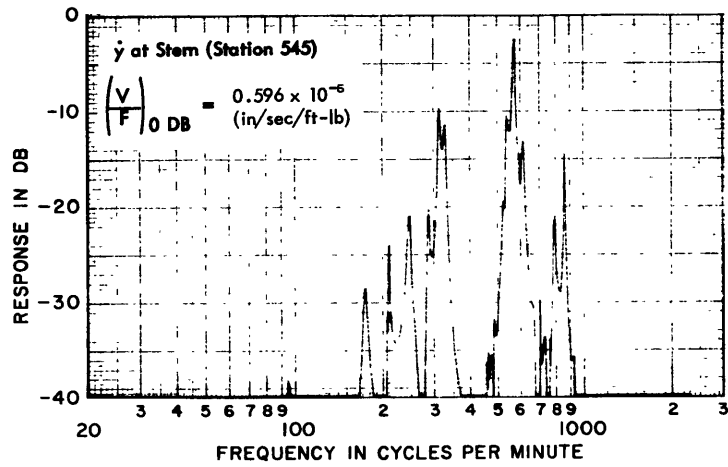


Figure 93

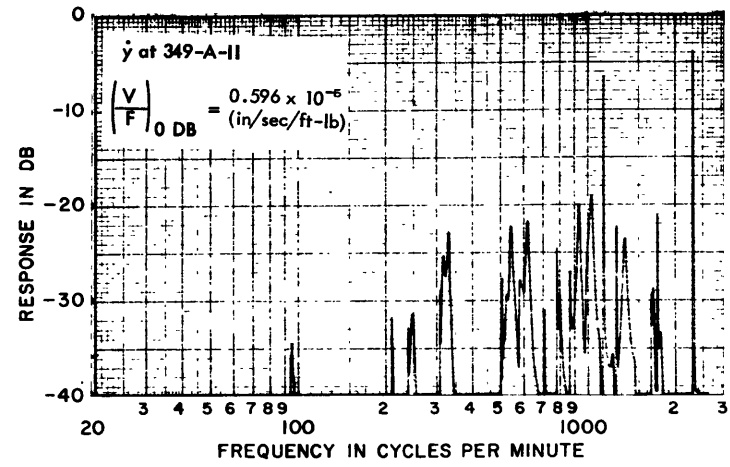


Figure 95

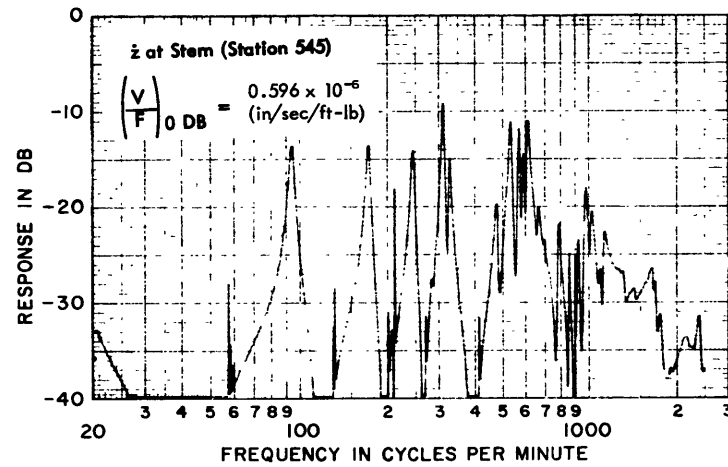


Figure 94

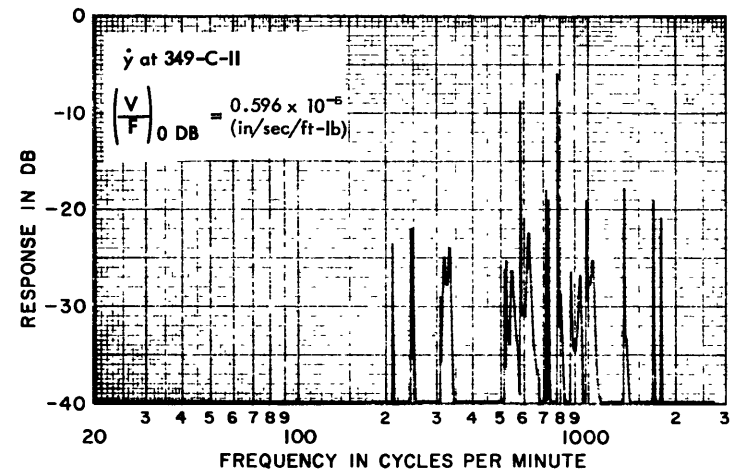


Figure 96

61

Excitation { Drive Point - Stem (Sta. 545)
 Moment in Configuration-Basic
 Type of Drive - Plane of Sym.

Coordinate at which response was measured is shown on each figure. The value of the velocity/force

at 0 DB (in/sec/lb) is shown by $\left(\frac{V}{F}\right)_{0\text{ DB}} =$

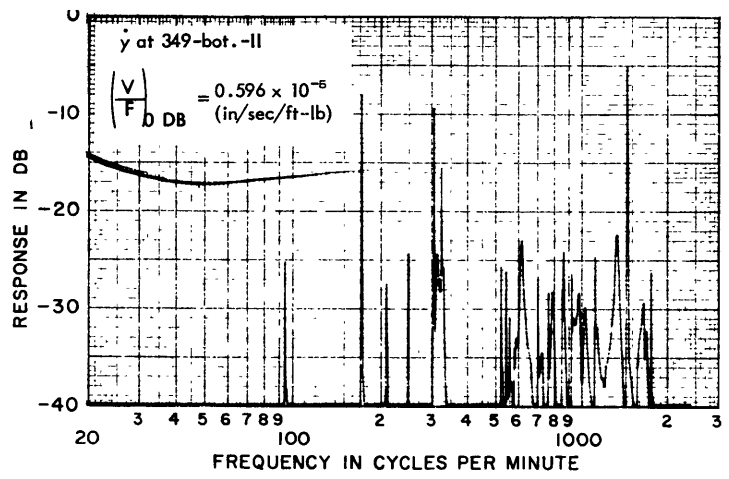


Figure 97

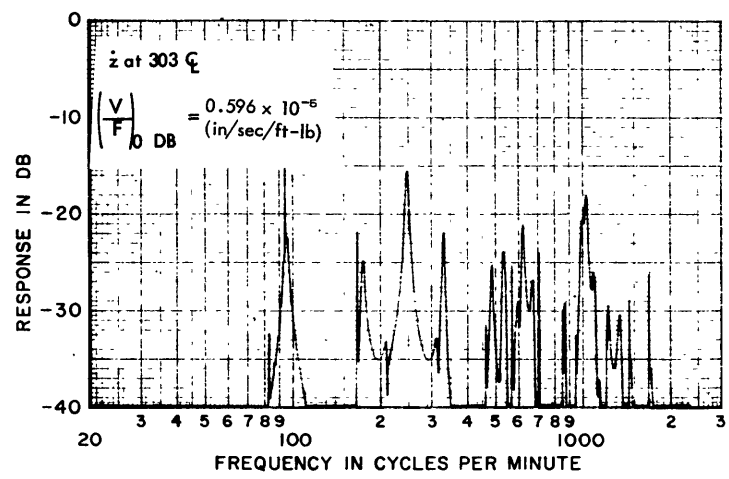


Figure 99

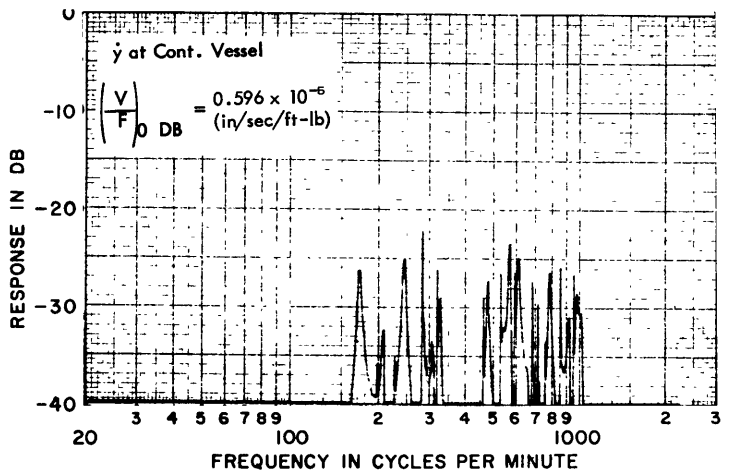


Figure 98

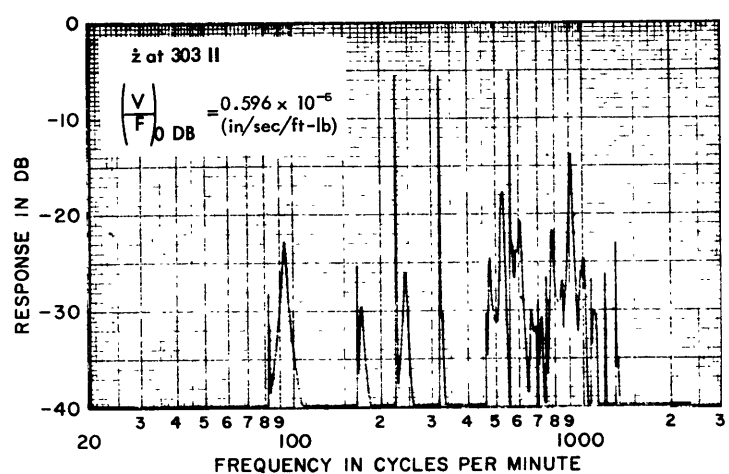


Figure 100

Excitation { Drive Point - Stem (Sta. 545)
 Type of Drive - Moment in Plane of Sym. Configuration-Basic

Coordinate at which response was measured is shown on each figure. The value of the velocity/force at 0 DB (in/sec/lb) is shown by $\left(\frac{V}{F}\right)_{0 \text{ DB}} =$

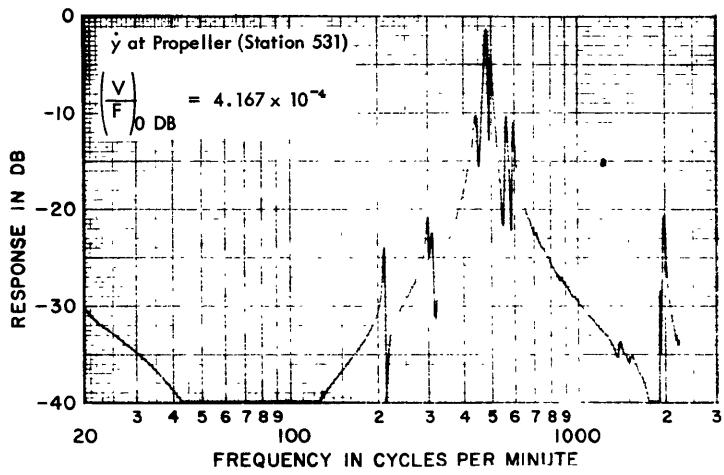


Figure 101

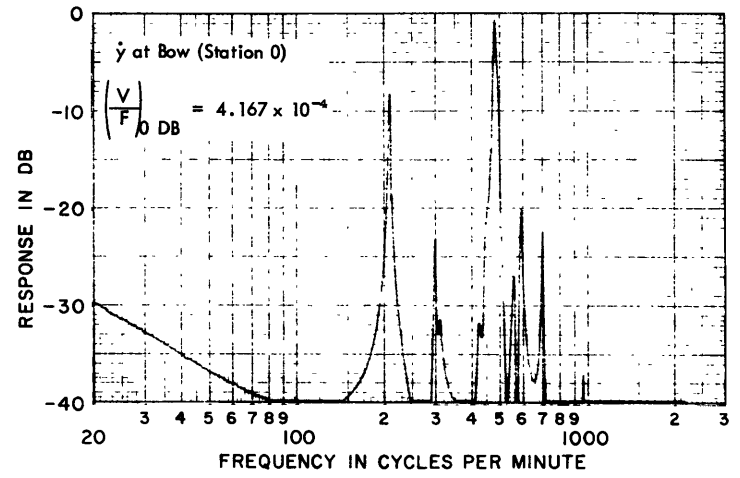


Figure 103

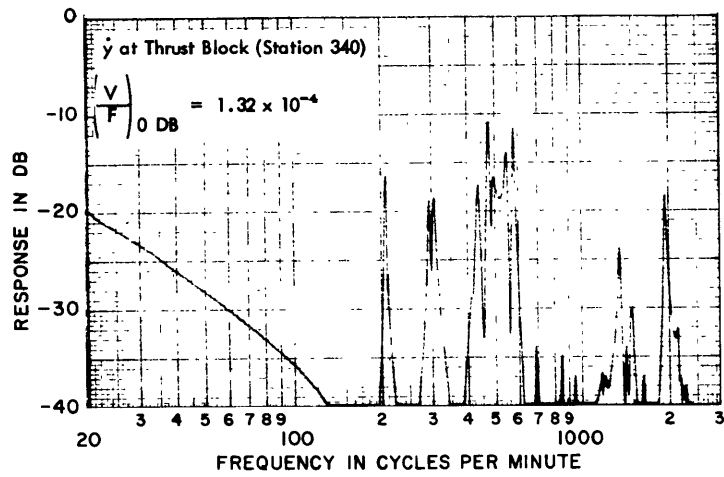


Figure 102

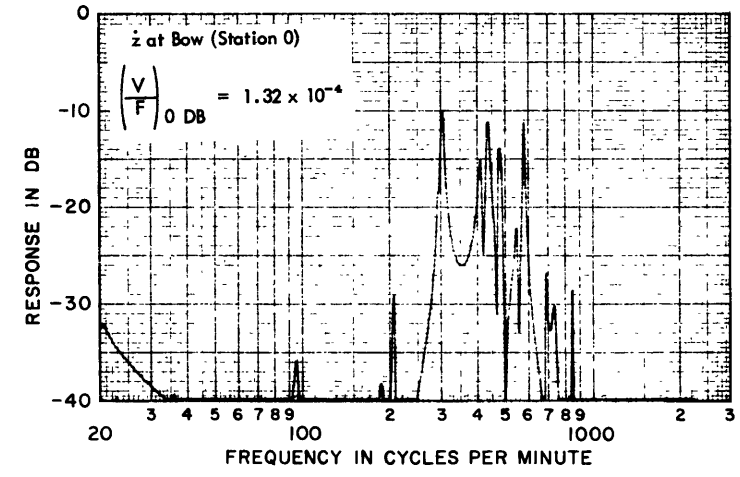


Figure 104

69

Excitation { Drive Point - Propeller
Type of Drive - Thrust

Configuration - Bulkheads Made Rigid

Coordinate at which response was measured is shown on each figure. The value of the velocity/force at 0 DB (in/sec/lb) is shown by $\left(\frac{V}{F}\right)_{0 \text{ DB}} =$

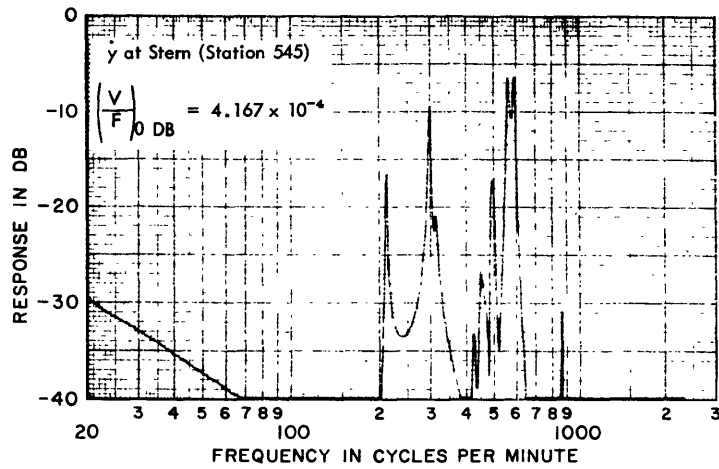


Figure 105

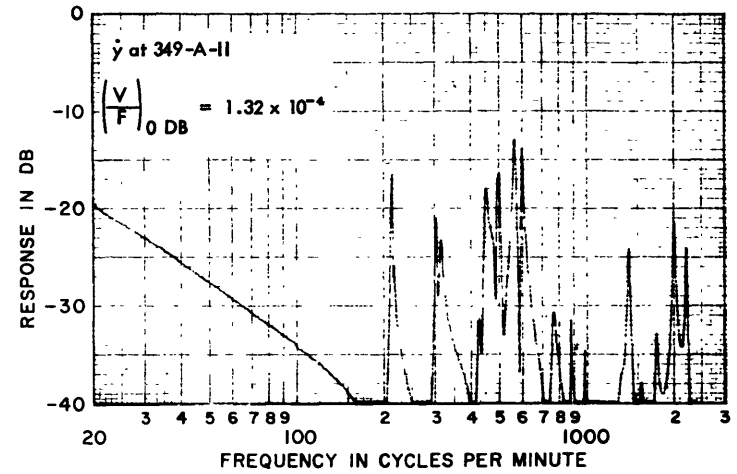


Figure 107

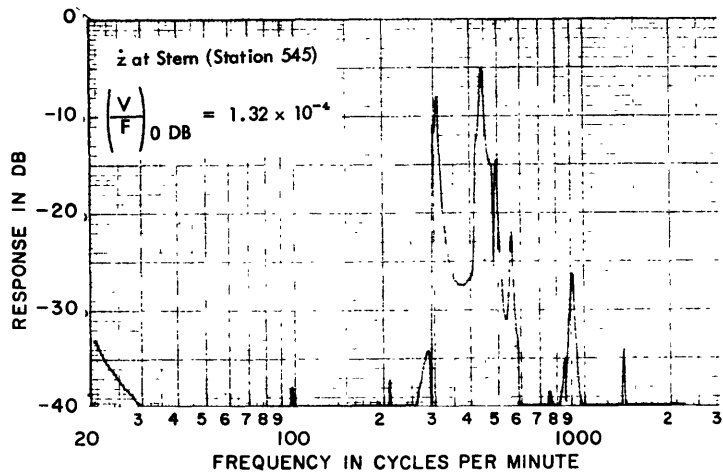


Figure 106

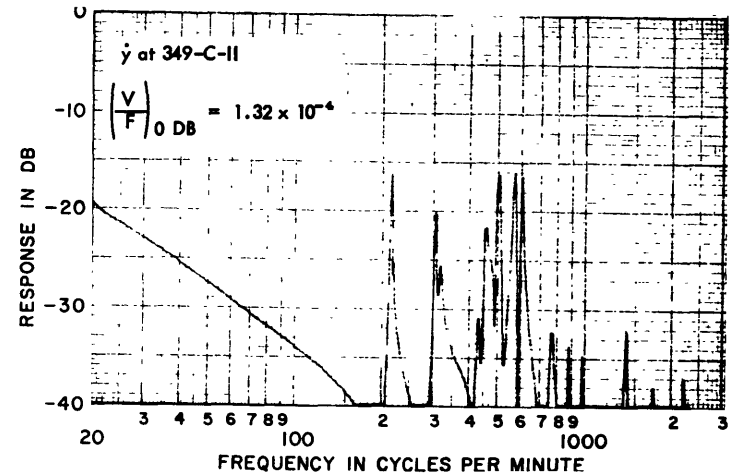


Figure 108

64

Excitation { Drive Point - Propeller
Type of Drive - Thrust

Configuration - Bulkheads Made Rigid

Coordinate at which response was measured is shown on each figure. The value of the velocity/force at 0 DB (in/sec/lb) is shown by $\left(\frac{V}{F}\right)_{0 \text{ DB}} =$

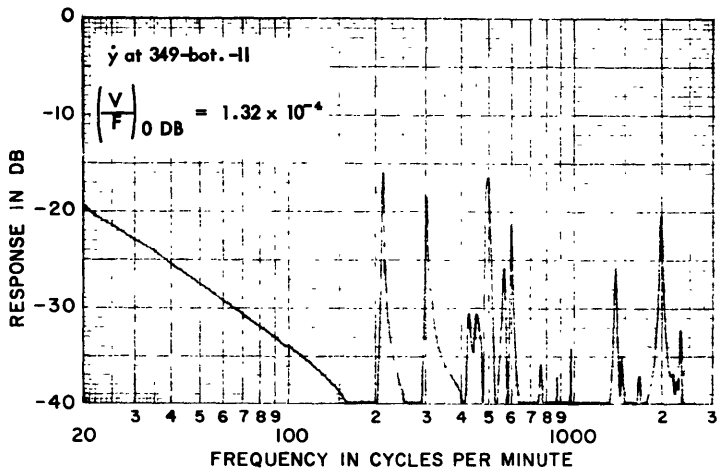


Figure 109

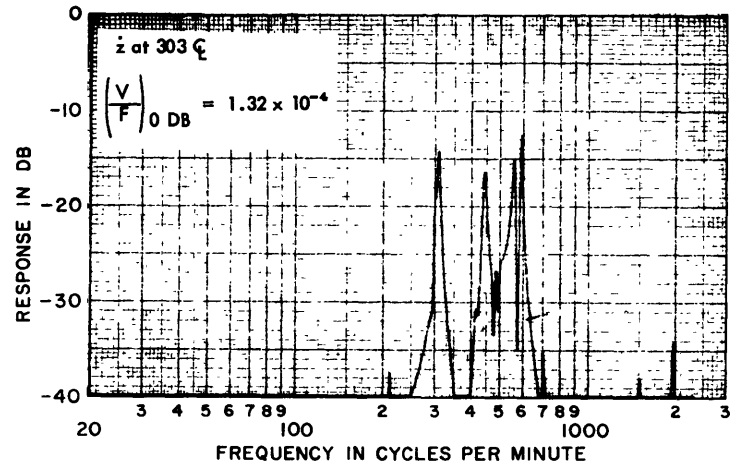


Figure 111

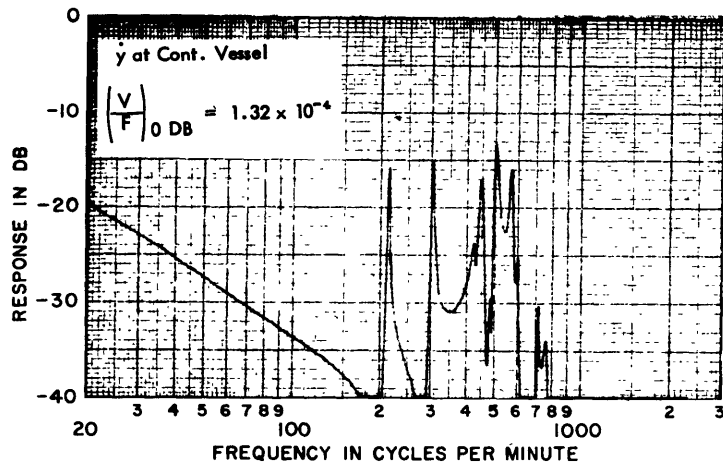


Figure 110

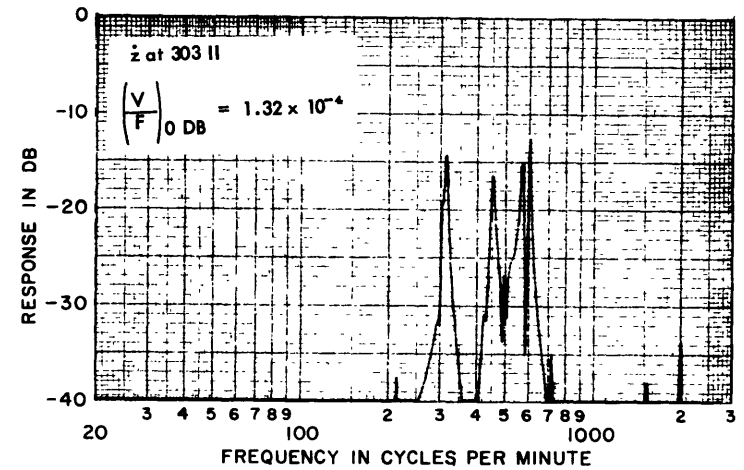


Figure 112

65

Excitation { Drive Point - Propeller
Type of Drive - Thrust

Configuration - Bulkheads Made Rigid

Coordinate at which response was measured is shown on each figure. The value of the velocity/force

at 0 DB (in/sec/lb) is shown by $\left(\frac{V}{F}\right)_{0\text{ DB}} =$

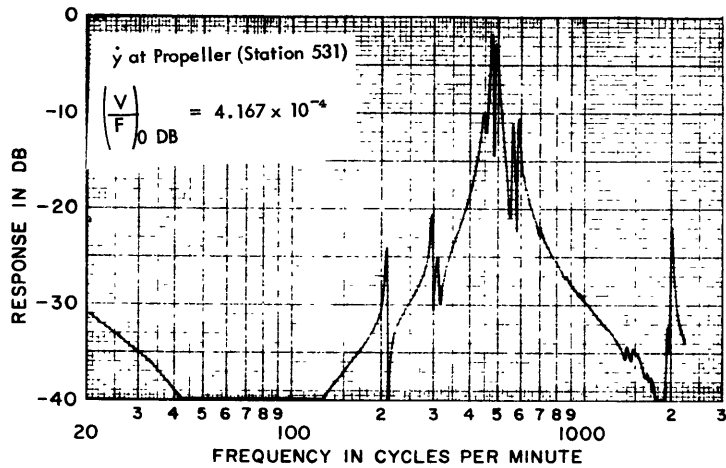


Figure 113

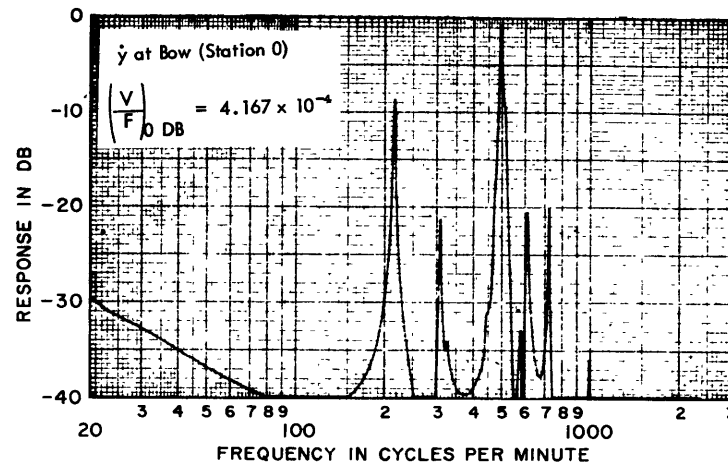


Figure 115

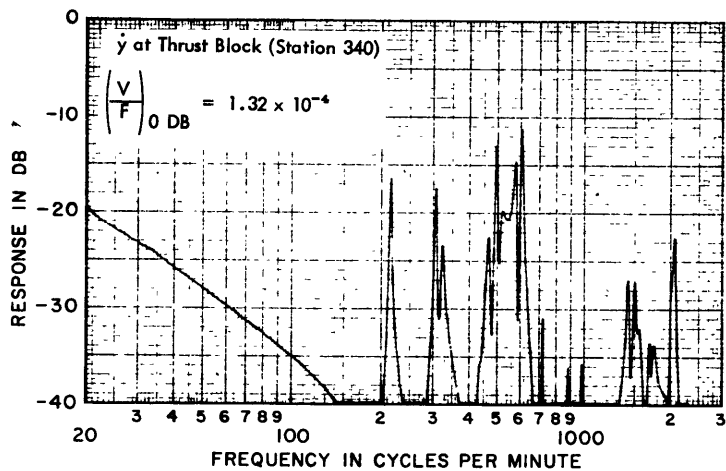


Figure 114

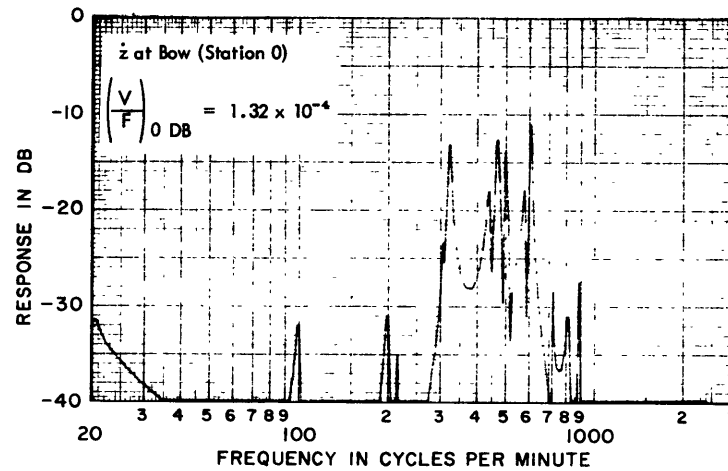


Figure 116

99

Excitation { Drive Point - Propeller
Type of Drive - Thrust

Configuration - Bulkheads and Decks Rigid

Coordinate at which response was measured is shown on each figure. The value of the velocity/force at 0 DB (in/sec/lb) is shown by $\left(\frac{V}{F}\right)_{0 \text{ DB}} =$

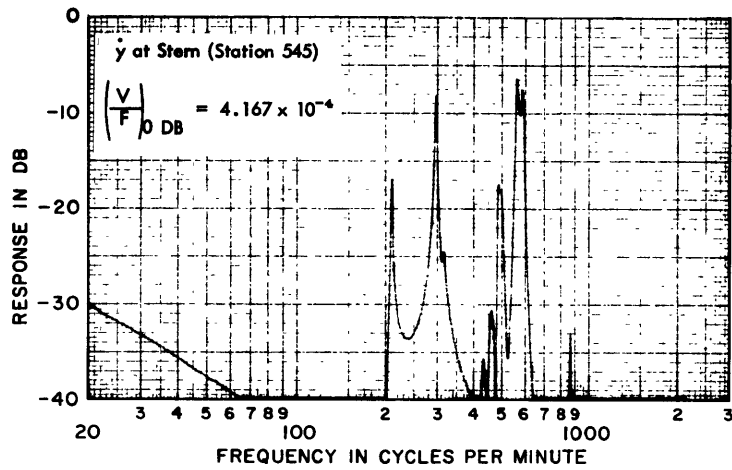


Figure 117

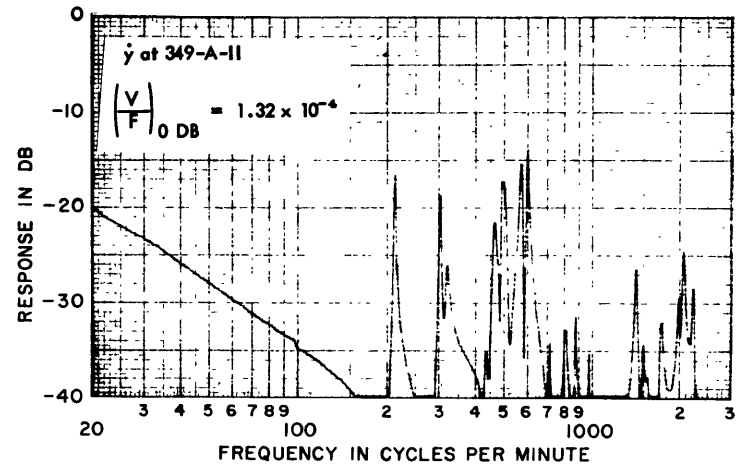


Figure 119

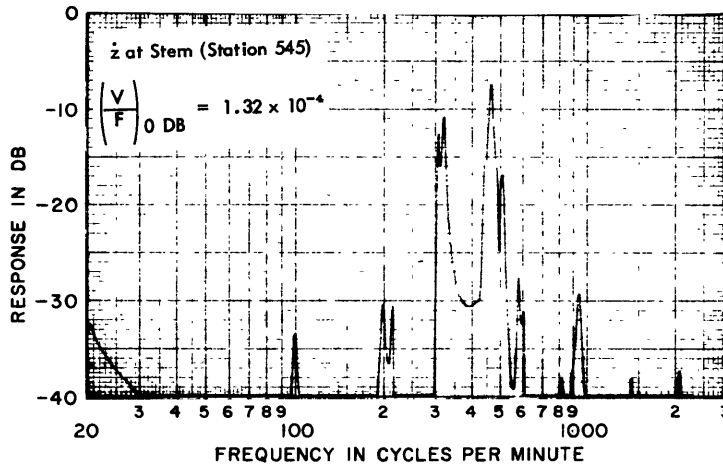


Figure 118

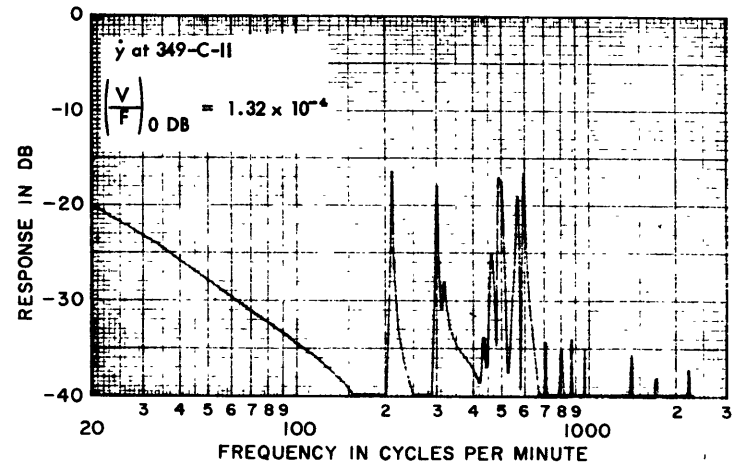


Figure 120

Excitation { Drive Point - Propeller
Type of Drive - Thrust

Configuration - Bulkheads and Decks Rigid

Coordinate at which response was measured is shown on each figure. The value of the velocity/force

at 0 DB (in/sec/lb) is shown by $\left(\frac{V}{F}\right)_{0 \text{ DB}} =$

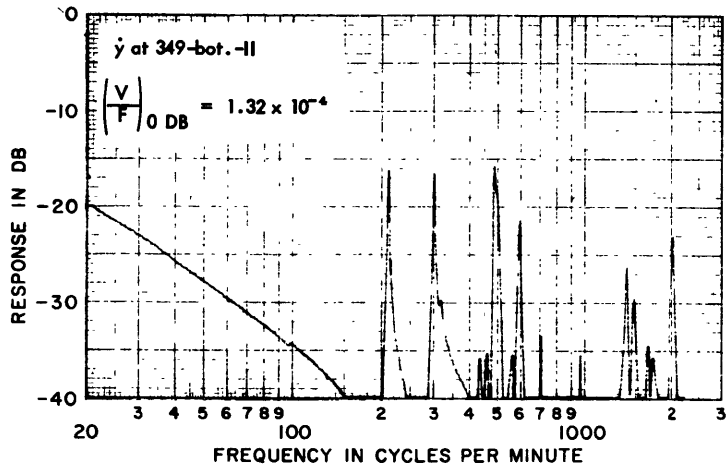


Figure 121

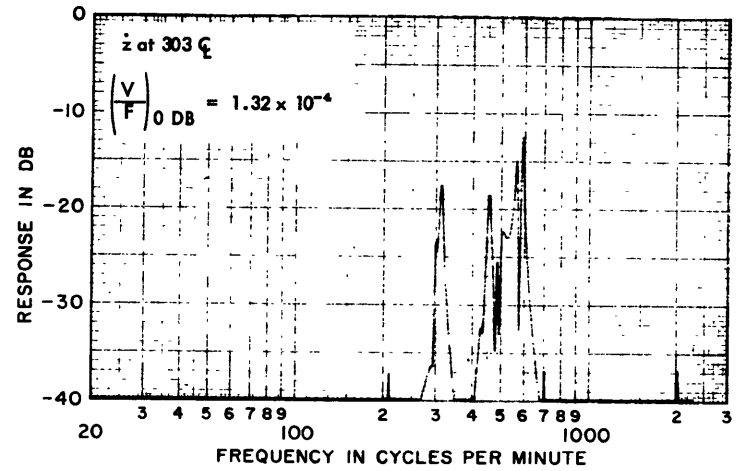


Figure 123

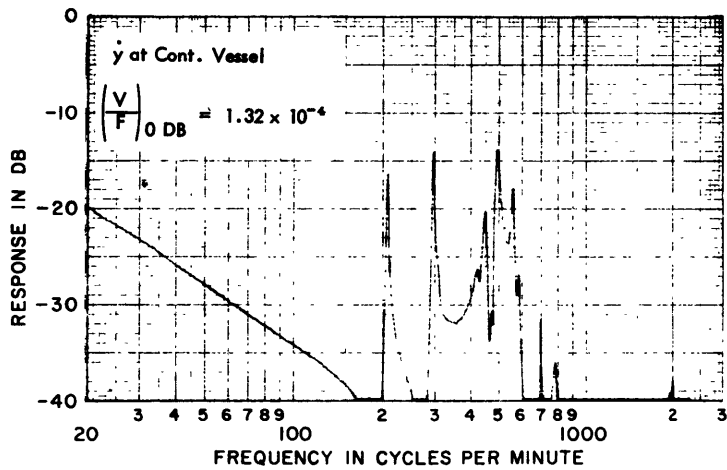


Figure 122

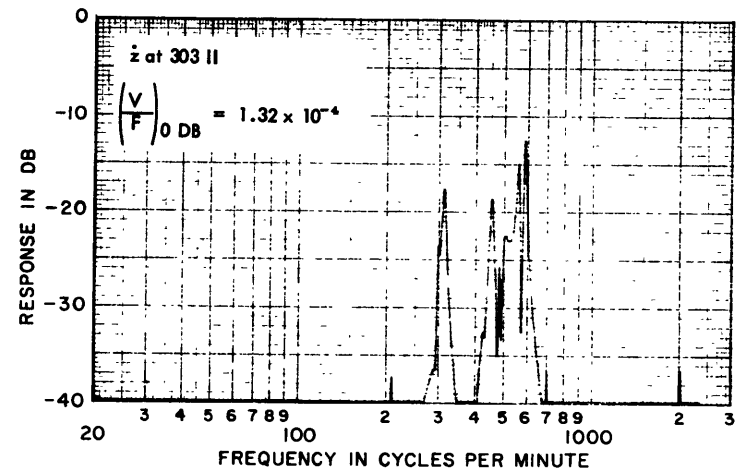


Figure 124

89

Excitation { Drive Point - Propeller
Type of Drive - Thrust

Configuration - Bulkheads and Decks Rigid

Coordinate at which response was measured is shown on each figure. The value of the velocity/force at 0 DB (in/sec/lb) is shown by $\left(\frac{V}{F}\right)_{0 \text{ DB}} =$

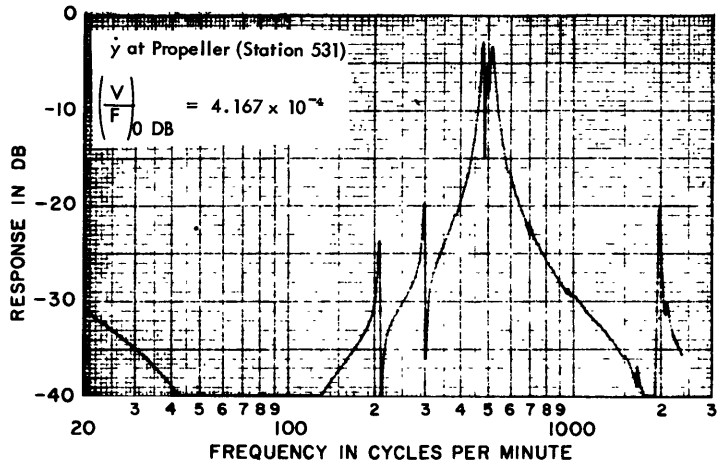


Figure 125

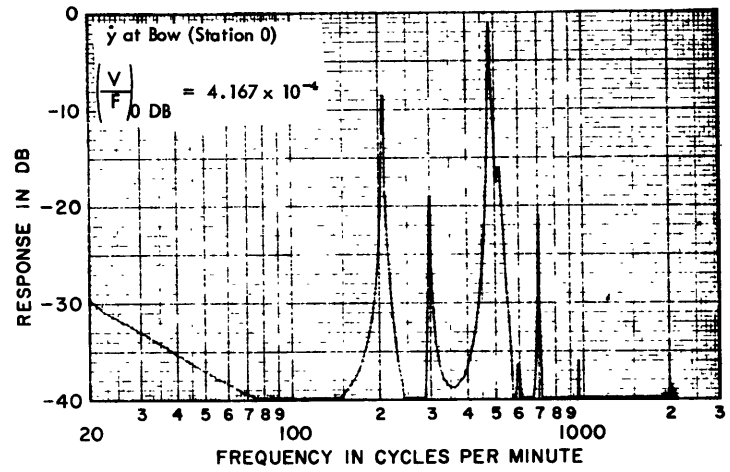


Figure 127

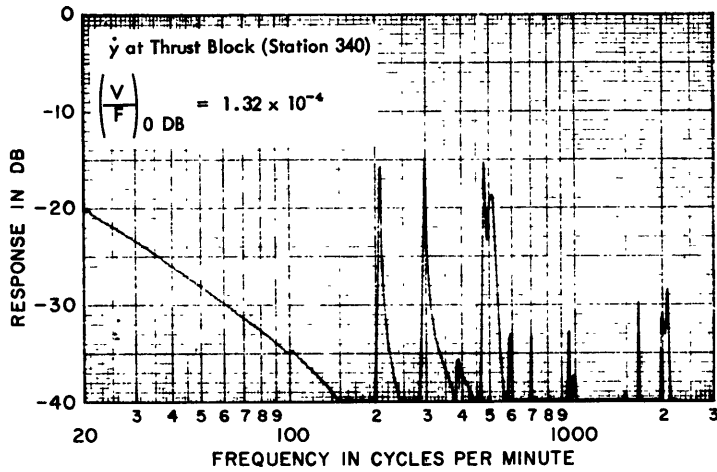


Figure 126

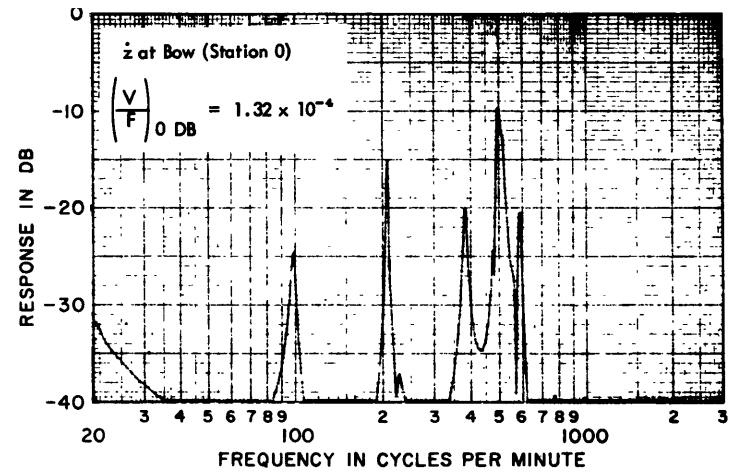


Figure 128

69

Excitation { Drive Point - Propeller
Type of Drive - Thrust

Configuration - Bulkheads, Decks, and Side Plating Rigid (Rigid Shell)

Coordinate at which response was measured is shown on each figure. The value of the velocity/force

at 0 DB (in/sec/lb) is shown by $\left(\frac{V}{F}\right)_{0 \text{ DB}} =$

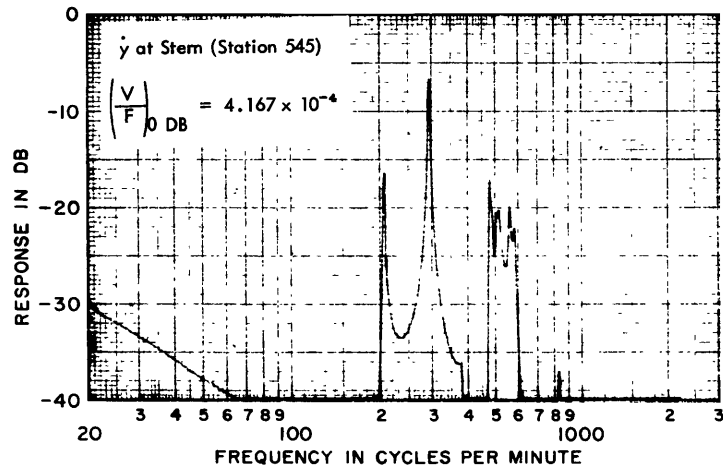


Figure 129

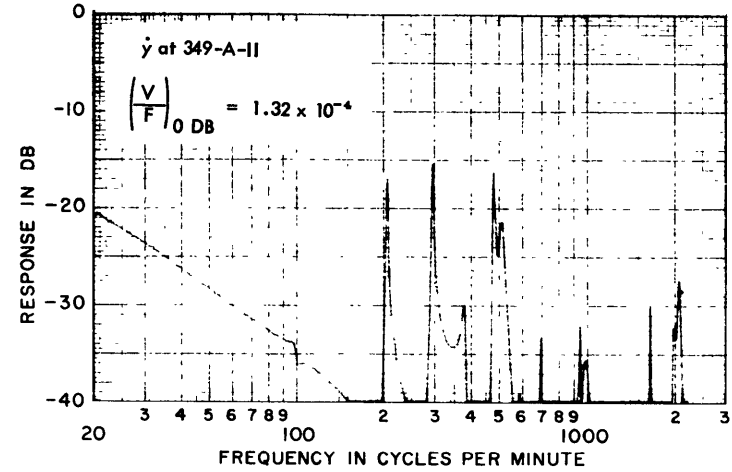


Figure 131

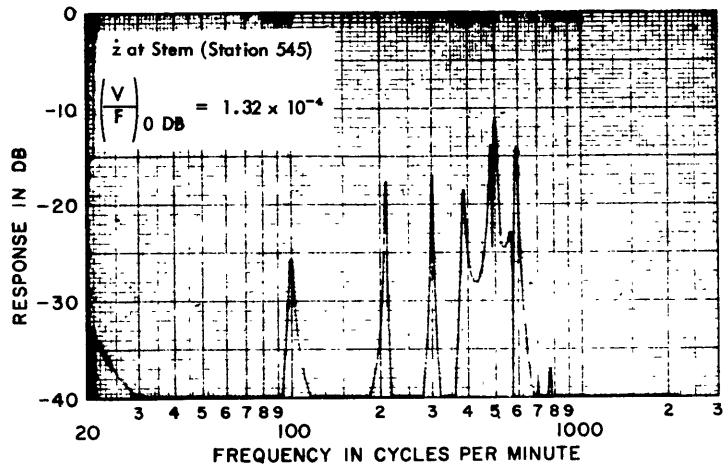


Figure 130

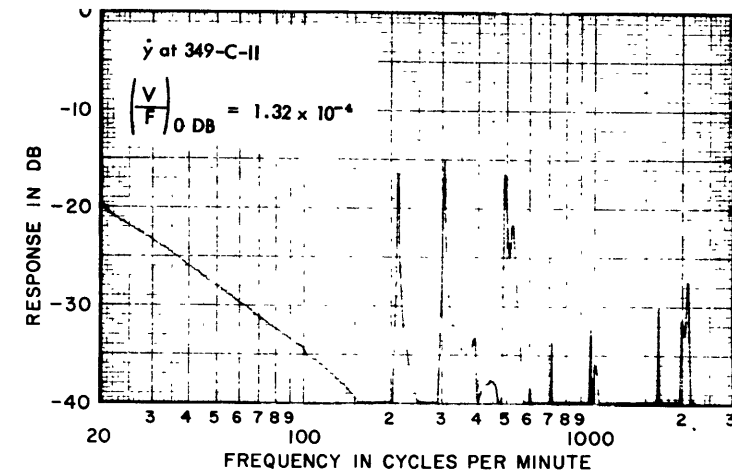


Figure 132

70

Excitation { Drive Point - Propeller
Type of Drive - Thrust

Configuration - Bulkheads, Decks, and Side
Plating Rigid (Rigid Shell)

Coordinate at which response was measured is shown on each figure. The value of the velocity/force at 0 DB (in/sec/lb) is shown by $\left(\frac{V}{F}\right)_{0 \text{ DB}} =$

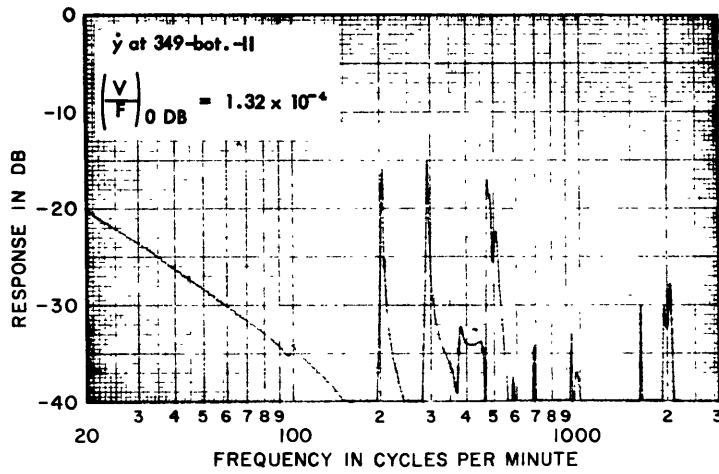


Figure 133

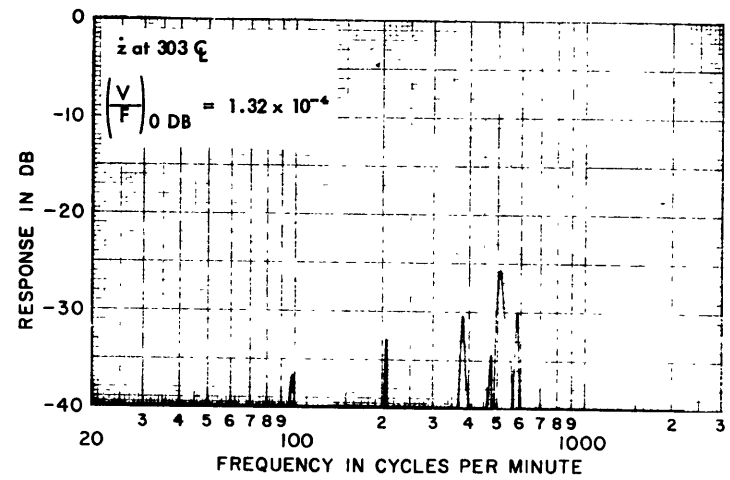


Figure 135

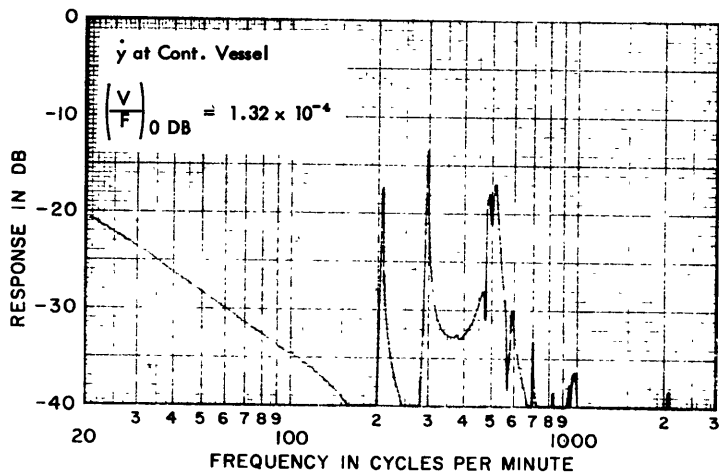


Figure 134

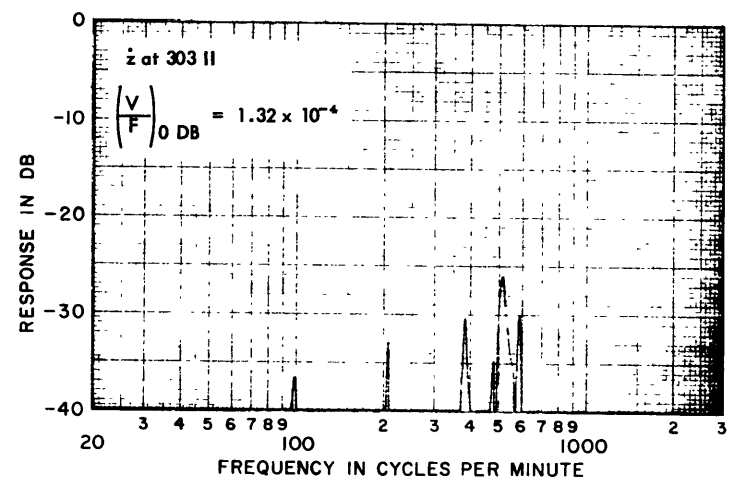


Figure 136

71

Excitation $\left\{ \begin{array}{l} \text{Drive Point - Propeller} \\ \text{Type of Drive - Thrust} \end{array} \right.$

Configuration - Bulkheads, Decks, and Side Plating Rigid (Rigid Shell)

Coordinate at which response was measured is shown on each figure. The value of the velocity/force

at 0 dB (in/sec/lb) is shown by $\left(\frac{V}{F}\right)_{0 \text{ DB}} =$

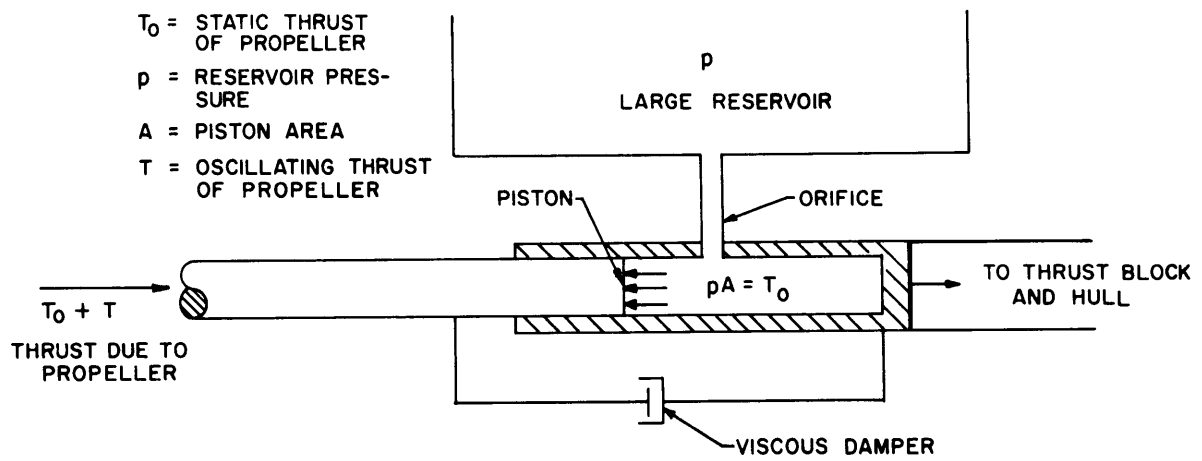


Figure 137 - Thrust-Coupling Mechanism

APPENDIX A

REPRESENTATION OF NS SAVANNAH AS A BEAM-SHELL-SPRUNG BODY SYSTEM

1. GENERAL DESCRIPTION OF SYSTEM REPRESENTATION

The idealized structural model adapted for the analysis is shown in Figure 1. The principal features of the model, comprised of the main structure of the ship (beam-shell system) excited by a propeller through a shafting system (sprung body), are described as follows:

a. The portion of the ship forward of Station 243 (Frame 102) is represented by a *beam* capable of bending in the vertical direction. The neutral axis of the beam is located 26.5 ft above the bottom of the ship.* Extension and contraction of the ship in the longitudinal direction is included by allowing the neutral axis of the beam to extend and contract. The distributed mass of the forward portion of the ship is concentrated at six stations along the neutral axis of the beam. The bending flexibility ($\Delta x/EI$) is concentrated at points midway between the mass stations, as is the axial flexibility ($\Delta x/EA$).

*The location of the neutral axis of the ship was determined as follows. The detailed shell representation in the central portion of the ship does not require *a priori* determination of the neutral axis. For the portion of the ship forward of Station 243 and the portion aft of Station 408, the ship was represented as a beam in vertical bending and as a longitudinal member carrying axial loads. In each case the neutral axis was considered to be at a constant height above the reference. The height was chosen to correspond to the actual neutral axis at the stations at which the beam representation was joined to the shell representation, that is, at Stations 243 for the forward section and 408 for the aft section. This agreement with the actual location of the neutral axis was obtained by reading from the curve of Figure 150.

b. The portion of the ship aft of Station 408 (Frame 168) is represented in the same manner as the forward section. The mass is concentrated at four stations along the neutral axis, and the neutral axis is located 33.5 ft above the bottom of the ship.

c. The middle part of the ship between Stations 243 and 408 is treated as a *shell*, the walls of which are formed by decks, bulkheads, and the sides of the ship, as shown in Figures 1 and 138. The panels of the shell are assumed to carry loads only in their own planes (both direct stress and shear stress).* The bending stiffness of the double bottom is represented by a pair of beams with neutral axes 2.5 ft above the bottom of the ship. Inertia is concentrated at 58 points within the structure, as shown in Figures 3 and 4. Axial flexibilities are concentrated between mass stations; see Figures 139 and 140. The calculation of axial flexibility ($\Delta x/EA$) is based upon the cross-sectional area of plates and stiffeners shown in the latter figures.** Shear panels, framed by mass stations, are also shown in these figures at the position of the deck and bulkhead shear panels. The middle portion of Decks C and D are cut out (portion between the centerline and Plane I).

*A shear panel is a two-dimensional structural element that resists the action of tangential forces applied to its edges (plus the action of other forces when absolutely necessary to preserve equilibrium) but does not resist the action of normal forces. Shear panels are created in the process of obtaining idealized modes for thin elastic sheets. If a sheet has heavy stiffeners, it is reasonable to lump the normal stress-resisting properties of the sheet into the stiffeners and to lump the shear-resisting properties of the sheet into the shear panels. This idealization can frequently be justified even if the sheet has light stiffeners or no stiffeners at all. The shape of a shear panel is determined by the directions of the bounding stiffeners and, although a rectangular shape can be considered as normal for a shear panel, many different shapes must be considered in practice. The discussion of shear panels is aided if the panels are classified according to shape (i.e., rectangular, quadrilateral, etc.).

**The manner in which the calculation of the terms $\frac{\Delta x}{EA}$ includes the area of the plates and stiffeners is discussed in Appendix E.

The major weight item in the reactor space of the ship is the containment vessel, which is sufficiently stiff to be assumed rigid. Therefore, the effect of this mass item on the response of the remainder of the ship was duplicated by representing the complete containment vessel as a single mass at its center of gravity. (In vertical motion the mass was located at two points at Station 270, half the mass being on the center-line, and half the mass being at buttock line I.) The coordinates for the location of this mass were created by rigid extensions from the bottom. The incorporation of this mass into the lumped mass of the ship structure is indicated in Tables 12 and 13 of Appendix D. The response of this structure is indicated only to the extent that response measurements of the coordinates of the bottom were obtained.

d. The longitudinal dynamics of the propeller shaft considered as a sprung body¹ are represented as shown in Figure 1. The mass of the propeller shaft is concentrated at six stations and the axial flexibility of the shaft is concentrated at points between mass stations. The thrust of the propeller is carried by a thrust block mounted on the double bottom of the ship. The bottom of the thrust block applies a moment to the bottom of the ship. A "thrust-coupling mechanism" is located between Stations 377 and 340 of the shaft; see Figure 1. A physical model of the coupling mechanism studied is shown in Figure 137.

2. DETAILED BREAKDOWN

One of the most generally useful approaches to the derivation of passive electric

analogies begins with an idealization of the actual structure into one composed entirely of a few basic types of simple structural elements. The decomposition, or analysis, of the original structure into an arrangement of simple elements often requires a considerable amount of engineering judgment and experience; however, once this step is taken, the rest is only science and adroitness.

Figure 1 shows the structural idealization adapted for the purpose of determining the symmetric vibrations of SAVANNAH. This idealization is composed entirely of the following simple elements:

- a. Axial elements (structural elements which carry only tension and compression).
- b. Beams.
- c. Shear panels.
- d. Torque box or torque tube.

Each of these structural elements is discussed separately. The interconnection of these simple elements and the corresponding form of the electrical analogy is considered in Appendix B.

a. Axial Elements

In the idealized model given in Figure 1, the part of the shell structure which carries tensile and compressive stress is "lumped" into the edges formed by intersection of decks, frames, and vertical Planes I and II (Plane II coincides with the plane of the side plating). Axial elements also occur in the portions of the ship forward and aft of the shell. Figure 141a shows an axial element with extensional stiffness EA .

b. Beams

In the idealized model of SAVANNAH, beams occur in the following places:

(1) Two beams are used to represent the bending stiffness of the double bottom in the vertical direction. These beams run along the intersection of Planes I and II with the bottom (see Figure 1).

(2) The hull forward and aft of the shell structure is represented by beams.

Figure 142a shows a beam element with bending rigidity EI .

c. Shear Panels

A shear panel is a two-dimensional structural element which does not carry direct stress. Decks, plating, and bulkheads of SAVANNAH are represented by combinations of shear panels and the axial elements discussed previously. A shear panel element is shown in Figure 143a.

Figure 144a illustrates the way in which axial elements and shear panels are connected to form a plate.

In the idealized model the shear of one deck with respect to another is resisted by the shear stiffness of the sides and the shear stiffness of the bulkheads.

Certain mechanical details tied to the analogy for SAVANNAH are discussed in Appendix B.

d. Torque Box

A torque box is composed of two parallel sheets of skin assumed to carry shear only, connected around the boundary by beam webs. In the representation of SAVANNAH, a rectangular torque box was used to represent the torsional stiffness of the double bottom. The torque box and its passive electrical analog are discussed in Appendix H.

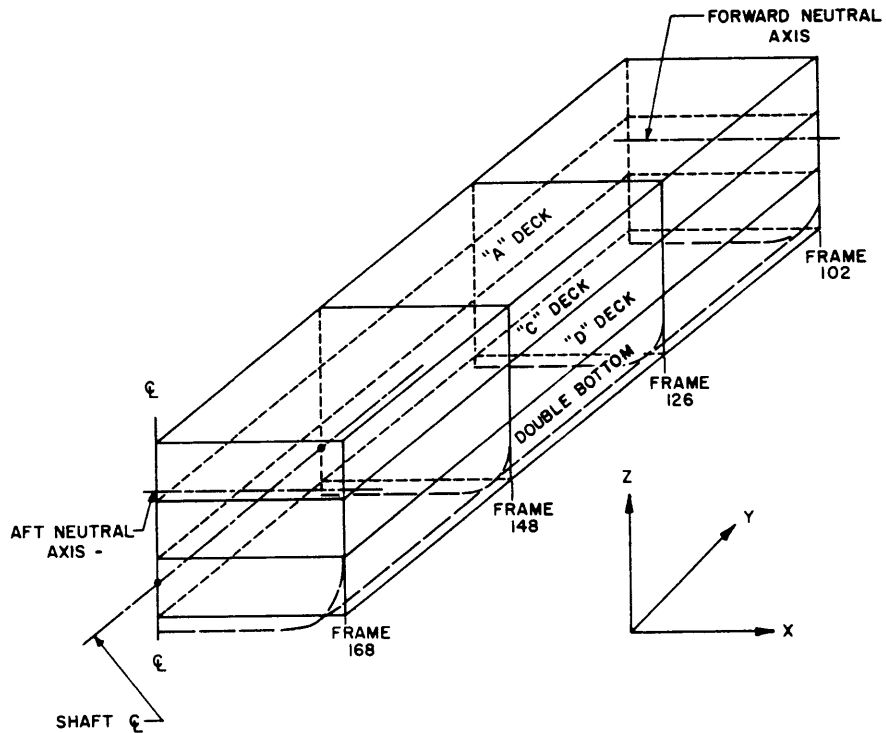


Figure 138 - Shell Structure

× INDICATES POSITION OF LUMPED FLEXIBILITY

FRAME 168 (STA. 408) FRAME 148 (STA. 358) FRAME 125 (STA. 303) FRAME 102 (STA. 243)

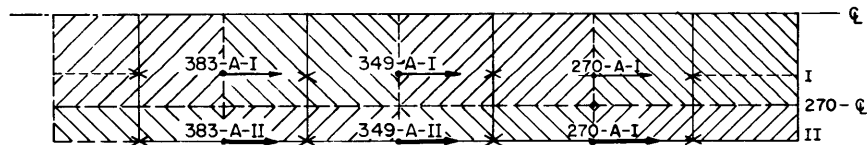


Figure 139a - Typical Deck Showing Location of Lumped Axial Flexibility and Areas Used to Calculate the Axial Flexibility (Longitudinal Direction)

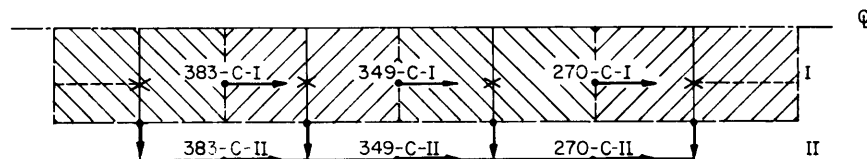


Figure 139b - Typical Deck Showing Location of Lumped Axial Flexibility and Areas Used to Calculate the Axial Flexibility (Lateral Direction)

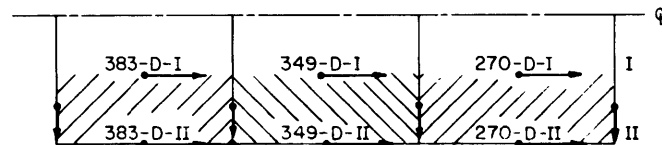


Figure 139c - Typical Deck Showing Location of Lumped Shear Flexibility and Areas Used to Calculate the Shear Flexibility

Figure 139 - Area Lumping for Decks

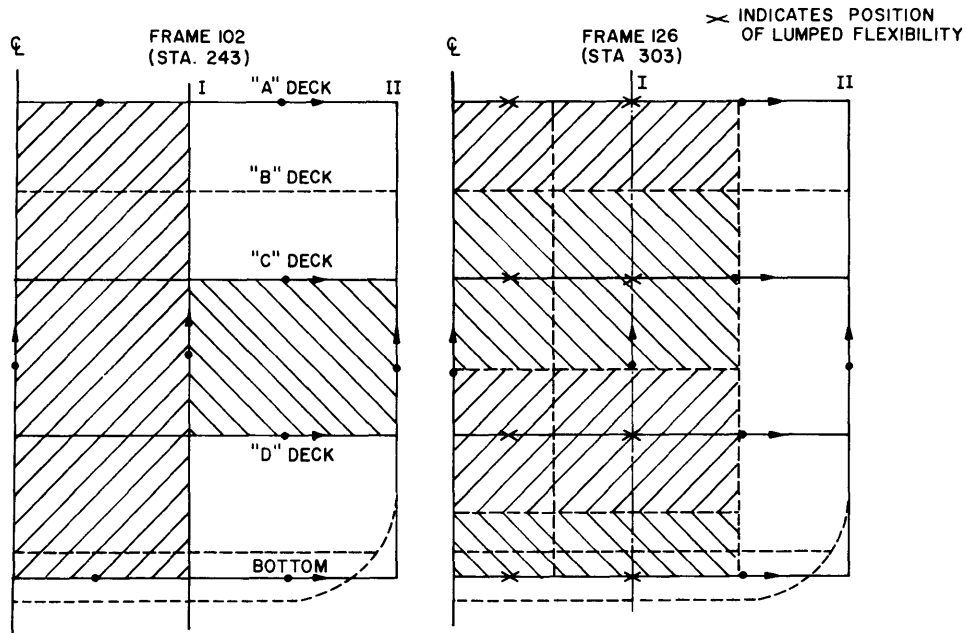


Figure 140a - Typical Bulkhead Showing Shear Panel Location

Figure 140b - Typical Bulkhead Showing Area Used to Calculate Axial Flexibilities

Figure 140 - Area Lumping for Bulkheads

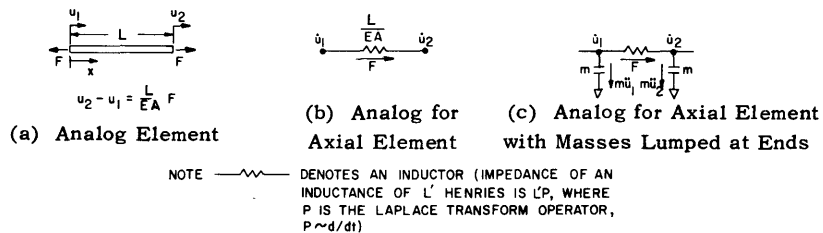


Figure 141 - Axial Element Analogy

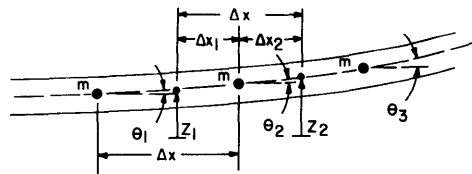


Figure 142a - Beam

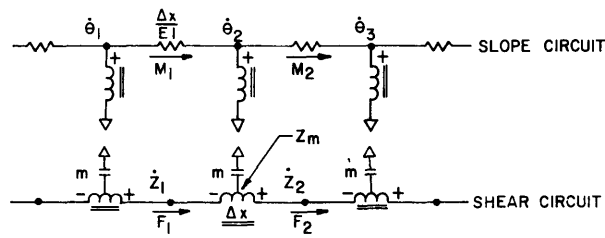


Figure 142b - Analog for Beam

Figure 142 - Beam Analogy

NOTE: Tap on transformers in shear circuit located Δx_1 turns from "-" end.

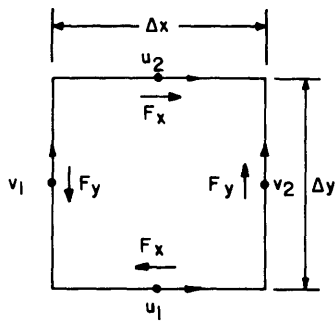


Figure 143a - Shell Panel

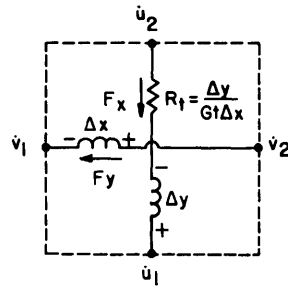


Figure 143b - Analog for Shell Panel

$$\Delta x F_y = \Delta y F_x$$

$$F_x = \frac{Gt\Delta x}{\Delta y} \left[u_2 - u_1 + \frac{\Delta y}{\Delta x} (v_2 - v_1) \right]$$

Figure 143 - Shear Panel Analogy

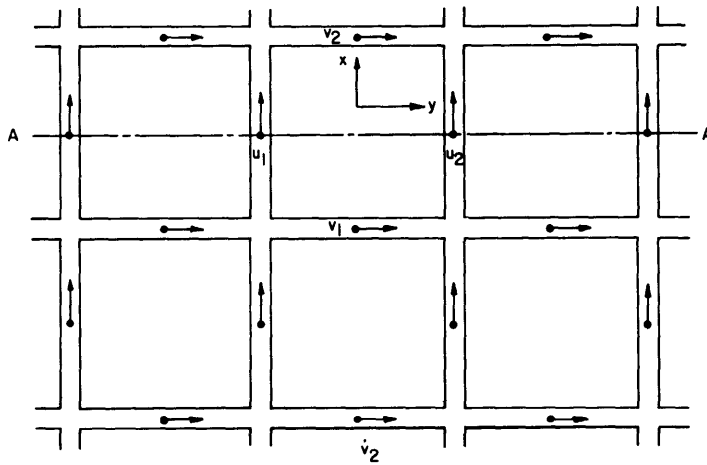


Figure 144a - Plate

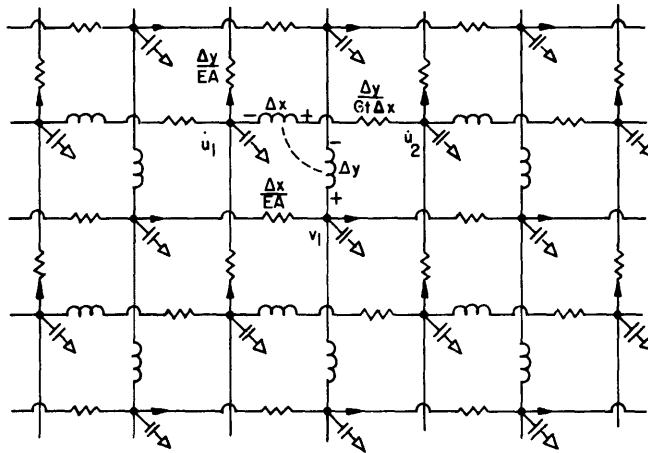


Figure 144b - Analog for Plate

Figure 144 - Electrical Analogy for a Plate

APPENDIX B

ANALOG OF STRUCTURAL ELEMENTS OF SHIP

In this appendix the analog of the simple structural elements discussed in Appendix A and their interconnections is developed.

1. AXIAL ELEMENTS

The passive electrical analogy for an axial element is especially simple since such elements are one-dimensional and do not require transformers for their simulation. Figure 141b is the circuit diagram for an axial element.

In this circuit, current is analogous to force and voltage is analogous to velocity. Thus capacitance is analogous to mass, a fact which results in an exceedingly simple electrical representation of inertia forces (see Figure 141c, where the current flowing through the capacitors represents the inertia force due to masses lumped at the ends of the axial element).

To show this we have, by Hooke's law,

$$\frac{du}{dx} = \frac{F}{EA}$$

where $u(x)$ is the axial displacement along x , F is the force, and A is the cross-sectional area. If u_1 and u_2 are displacements at the ends parallel to the axis of the rod of length L , then

$$u_2 - u_1 = F \int_0^L \frac{dx}{EA} = \frac{L}{EA} F$$

differentiating with respect to time t

$$\dot{u}_2 - \dot{u}_1 = \left(\frac{L}{EA} \right) \frac{dF}{dt}$$

This is analogous to $E = L' \frac{di}{dt}$ which gives the relationship between the voltage E across and current I through an inductance L' . Moreover, for masses lumped at the ends, inertia forces $F_1 = m\ddot{u}_1$ and $F_2 = m\ddot{u}_2$ are analogous to $i' = C' \frac{dE'}{dt}$ and $i'' = C'' \frac{dE''}{dt}$ which gives the relationship between the currents i' , i'' through and voltages E' , E'' across capacitors C' , C'' , respectively.

2. BEAMS

Passive electrical analogies for beams are well known and have been described in many publications (see, for example, References 1 and 3). A basic analogy is shown in Figure 142. The currents flowing between nodes in the slope circuit represent bending moments, whereas the currents flowing between nodes of the shear circuit represent shear forces. Bending flexibility of the beam is represented by inductors. The circuit given in Figure 142 satisfies the following equations:*

$$\begin{aligned} z_2 - z_1 &= \Delta x \theta_2 & M_2 - M_1 &= \Delta x_2 F_2 - \Delta x_1 F_1 \\ \theta_2 - \theta_1 &= \frac{\Delta x}{EI} M_1 & F_2 - F_1 &= m\ddot{z}_m \end{aligned}$$

3. SHEAR PANELS

The basic stress-strain relationship for a plane element subject to shear is (see page 41 of Reference 5):

*For rigorous derivations of these quantities, see Appendix A and Equations [2.5] to [2.8] of Reference 1. The corresponding analog given here is discussed in Reference 3.

$$\tau = G\gamma = G \left(\frac{\partial U_x}{\partial y} + \frac{\partial U_y}{\partial x} \right)$$

where τ is the shear stress,

γ is the shear strain,

G is the shear modulus of elasticity, and

U_x and U_y are components of displacement parallel to the x - and y -axes, respectively.

For the rectangular panel, it is convenient to introduce a coordinate along the circumferential direction of the cross section and to speak of the "shear flow" q as meaning the shearing force per unit of circumference. Then (see Section 1.2 of Reference 6):

$$q = \tau t = \frac{F_x}{\Delta x} = \frac{F_y}{\Delta y}$$

where t is the thickness of the panel and the forces F_x and F_y (see Figure 143) represent the total shear forces sustained by the panel. They appear as currents in the electrical analogy. These shear forces are closely related by the equation

$$F_y \Delta x = F_x \Delta y$$

which expresses the condition that the sum of the moments on the shear panel about a corner is zero. This relation is satisfied by the currents flowing in the transformer windings.

The current F_x is then

$$F_x = Gt\Delta x \left(\frac{\partial U_x}{\partial y} + \frac{\partial U_y}{\partial x} \right)$$

and, replacing partial derivatives by finite derivatives, we obtain the relationship

between the current F_x appearing in the circuit diagram and the voltages $u_1, u_2, v_1,$

v_2 :

$$F_x = \frac{Gt\Delta x}{\Delta y} \left[(u_2 - u_1) + \frac{\Delta y}{\Delta x} (v_2 - v_1) \right]$$

A similar result is obtained for F_y .

Since all of the shear panels are rectangular (see Figure 1), the electrical analogy takes the simple form of the circuit in Figure 143b.

Passive electric analogies for trapezoidal shear panels can be found in Reference 3.

To form the complete electrical analogy, the simple circuits just discussed must be properly interconnected. Here we are guided by two simple physical principles which govern the interconnection of elastic elements:

- a. The sum of the forces acting on a point of the structure is zero.
- b. The sum of the displacements around a close curve in the structure must add

up to zero.

In the language of electric circuits, these statements become Kirchoff's laws:

- a. The sum of the currents entering a node is zero.
- b. The sum of the voltages around a closed path of the circuit must vanish.

Both of these conditions will be satisfied simultaneously if we merely observe the following rules of interconnection:

- a. If two voltages represent the displacement of the same point of the elastic structure, then these two voltages must be equal and the nodes at which these voltages are defined must, therefore, be connected.

- b. The currents representing the forces acting at a point of the structure must

all enter the same node.

Figure 144 shows the way in which axial elements and shear panels may be connected to form a plate; the corresponding electrical network is also shown.

If motion is symmetric with respect to the line A-A (Figure 144), then the circuit takes the form given in Figure 145. The circuit is then identical to that used to represent half the deck of SAVANNAH. There are four such circuits, three for A, C, D, and one for the bottom.

In the idealized model, the shear of one deck with respect to another is resisted by the shear stiffness of the sides and the bulkheads. Figure 146 shows how the deck circuits are connected by shear panel circuits representing the sides of the ship and the bulkheads.

Several details of the electrical analogy for SAVANNAH require special discussion:

a. How are the forces and moments due to the forward part of the ship distributed among the decks of the shell structure? At Frame 114, where the beam representation interconnects with the shell structure (see Figure 1), it is assumed that the frame deforms in such a way that it remains plane. Thus, at this frame there is a geometrical relationship between the longitudinal displacements and the slope of the beam representing the forward part of the ship. The interconnection circuit used at Frame 114 is shown in Figure 147. The vertical displacement of the beam at Frame 114 is taken to be the average of the vertical displacements over the frame. The transformer circuit which interconnects the vertical displacements of this frame to the shear circuit of the beam analogy furnishes the required relation.

Identical circuits are employed at Frame 158, where the beam analogy for the aft part of the ship interconnects with the shell structure.

b. It is assumed that z-deflections in the plane of symmetry follow the vertical deflections of the beam along the double bottom at the centerline. This also applies for vertical deflections in the vertical Plane I.

c. Differential bending of the two beams that represent the bending properties of the double bottom is elastically restrained. This effect is included in the circuit analogy by placing inductors between the slope circuits of the two beams.

4. TORQUE BOX

This element and its electrical analog are discussed in Appendix H.

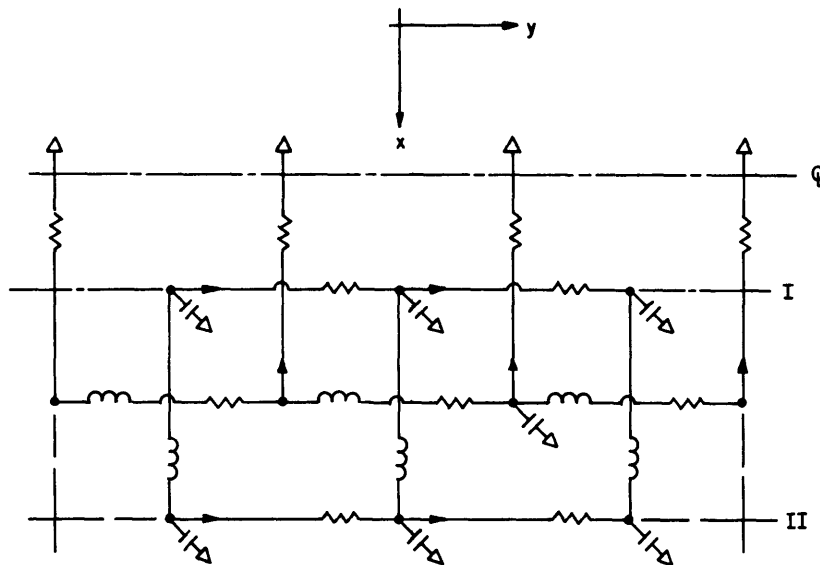


Figure 145 - Electrical Analogy for a Half Deck

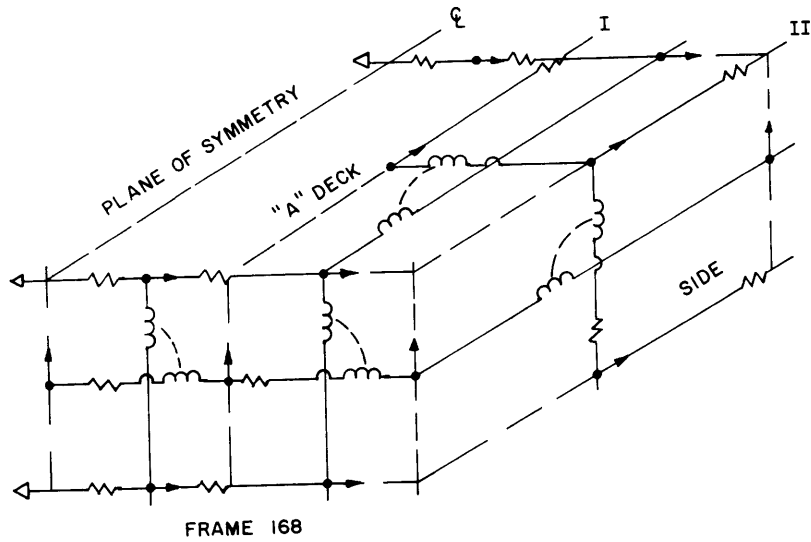


Figure 146 - Interconnection of Decks by Shear Panels

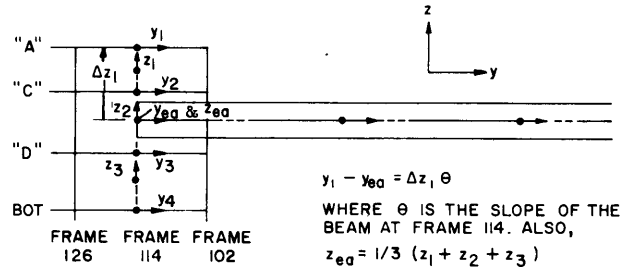


Figure 147a - Beam-Shell System

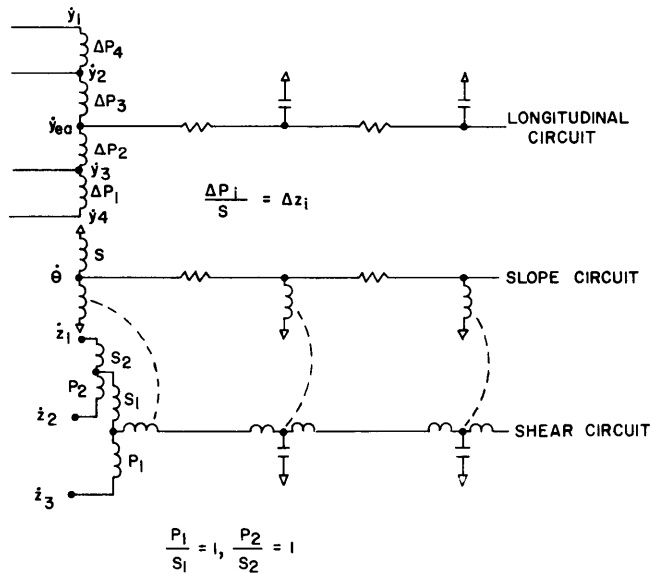


Figure 147b - Analog for Beam-Shell System

Figure 147 - Interconnection of Beam Analogy and Shell Analogy

BLANK

APPENDIX C

SYMMETRIC AND ANTISYMMETRIC ANALYSES

Only the symmetric analysis for NS SAVANNAH was made in this investigation. For completeness, however, both the symmetric and antisymmetric analyses are discussed here.

1. SYMMETRIC ANALYSIS

The ship is represented as in Figure 1 and consists of the structural elements discussed in Appendix A. The structure (in general) has bending and shear flexibility for vertical translation and extensional flexibility for longitudinal translation. Coupling between longitudinal, vertical, and transverse motion is considered necessary because the point of thrust excitation is well below the center of gravity. The shaft is considered to be flexible in extension and its mass is lumped at several points. The thrust is applied directly to the propeller shafts.

Large pieces of machinery with known natural frequencies may be represented as sprung bodies.

Apparent (or virtual) hydrodynamic mass is added to the hull mass for lateral but not for longitudinal motions.

Rotary inertia of the hull cross sections can be included where appropriate and desirable.

Structural damping is simulated by the inherent damping of the analog computer. Since the amount of computer damping will not, in general, correspond to the amount

of structural damping in the ship, the computer results must be adjusted for this fact. Except near resonances, structural damping has little effect. At a resonance the magnitude of response is inversely proportional to the damping. The computer damping at resonance can be measured easily. Thus the adjustment consists of multiplying the peak amplitudes at resonance points, as measured on the computer, by the ratio of computer damping to structural damping. Computer damping is approximately 1 to 2 percent of critical damping.

Now let us consider the representation of the thrust-bearing support in symmetric analysis. The transmission of thrust from the propeller shaft to the ship hull requires detailed representation. The configuration of the idealized support structure depends on the details of the actual configuration. Let it be assumed for illustration that the thrust bearing is supported by framing from the bottom hull girders. The framing will introduce vertical and horizontal loads into the hull girders; the vertical loads will be carried to adjacent bulkheads by bending of the girders, and bending of transverse beams may also be involved. The horizontal loads will be transmitted to other girders by "shear lag" in such a way that, at a large distance forward, the stress distribution in the hull will be approximately planar.

Well-known and thoroughly tested methods are available for simulating the structural deformations of plates and shells on an analog computer.^{7, 8} In this instance, the main problem in simulation is to distribute the available quantity of computer elements so as to afford an optimum structural representation. All girders and all frames cannot be represented because of the limited amount of available equipment. Beams and girders compete with the elements required to simulate shear lag and with the

elements required to represent the beam properties of the ship as a whole. Shear lag should probably be considered over a fore-aft dimension at least equal to the beam of the ship. At the ends of this region, a planar stress distribution can be imposed.

The limiting factor in the computer is the availability of elements to represent stiffness (inductors).

2. ANTISYMMETRIC ANALYSIS

The following presentation is conceptual only. In the actual execution of this analysis for a particular ship, the details may be different. In antisymmetric vibration, the principal motions of the ship hull are lateral bending and torsion. Hydrodynamic excitation is produced by propeller torque fluctuations and pulsating lateral force on the rudder. In twin-screw propulsion, differential propeller thrust produces a couple that excites lateral bending of the hull; therefore single-screw and twin-screw idealizations of the ship structure are somewhat different. Thus there are either two or three sources of excitation, depending upon whether there is one screw or two.

A simplified antisymmetric model for a single-screw ship is shown in Figure 148. In this model the torsional coupling between the stator of the motor and hull of the ship is represented by a single equivalent torsional spring. In practice, it may be necessary to represent this coupling by a detailed simulation of elements in the support structure, similar to the representation of the thrust-bearing support structure in symmetric analysis.

The propeller drive torque is presumed to be provided by an electrical motor. The relationship between torque and angular velocity (or angular displacement) for any type of electrical motor can be simulated in an analog computer by lumped

electrical elements.

A pulsating lateral force is produced on the rudder as a result of fluctuations in the wake of the propeller. Additional hydrodynamic forces on the rudder are produced by motions of the rudder. These additional forces can be simulated in a manner similar to that employed in Reference 9, which utilizes incompressible aerodynamic flow theory for the calculation of unsteady hydrodynamic force coefficients. The motions of the rudder will be simulated by circuits similar to those given in Reference 10.

The hull of the ship is represented by a beam with bending, shear, and torsional flexibility. Coupling between lateral bending and torsion is provided by jogs in the elastic axis and by off-center inertia forces.

Apparent hydrodynamic mass is added to the mass of the hull for lateral translation and the hydrodynamic mass is presumed to act at the center of gravity of the submerged cross section. The torsional inertia of the hydrodynamic mass about this point is assumed to be zero. Rotary inertia (about a vertical axis) of the hull cross sections is included.

For a twin-screw ship, the thrust transmission properties of the propeller shafts are included. The thrust-bearing support structure may be represented in a manner similar to that for symmetric analysis, including shear lag effects. In antisymmetric analysis, thrust is reacted by lateral bending of the hull.

In the antisymmetric case also, the motor torque characteristic and the hydrodynamic force coefficients of the rudder are sources of damping in addition to structural damping. Although these additional sources may have little influence on the principal vibration modes of the ship hull, they will have important effects on the magnitude of

propeller-induced vibration because of their proximity to the sources of excitation.

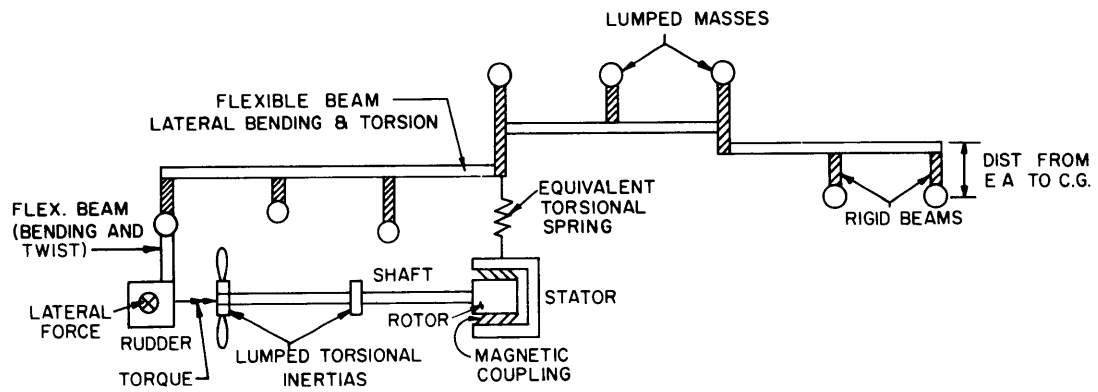


Figure 148 - Simplified Antisymmetric Model (Single-Screw)

APPENDIX D

SHIP DATA

This appendix presents tables and figures showing principal characteristics and other ship data concerning NS SAVANNAH used in calculating the normal modes and frequencies on the digital and analog computers and the steady-state response characteristics on the analog computer.

Table 3 lists the characteristics of SAVANNAH and Figure 149 gives the inboard profile and plan view of that ship. The raw data useful in calculating ship parameters and evaluating the results are shown in Figure 150. These data include the vertical and horizontal virtual weight curves; longitudinal ship weight distribution curve; moment of inertia curves I_y and I_z about the y - and z -axes,* respectively; curves for vertical, horizontal, and total areas; and true neutral axis and half-beam curves.

Figure 151 shows the six sections of the hull for which moments of inertia are given. Table 4 presents the mass and stiffness data, from Figures 2b through 2g, used for the vertical vibrations calculated on the digital computer. The method of evaluating the parameters for analog computation is given in Appendix F.

*For the digital computer calculations only, a right-handed system of axes was used with the y -axis vertical, the z -axis horizontal, and the x -axis passing through the equilibrium position of the centroid of the cross section (see page 4 of Reference 1); this is in contrast to the axial system, shown in Figure 138, used for the analog computer calculation.

TABLE 3

Principal Characteristics of NS SAVANNAH

| | |
|-------------------------------------|-------------|
| Length between perpendiculars | 539 ft |
| Molded beam | 78 ft |
| Depth to A deck amidships | 50 ft |
| Design draft | 29 ft 6 in. |
| Light draft (approximately) | 18 ft 6 in. |
| Length-to-beam ratio, L/B | 6.9 |
| Length-to-depth ratio, L/D | 10.8 |
| Beam-to-depth ratio, B/D | 1.6 |
| Full load displacement | 21,840 tons |
| Light displacement | 11,850 tons |
| Design speed | 21.2 knots |
| Maximum continuous shaft horsepower | 22,000 hp |
| Maximum shaft speed | 110 rpm |

TABLE 4

Mass and Stiffness Data

| Col. A | Col. B | Col. C | Col. D |
|-----------|--|-----------------------------------|------------------------------------|
| Station | $\mu \Delta x$ | $\frac{\Delta x}{EI} \times 10^8$ | $\frac{\Delta x}{KAG} \times 10^6$ |
| | $\frac{\text{ton-sec}^2}{\text{feet}}$ | $\frac{1}{\text{ton feet}}$ | $\frac{\text{feet}}{\text{ton}}$ |
| 0 (Stern) | | | 10.087 |
| 1/2 | 7.510 | 1.189 | |
| 1 | | | 7.211 |
| 1 1/2 | 14.20 | 0.4125 | |
| 2 | | | 5.290 |
| 2 1/2 | 27.73 | 0.2501 | |
| 3 | | | 4.833 |
| 3 1/2 | 40.01 | 0.1835 | |
| 4 | | | 4.622 |
| 4 1/2 | 54.91 | 0.1485 | |
| 5 | | | 4.483 |
| 5 1/2 | 59.04 | 0.1290 | |
| 6 | | | 4.491 |
| 6 1/2 | 62.18 | 0.1182 | |
| 7 | | | 4.588 |
| 7 1/2 | 71.99 | 0.1138 | |
| 8 | | | 4.584 |
| 8 1/2 | 75.69 | 0.1139 | |
| 9 | | | 4.475 |
| 9 1/2 | 101.48 | 0.1114 | |
| 10 | | | 4.429 |
| 10 1/2 | 101.63 | 0.1195 | |
| 11 | | | 4.656 |
| 11 1/2 | 60.09 | 0.1434 | |
| 12 | | | 5.172 |
| 12 1/2 | 54.88 | 0.1543 | |
| 13 | | | 5.556 |
| 13 1/2 | 54.03 | 0.1580 | |
| 14 | | | 5.643 |

TABLE 4
Mass and Stiffness Data (Continued)

| Col. A | Col. B | Col. C | Col. D |
|----------|--|-----------------------------------|------------------------------------|
| Station | $\mu \Delta x$ | $\frac{\Delta x}{EI} \times 10^8$ | $\frac{\Delta x}{KAG} \times 10^6$ |
| | $\frac{\text{ton-sec}^2}{\text{feet}}$ | $\frac{1}{\text{ton feet}}$ | $\frac{\text{feet}}{\text{ton}}$ |
| 14 1/2 | 47.15 | 0.1651 | |
| 15 | | | 5.386 |
| 15 1/2 | 35.95 | 0.1787 | |
| 16 | | | 5.064 |
| 16 1/2 | 25.20 | 0.2032 | |
| 17 | | | 4.805 |
| 17 1/2 | 14.55 | 0.2501 | |
| 18 | | | 4.580 |
| 18 1/2 | 8.235 | 0.3718 | |
| 19 | | | 5.274 |
| 19 1/2 | 7.647 | 1.0219 | |
| 20 (Bow) | | | 6.707 |

$\Delta x = 13.625$ feet at Stations 0 and 20 and 27.25 feet at all other Stations.

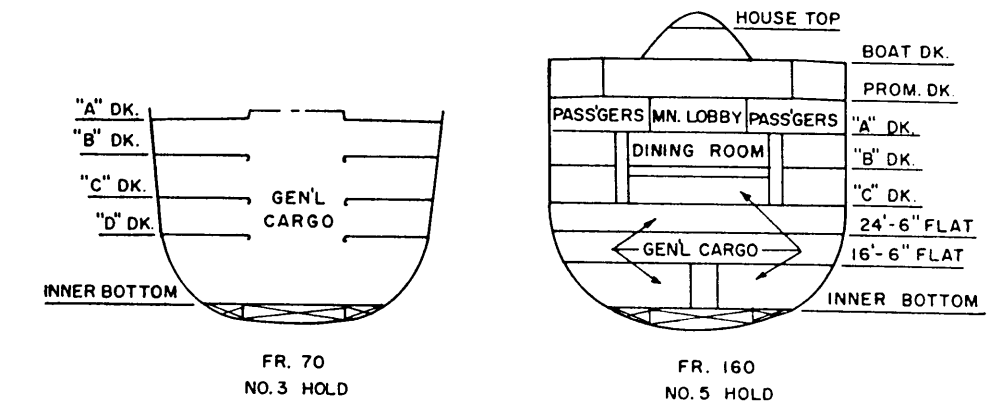
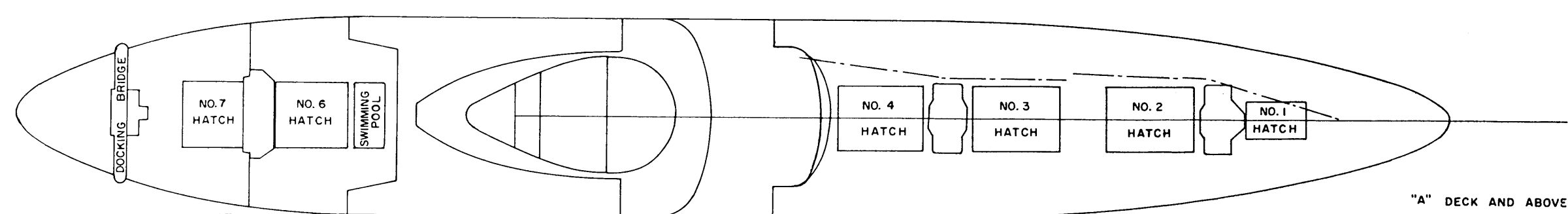
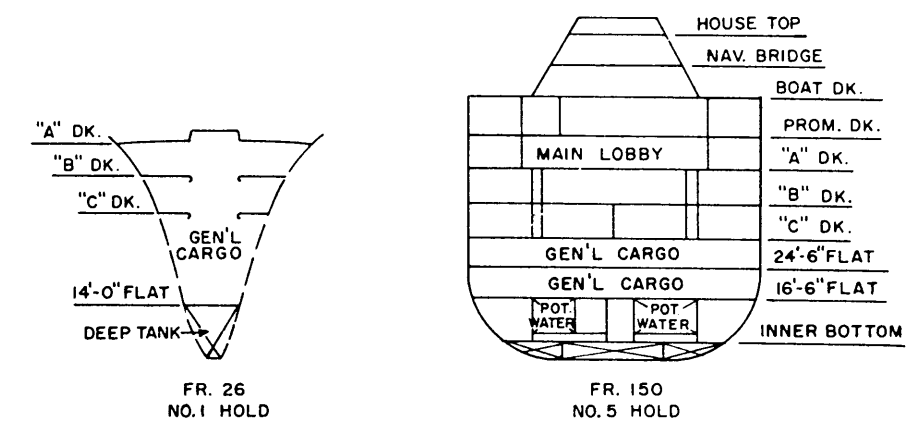
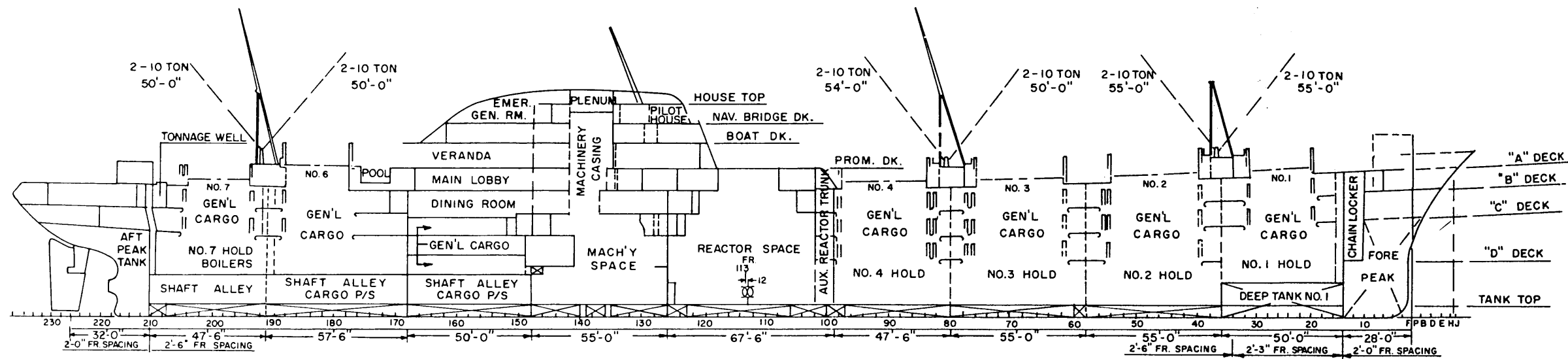
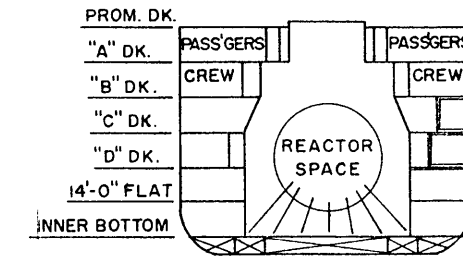
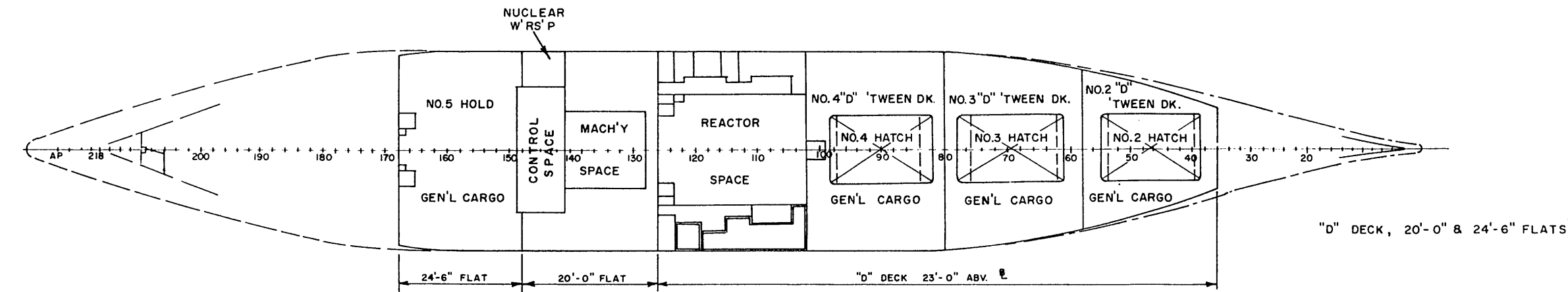
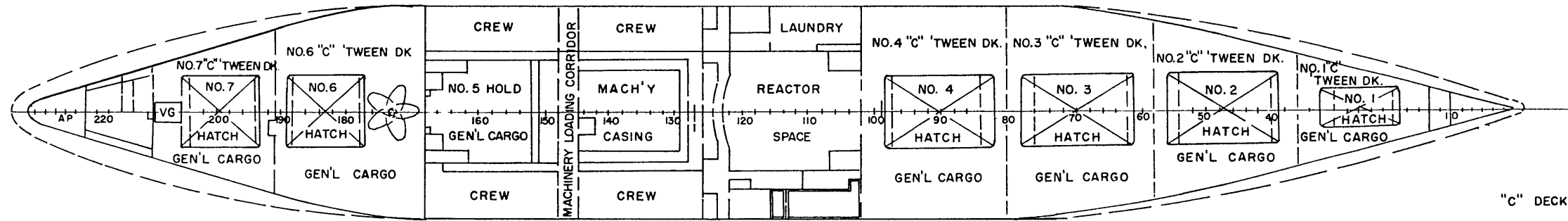
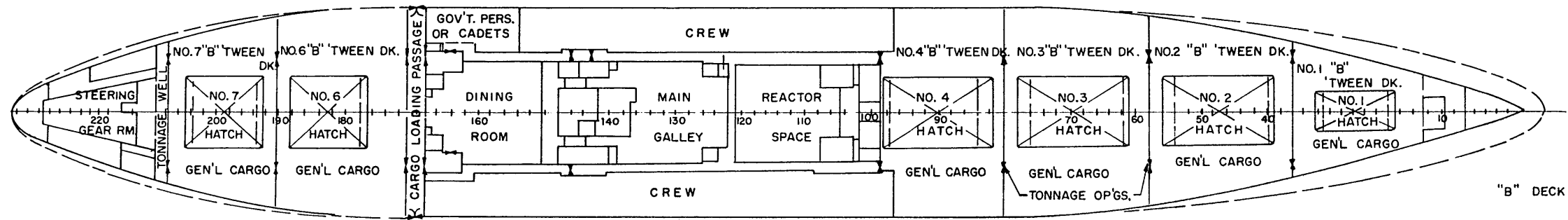
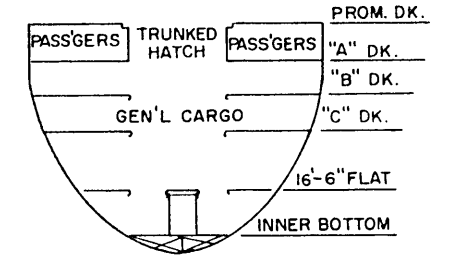


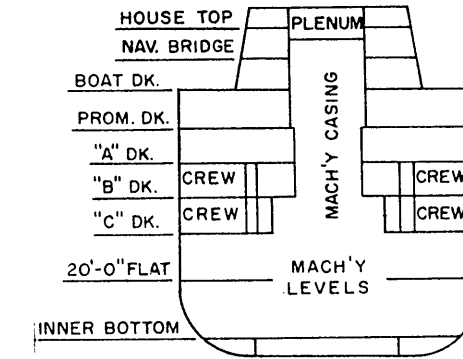
Figure 149 - Inboard Profile and Plan View of NIC SAVANINAH



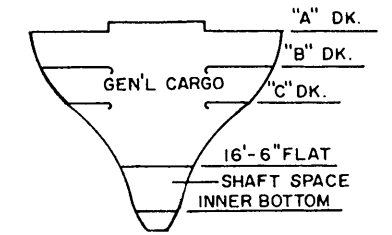
FR. 114 REACTOR SPACE



FR. 180 NO. 6 HOLD



FR. 140 MACH'Y SPACE



FR. 200 NO. 7 HOLD

Figure 149 (Continued)

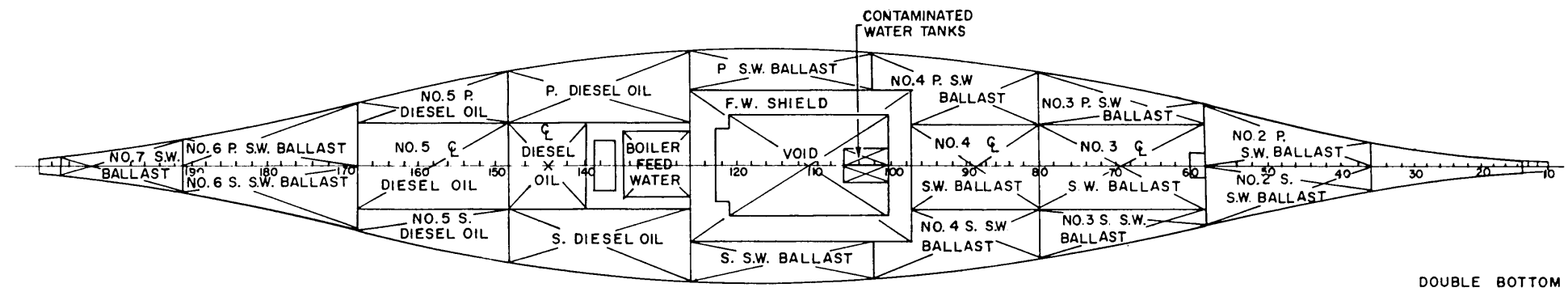
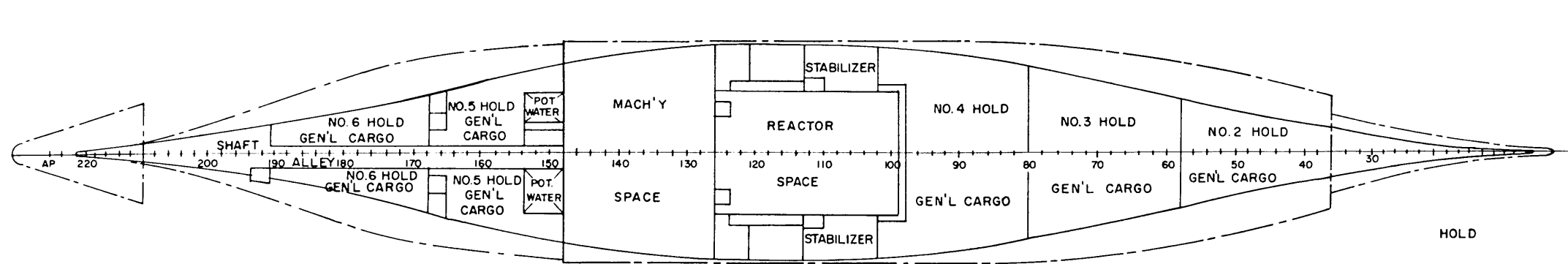
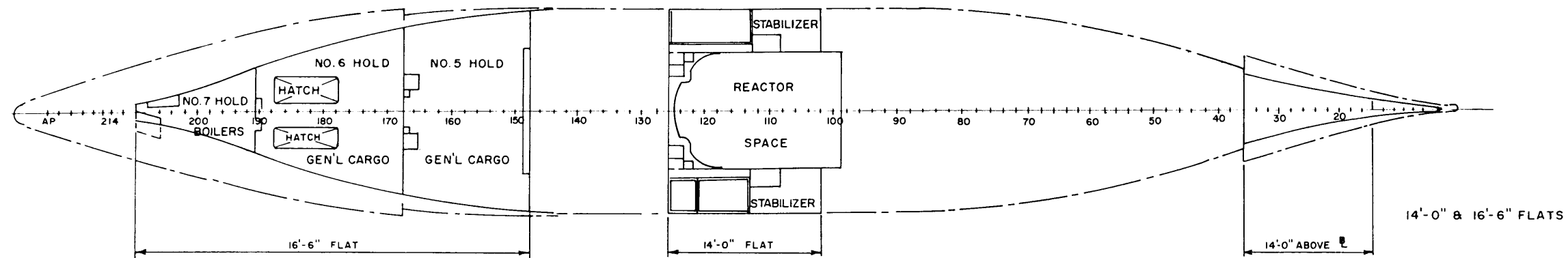
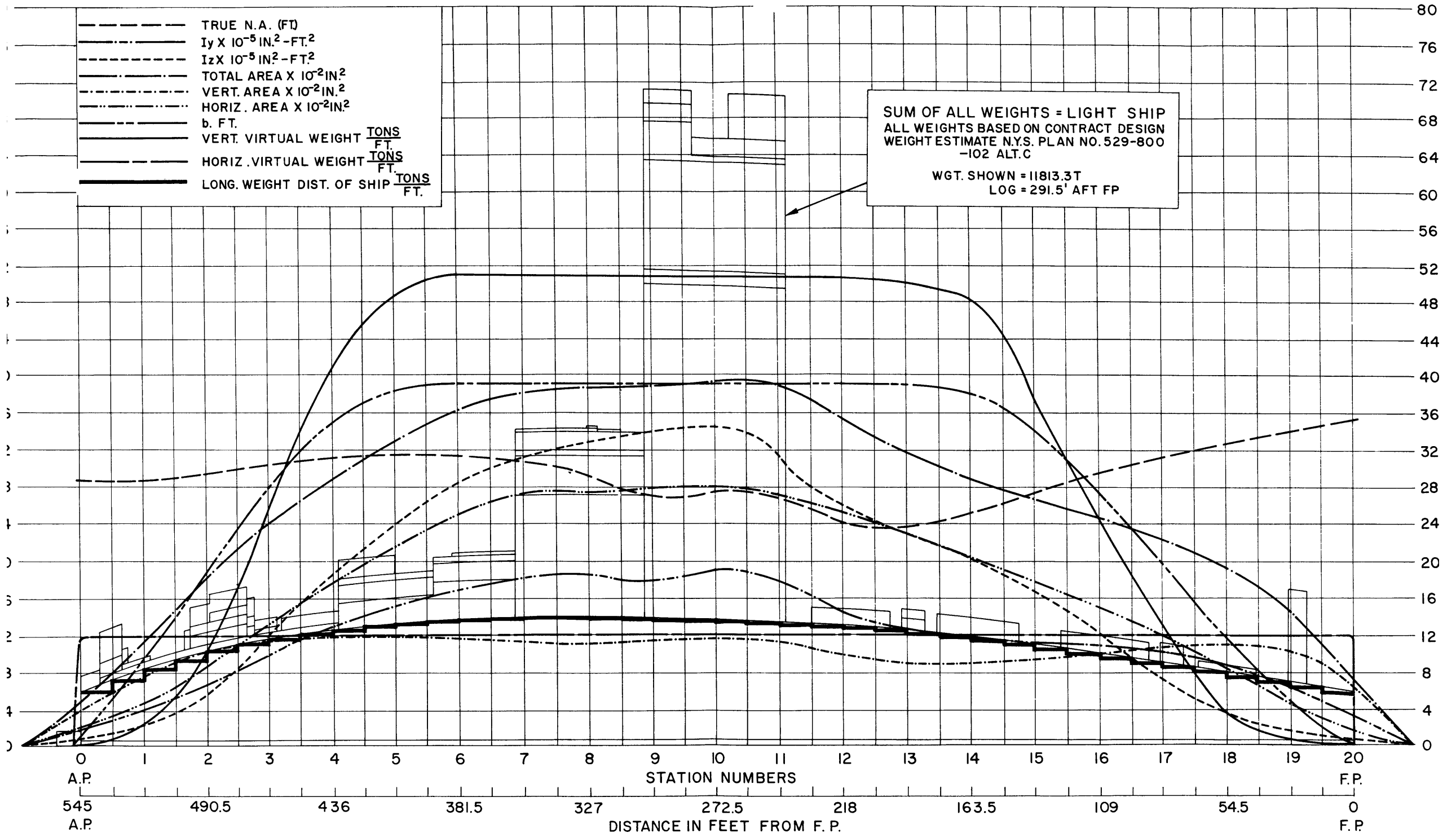
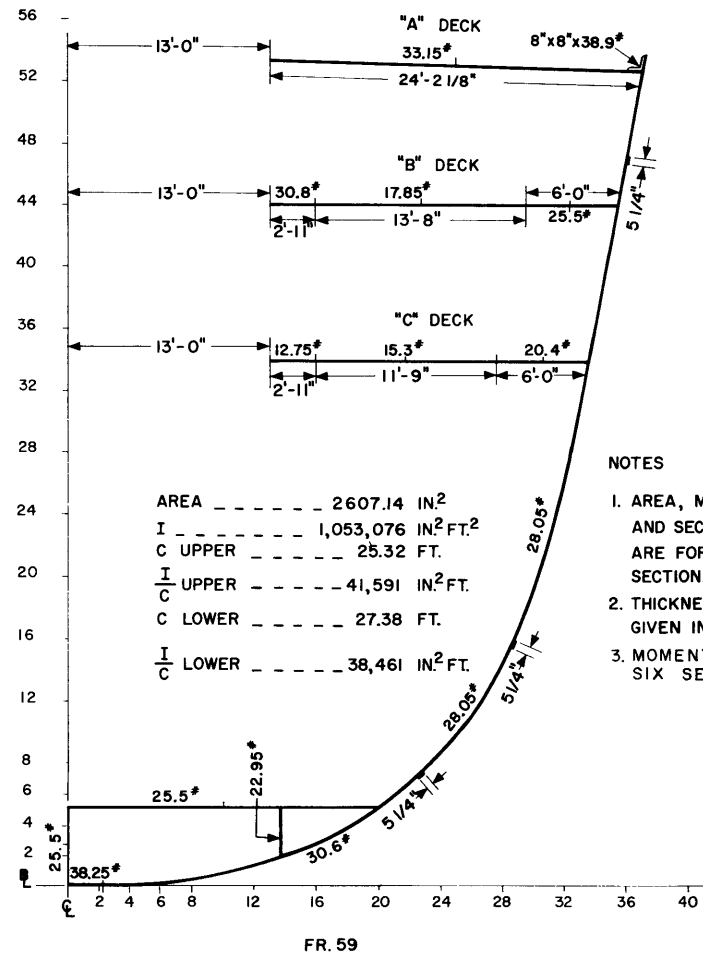
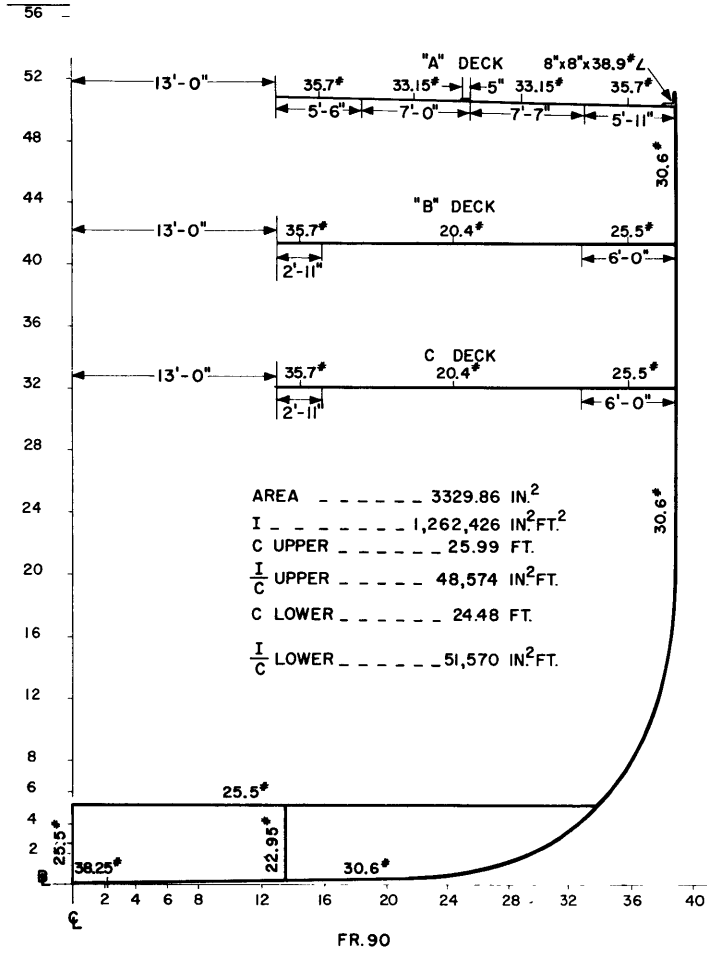


Figure 149 (Continued)





NOTES

1. AREA, MOMENT OF INERTIA, AND SECTION MODULUS VALUES ARE FOR BOTH SIDES OF SECTION.
2. THICKNESS OF PLATES ARE GIVEN IN WEIGHT (LBS/SQ.FT.)
3. MOMENTS OF INERTIA FOR SIX SECTIONS OF HULL

Figure 151 - Hull Sections and Corresponding Moments of Inertia (Sheet 1 of 3)

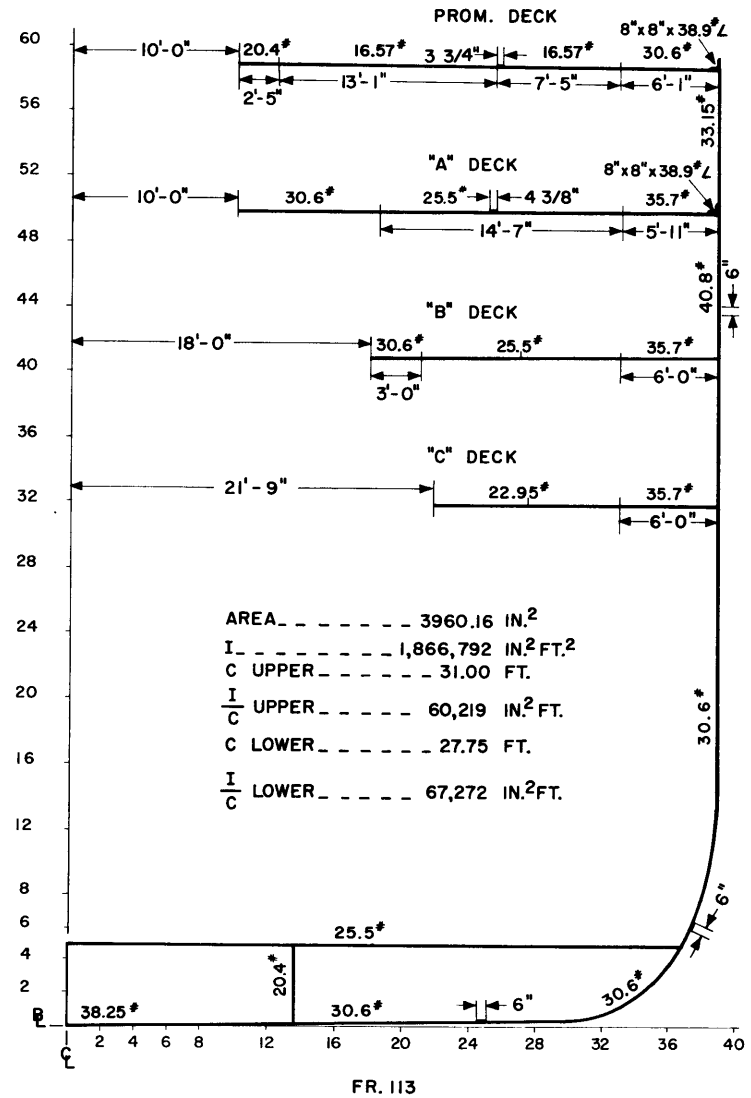
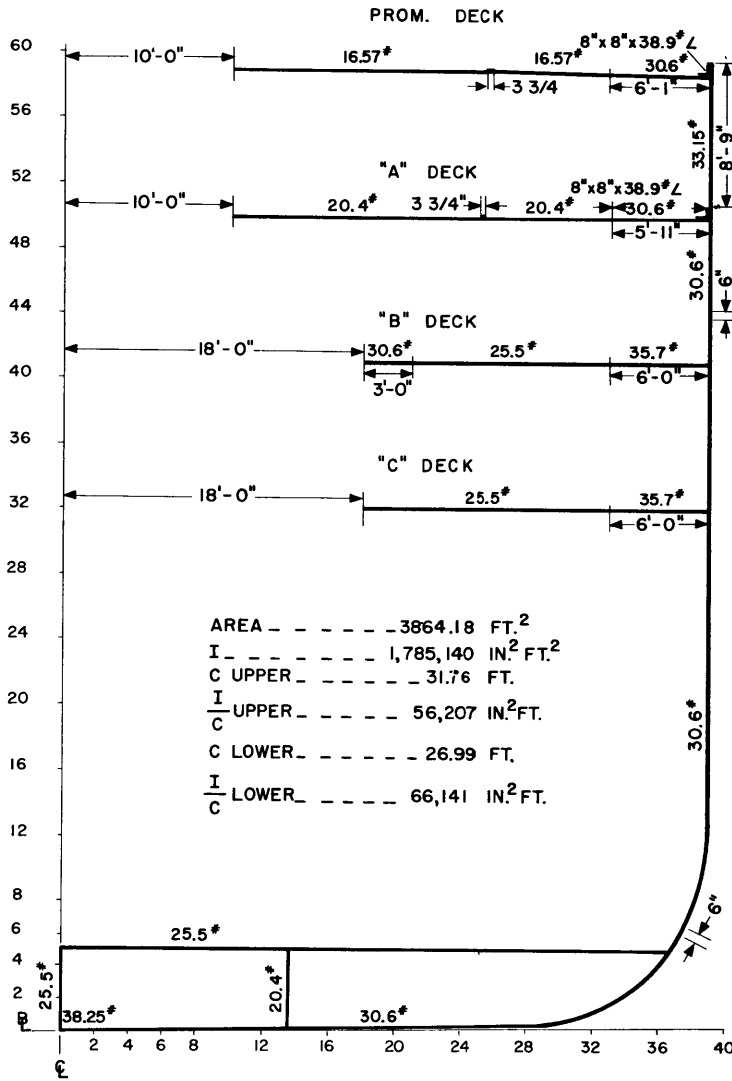


Figure 151 - Hull Sections and Corresponding Moments of Inertia
(Sheet 2 of 3)

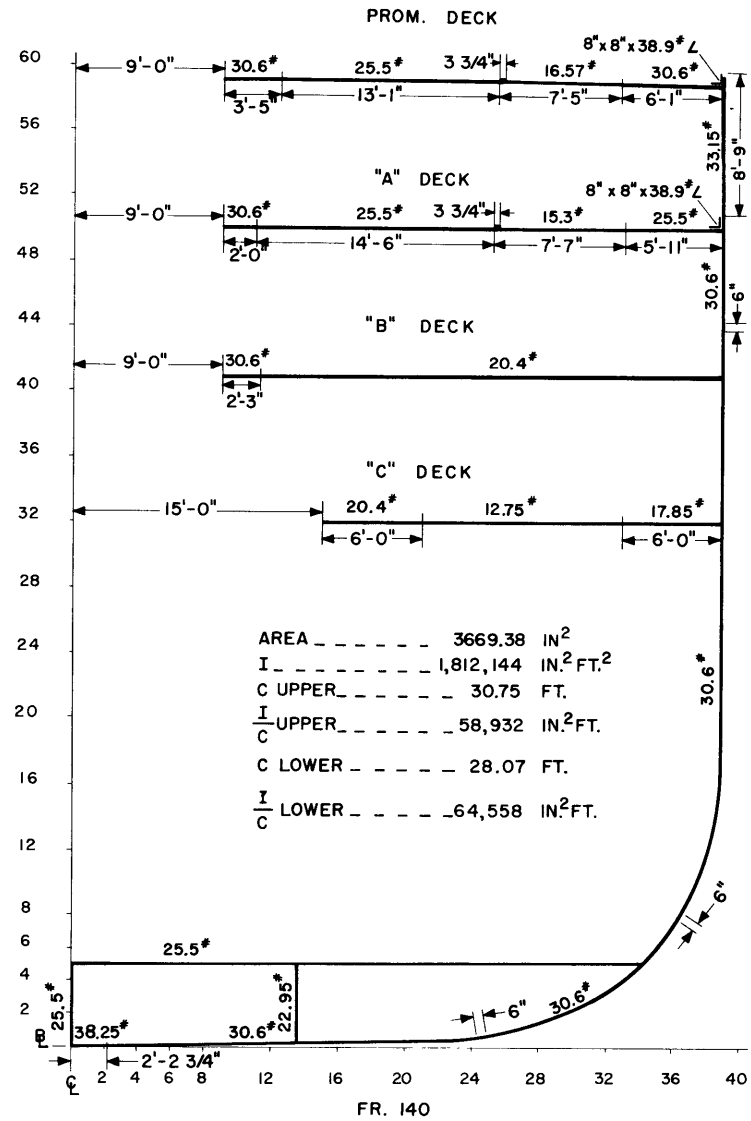
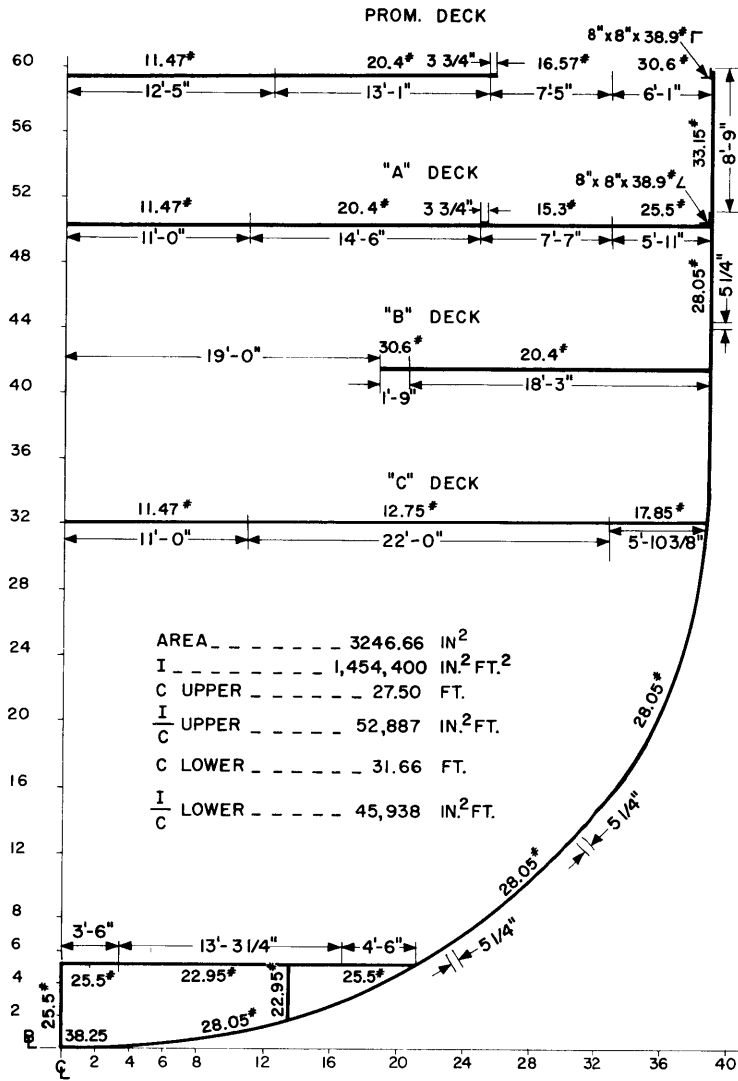


Figure 151 - Hull Sections and Corresponding Moments of Inertia
(Sheet 3 of 3)

APPENDIX E

METHOD OF EVALUATING PARAMETERS FOR ANALOG COMPUTATION

Four types of parameters are discussed in this appendix:

1. Axial flexibilities
 - a. Longitudinal flexibilities
 - b. Lateral flexibilities
2. Bending flexibilities
3. Shear flexibilities
4. Lumped inertias

The general method for lumping the flexibilities shown in Figures 139 and 140, is given in detail here, and the lumping limits of axial and shear elements are outlined in the tables attached thereto. The flexibilities for the lateral and longitudinal directions of a deck are obtained in a different manner, which is due to two reasons. First, the nature of the finite difference circuit which is employed provides that coordinates for motion in one direction do not always appear at the same points at which coordinates for motion in the other direction appear. Second, the boundary conditions play a different role in the cases of longitudinal force and lateral force, thereby requiring a different treatment. For example, along the outer edge of a deck longitudinal force may be transmitted in a fore-and-aft direction, as well as through the edge into the outer shell of the ship. However, in the same region no lateral force may be carried at all. As a consequence, the location of flexibility elements for longitudinal and lateral direction are independent of each other, and the lumping limits do not

necessarily agree .

With regard to the lumped shear flexibilities, a single lumped spring represents the strain energy of shear deformation of an entire rectangular panel. As long as this representation is correct and as long as the equilibrium relations of the forces applied to the perimeter of the panel are correctly simulated, there is no significance attached to the exact location of the lumped spring. Consequently, this location is not given.

With regard to the method of lumping the inertias in Figures 3 and 4, reference is made to Tables 3 and 4 of Appendix D, which details the mass distribution. It is noted that in this area of the model of the ship "distribution" is more applicable than "lumping" in describing the process employed to arrive at point masses. Most of the mass distributions of the ship are based on a longitudinal mass distribution (Appendix D). The method used for distribution of mass in that portion of the ship represented as a shell was one of judicious assumption.

1. AXIAL FLEXIBILITIES

a. Longitudinal flexibilities

In the midsection of the ship (Frames 102-168), the structure was idealized as indicated in Figures 1 and 138. Two longitudinal reference lines were located on each deck. Reference line I was located 18 ft from the centerline and reference line II was located at the outer shell (39 ft from the centerline). Since the decks were not of uniform thickness, the longitudinal flexibilities were calculated as

$$\frac{1}{K_{\text{long.}}} = \int_{y_1}^{y_2} \frac{dy}{EA} \approx \sum_{y_1}^{y_2} \frac{\Delta y}{EA_y}$$

For reference line I, an effective deck width of 28.5 ft was used. The effective area was simply the cross-sectional area (28.5 x thickness) plus the cross-sectional area of any longitudinal deck stiffener in the region from the centerline to 28.5 ft from the centerline. For reference line II, an effective deck width of 10.5 ft (from 28.5 ft to outer shell) was used. The effective area was the cross-sectional deck area, i.e., 10.5 x thickness plus the cross-sectional area of stiffeners in the region from 28.5 ft to 39 ft plus 1/2 the cross-sectional area of the outer shell between two decks.

A slightly different technique was used to calculate longitudinal flexibilities of the bottom. In addition to the reference lines I and II, a third line located at the centerline was used. The effective width for flexibilities at the centerline was 9 ft. The effective width for flexibilities at I was 28.5 - 9 = 19.5 ft; for flexibilities at II, 39 - 28.5 = 10.5 ft.

The longitudinal flexibilities for the portion forward of Station 243 and aft of Station 408 were based on the cross-sectional area of the ship as given in the data of Appendix D.

b. Lateral Flexibilities

Lateral flexibilities were calculated as

$$\frac{1}{k_{lat.}} = \sum_{x_1}^{x_2} \frac{\Delta x}{EA_x}$$

Two regions were originally considered. One region had the limits $x_1 = \text{centerline}$, $x_2 = 28.5 \text{ ft}$, while the other region had the limits $x_1 = 28.5 \text{ ft}$, $x_2 = 39 \text{ ft}$ (outer shell). Investigation of the magnitude of flexibilities in the region $x_1 = 28.5 \text{ ft}$, $x_2 = 39 \text{ ft}$ indicated that the deck in this region could be considered rigid relative to the inner

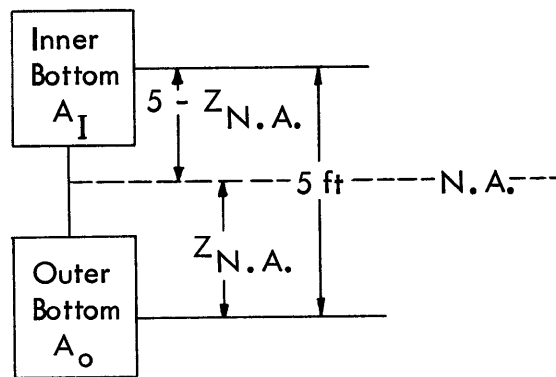
portion of the deck. The effective cross-sectional area was composed of the incremental longitudinal length x thickness plus the cross-sectional area of any stiffeners in the longitudinal section plus 1/2 the cross-sectional area (between two decks) of any bulkhead in the longitudinal section.

2. BENDING FLEXIBILITIES

The bending flexibilities were calculated as

$$\frac{1}{k_{\text{bend.}}} = \sum_{y_1}^{y_2} \frac{\Delta y}{EI}$$

For the double bottom between Stations 243 and 408, the inner and outer bottoms were considered 5 ft apart. The idealized cross section of the double bottom was then as shown below:



The distance of the neutral axis above the outer bottom is

$$Z_{N.A.} = \frac{5 \times A_I}{A_O + A_I}$$

and the moment of inertia is simply

$$I_{N.A.} = A_O (Z_{N.A.})^2 + A_I (5 - Z_{N.A.})^2$$

The bending flexibilities of the beam forward of Station 243 and aft of Station 408 were based on moment of inertia data (Appendix D).

3. SHEAR FLEXIBILITIES

Shear flexibilities were calculated as:

$$\begin{aligned}\frac{1}{K} &= \frac{\Delta y}{G t \Delta x} && \text{Decks} \\ &= \frac{\Delta x}{G t \Delta z} && \text{Bulkheads} \quad [1] \\ &= \frac{\Delta z}{G t \Delta y} && \text{Outer Shell}\end{aligned}$$

For a deck Δx = width of deck between I and II, Δy = spanwise section as indicated in Figure 139, and t is the thickness of the section. A bulkhead is idealized as two shear panels. One shear panel has a width from the centerline to I and the other shear panel has a width from I to II. Both shear panels have a Δz equal to the height from "A" deck to the bottom. The outer shell has a Δz equal to the distance between two decks, and the Δy is the same as used for the shear panel of the decks.

4. LUMPED INERTIAS

The running weight distribution data were provided in the data in Appendix D. The weight was lumped at stations indicated in Figure 1. For Decks A, C, and D the lumped inertia was distributed equally at 270 I and II, 349 I and II, and 383 I and II. The distribution on the bottom was such that the inertias at 270-I, 349-I, and 383-I were twice as large as those at 270-II, 349-II, and 383-II.

The total weights are composed of two parts, the weight of the ship structure and associated equipment, and the virtual weight due to the motion of the displaced water. In all cases a "light" ship was used in which no cargo weight was added. A tabulation of the parameters used is given in Tables 5-18.

TABLE 5

Longitudinal Flexibilities
(Inches per Pound)










| Δy | Decks | | | |
|-----------------------------------|--|--|---|--|
| | A | C | D | Bottom |
| (349-I) - (270-I) | 0.108×10^{-6} | 0.254×10^{-6} | 0.0853×10^{-6} | 0.063×10^{-6} |
| (383-I) - (349-I) | 0.0987  | 0.116  | 0.123  | 0.0652  |
| (349-II) - (270-II) | 0.114  | 0.0888  | 0.103  | 0.0939 |
| (383-II) - (349-II) | 0.112×10^{-6} | 0.0993×10^{-6} | 0.219×10^{-6} | 0.0942  |
| (349- ζ) - (270- ζ) | -- | -- | -- | 0.113  |
| (383- ζ) - (349- ζ) | -- | -- | -- | 0.114×10^{-6} |

TABLE 6

Lateral Flexibilities
(Inches per Pound)









| Station | Decks | | | |
|---------|--|--|---|--|
| | A | C | D | Bottom |
| 243 | 0.018×10^{-6} | 0.0352×10^{-6} | 0.0404×10^{-6} | 0.0156×10^{-6} |
| 303 | 0.0215  | 0.0228  | 0.0364  | 0.0162  |
| 358 | 0.0198  | 0.0258  | 0.0226  | 0.0190  |
| 408 | 0.0237×10^{-6} | 0.0237×10^{-6} | 0.040×10^{-6} | 0.007×10^{-6} |

TABLE 7
Deck Shear Flexibilities
(Inches per Pound)

| Deck | Δx | Δy | | |
|--------|------------|-------------------------|-------------------------|-------------------------|
| | | (303-243) | (358-303) | (408-358) |
| A | II-I | 0.2052×10^{-6} | 0.2590×10^{-6} | 0.2442×10^{-6} |
| C | II-I | 0.2119 | 0.3158 | 0.3037 |
| D | II-I | 0.3246 | 0.2976 | 0.4884 |
| Bottom | II-I | 0.1598 | 0.1465 | 0.1332 |
| Bottom | I-C | 0.1865×10^{-6} | 0.1709×10^{-6} | 0.1554×10^{-6} |

TABLE 8
Double Bottom Beam Flexibilities
(Radians per Inch-Pound)

| Interval Lumped (Δy) | Location of Lumped Flexibility Station | Location | |
|--------------------------------|--|-------------------------|--------------------------------|
| | | At Centerline | At I (18 Feet from Centerline) |
| 270 - 243 | 256.5 | 60.36×10^{-12} | 33.96×10^{-12} |
| 303 - 270 | 286.5 | 71.33 | 40.13 |
| 349 - 303 | 326 | 93.28 | 52.48 |
| 358 - 349 | 353.5 | 24.44 | 15.44 |
| 383 - 358 | 370.5 | 60.94 | 39.34 |
| 408 - 383 | 395.5 | 60.94×10^{-12} | 39.34×10^{-12} |

TABLE 9

Double Bottom Torque Tube Flexibilities
(Radians per Inch-Pound)

| Between Centerline and I | Station | | | | |
|-----------------------------|------------------------|------------------------|------------------------|------------------------|-------------------------|
| | 270 | 303 | 349 | 358 | 383 |
| | 4.82×10^{-12} | 7.59×10^{-12} | 4.40×10^{-12} | 6.69×10^{-12} | 11.16×10^{-12} |

TABLE 10

Outer Shell Shear Panel Flexibilities
(Inches per Pound)

| Location | Δz | Δy | | |
|----------|------------|-------------------------|-------------------------|-------------------------|
| | | (303 - 243) | (358 - 303) | (408 - 358) |
| II | A-C | 0.0308×10^{-6} | 0.0336×10^{-6} | 0.0381×10^{-6} |
| II | C-D | 0.0265×10^{-6} | 0.0289×10^{-6} | 0.0328×10^{-6} |
| II | D-Bottom | 0.0239×10^{-6} | 0.0261×10^{-6} | 0.0296×10^{-6} |

TABLE 11

Bulkhead Shear Panel Flexibilities
(Inches per Pound)

| Location | ΔX | ΔZ |
|----------|------------|-------------------------|
| | | (A-Bottom) |
| 243 | II-I | 0.0907×10^{-6} |
| 243 | I- ϕ | 0.0777 |
| 303 | II-I | 0.0907 |
| 303 | I- ϕ | 0.0777 |
| 358 | II-I | 0.0907 |
| 358 | I- ϕ | 0.0777 |
| 408 | II-I | 0.0907 |
| 408 | I- ϕ | 0.0777×10^{-6} |




TABLE 12

Longitudinal Weight Distribution

| Location (Station) | Light Weight tons | Location (Station) | Light Weight tons |
|-----------------------|-------------------------|-----------------------|-------------------------|
| 270-A-I | 77 | 270-D-I | 54 |
| 270-A-II | 77 | 270-D-II | 54 |
| 349-A-I | 117 | 270-Bot. -C | 1664* |
| 349-A-II | 117 | 349-D-I | 64 |
| 383-A-I | 95 | 349-D-II | 64 |
| 383-A-II | 95 | 383-D-I | 48 |
| 270-C-I | 54 | 383-D-II | 48 |
| 270-C-II | 54 | 270-Bot. -I | 152 |
| 349-C-I | 64 | 270-Bot. -II | 76 |
| 349-C-II | 64 | 349-Bot. -I | 376 |
| 383-C-I | 48 | 349-Bot. II | 188 |
| 383-C-II | 48 | 383-Bot. -I | 96 |
| | | 383-Bot. -II | 48 |

*Represents weight of reactor and containment vessel.

TABLE 13

Vertical Weight Distribution

| Location | Empty Weight tons | Virtual Weight tons | Light Weight tons |
|----------|-------------------|---------------------|-------------------|
| 243-C | 106 | 250 | 356 |
| 243-I | 211 | 500 | 711 |
| 243-II | 106 | 334 | 440 |
| 270-C | 832* | 175 | 1007 |
| 270-I | 832* | 350 | 1182 |
| 303-C | 188 | 184 | 372 |
| 303-I | 376 | 368 | 744 |
| 303-II | 188 | 366 | 554 |
| 349-C | 93 | 174 | 267 |
| 349-I | 93 | 348 | 441 |
| 358-C | 197 | 168 | 365 |
| 358-I | 384 | 336 | 720 |
| 358-II | 192 | 334 | 526 |
| 383-C | 12 | 153 | 165 |
| 383-I | 0 | 306 | 306 |
| 408-C | 97 | 208 | 305 |
| 408-I | 194 | 416 | 610 |
| 408-II | 97 | 278 | 375 |

*Represents weight of reactor and containment vessel.

TABLE 14

Lateral Weight Distribution

| Location | Empty Weight | Virtual Weight tons | Light Weight tons |
|------------|--------------|---------------------|-------------------|
| 243-A | 77 | 0 | 77 |
| 303-A | 97 | 0 | 97 |
| 358-A | 106 | 0 | 106 |
| 408-A | 95 | 0 | 95 |
| 243-C | 54 | 0 | 54 |
| 303-C | 59 | 0 | 59 |
| 358-C | 56 | 0 | 56 |
| 408-C | 48 | 0 | 48 |
| 243-D | 54 | 180 | 234 |
| 303-D | 59 | 172.5 | 231.5 |
| 358-D | 56 | 157.5 | 213.5 |
| 408-D | 48 | 150 | 198 |
| 243-Bottom | 76 | 180 | 256 |
| 303-Bottom | 132 | 172.5 | 304.5 |
| 358-Bottom | 118 | 157.5 | 275.5 |
| 408-Bottom | 48 | 150 | 198 |

TABLE 15

Axial and Beam Flexibilities

| Between Stations | Axial Flexibility (Inches per Pound) | Beam Flexibility (Radians per Inch-Pound) |
|------------------|---|--|
| 0 - 63 | 0.03639×10^{-6} | 56.92×10^{-14} |
| 63 - 108 | 0.01589 | 25.26 |
| 108 - 153 | 0.01358 | 23.14 |
| 153 - 198 | 0.01184 | 21.46 |
| 198 - 243 | 0.01013 | 17.00 |
| 243 - 273 | 0.00618 | 9.20 |
| 383 - 408 | 0.00584 | 8.88 |
| 408 - 453 | 0.01218 | 19.38 |
| 453 - 498 | 0.01698 | 29.94 |
| 498 - 545 | 0.03530×10^{-6} | 69.62×10^{-14} |

TABLE 16
Weight Distribution

| Station | Longitudinal | Vertical | | |
|---------|-------------------|-------------------|---------------------|-------------------|
| | Light Weight tons | Empty Weight tons | Virtual Weight tons | Light Weight tons |
| 0 | 152.2 | 152.2 | 113 | 265.2 |
| 63 | 237.4 | 237.4 | 306.4 | 543.8 |
| 108 | 235.1 | 235.1 | 550.1 | 785.2 |
| 153 | 259.5 | 259.5 | 945.0 | 1204.5 |
| 198 | 296.2 | 296.2 | 1132.9 | 1429.1 |
| 243 | 145.1 | | | |
| 408 | 137.7 | | | |
| 453 | 350.2 | 350.2 | 720 | 1070.2 |
| 498 | 260.6 | 260.6 | 264.5 | 525.1 |
| 545 | 121.9 | 121.9 | 12.4 | 134.3 |

TABLE 17

Shaft Axial Flexibility

| Between Stations | Axial Flexibility (Inches per Pound) |
|------------------|---|
| 340 - 377 | 0.1442×10^{-6} |
| 377 - 415 | 0.0782 |
| 415 - 453 | 0.0782 |
| 453 - 491 | 0.0782 |
| 491 - 531 | 0.0782×10^{-6} |

TABLE 18

Shaft Weight Distribution

| Station | Virtual Weight tons | Weight Total tons |
|---------|------------------------|----------------------|
| 340 | 0 | 56 |
| 377 | 0 | 11.2 |
| 415 | 0 | 11.2 |
| 453 | 0 | 11.2 |
| 491 | 0 | 11.2 |
| 531 | 80 | 107 |

APPENDIX F
SCALE FACTORS

The scale factors define the relationship between electrical quantities in the analogy and mechanical quantities in the idealized mechanical model. The scale factors used in this analysis are defined as follows (see Reference 3):

| <u>Mechanical Quantity</u> | | <u>Electrical Quantity</u> |
|-----------------------------------|---|----------------------------|
| Velocity | $v_i = \frac{Ka}{N} e_i$ | Voltage |
| Force | $F_i = \frac{K}{a} l_i$ | Current |
| Angular Velocity | $\dot{\theta} = \frac{Ka}{P_\theta N} e_\theta$ | Voltage |
| Moment | $M = \frac{KP_\theta}{a} l_\theta$ | Current |
| Time | $t_m = Nt_e$ | Time |
| Frequency | $f_m = \frac{1}{N} f_e$ | Frequency |
| Axial and Shear Flexibility | $\frac{1}{K_i} \frac{1}{a^2} = L_i$ | Inductance |
| Bending and Torsional Flexibility | $\frac{1}{K_\theta} \frac{p^2}{a^2} = L_\theta$ | Inductance |
| Mass | $M_i \frac{a^2}{N^2} = C_i$ | Capacitance |

The numerical values of the scale factor coefficients are shown for the indicated sections of the analogy:

$$\text{(everywhere) } N = 60$$

$$\text{(everywhere) } a = 4.4721 \times 10^{-4} \left(\frac{\text{in.}}{\text{lb}} \frac{\text{amp}}{\text{volt sec}} \right)^{1/2}$$

$$\text{(Fore-and-Aft Ship) } P_{\theta} = 840 \text{ in.}$$

$$\text{(Double Bottom) } P_{\theta} = 56 \text{ in.}$$

Other constants employed in this analysis are:

$$1 \text{ ton} = 2240 \text{ lb}$$

$$E = 30 \times 10^6 \text{ lb/in}^2$$

$$G = 13 \times 10^6 \text{ lb/in}^2$$

APPENDIX G

QUANTITATIVE EVALUATION OF EFFECT OF A MOMENT APPLIED TO PROPELLER

The importance of the oscillating moment component of the thrust when applied to the propeller disk eccentrically to the shaft is shown by a comparison of Figures 89 through 100 with Figures 5 through 16. Assume that application of the actual oscillating component of thrust to the propeller occurs at some point greater than $\frac{r}{6}$ but less than $\frac{r}{2}$, where $r = 11$ ft is the radius of the propeller. Then, for an effective eccentricity ranging from approximately 2 to 6 ft, the oscillating component of moment M lies between the bounds $2T < M < 6T$.

The response of the ship due to thrust applied eccentrically to the shaft can be found by the superposition of the case where the thrust is applied to the center of the shaft (Figures 5 through 16) with the case where a moment is applied to the propeller (Figures 89 through 100) equal to the thrust times the eccentricity. The importance of the moment component can be evaluated from the ratio of the response in Figures 5 through 16 to the response in Figures 89 through 100 when a moment is applied equal to the magnitude of the eccentricity.

A good indication of this ratio can be obtained by using the magnitude of the response at the 0-db level of the various runs from Table 2:

- | | |
|---------------------------------------|--|
| a. Figures 5-16 | $0 \text{ db} = 4.167 \times 10^{-4} \frac{\text{in/sec}}{\text{lb}}$ |
| b. Figures 89-100 | $0 \text{ db} = 0.596 \times 10^{-5} \frac{\text{in/sec}}{\text{in lb}}$ |
| c. Figures 89-100 (2-ft eccentricity) | $0 \text{ db} = 0.1192 \times 10^{-4} \frac{\text{in/sec}}{\text{lb}}$ |

d. Figures 89-100 (6-ft eccentricity) $0 \text{ db} = 0.3576 \times 10^{-4} \frac{\text{in/sec}}{\text{lb}}$

Then the ratios of interest are:

$$\frac{0 \text{ db (c)}}{0 \text{ db (a)}} = \frac{0.1192 \times 10^{-4}}{4.167 \times 10^{-4}} = 0.0286 = 30.8 \text{ db}$$

$$\frac{0 \text{ db (d)}}{0 \text{ db (a)}} = \frac{0.3576 \times 10^{-4}}{4.167 \times 10^{-4}} = 0.0858 = 21.3 \text{ db}$$

Since the dynamic response of the ship due to the moment component of the eccentric thrust is more than 20 db below the response due to the concentric thrust, it is concluded that the moment component is of negligible importance.

APPENDIX H

ELECTRICAL ANALOG OF TORQUE BOX

A rectangular torque box element was used to represent the torsional stiffness of the double bottom of NS SAVANNAH.

A torque box is composed of two parallel sheets of skin, assumed to carry shear only, connected around the boundary by beam webs; see Figure 153a. The moments M_x and M_y of Figure 153a are carried by shearing of the upper and lower skin. When the torque box is carrying a pure torsional loading, this loading is antisymmetric about the neutral plane, and the torsional properties of the torque box can be represented by the same form of analogy as used for a shear panel, provided the value of the inductor is multiplied by $\frac{2}{h^2}$. This is indicated in Figure 153b.

If the webs of the beams on the periphery of the torque box are considered rigid to vertical shear, then it can be shown (see, for example, page 120 of Reference 3) that the circuit can be further simplified to a single inductor connected between either pair of slope coordinates on opposite sides of the torque box. For example, a single inductor representing a torque tube connected between the M_x coordinates of Figure 153b would have the value $\frac{\Delta y}{2Gt \Delta x h^2}$.

In the representation of the double bottom of SAVANNAH in this analysis, Figure 152 illustrates the manner in which this analogy is applied. Two separate circuits give the out-of-plane motion of the double bottom and the in-plane motion of the double bottom. The entire motion of the double bottom can be resolved into an

out-of-plane component and an in-plane component. The circuit for in-plane motion of the double bottom is similar to the circuitry for any of the other decks, as it accounts for the symmetric shearing of the two bottoms and the symmetric axial extension of the two bottoms. (The term symmetric, in this respect, means that the inner bottom and the outer bottom are undergoing equal forces and deformations. Antisymmetric implies opposite forces and deformations. For example, if both the inner bottom and outer bottom are in longitudinal tension, this is a symmetric force and will produce in-plane motion. If the inner bottom is in tension but the outer bottom is in compression, this is an antisymmetric force and will produce vertical bending, an out-of-plane motion.) In out-of-plane motion the double bottom is represented by two beams in vertical bending, one lying along the centerline, and the other along the buttock line represented by 1. The inductors representing torque tubes lie in a lateral direction and connect pairs of slope circuit nodes of the beams.

Connections

- (A) To bulkhead circuit for vertical motion
- (B) To circuit for shaft longitudinal motion
- (C) To outer shell circuit for longitudinal motion
- (D) To bulkhead circuit for lateral motion

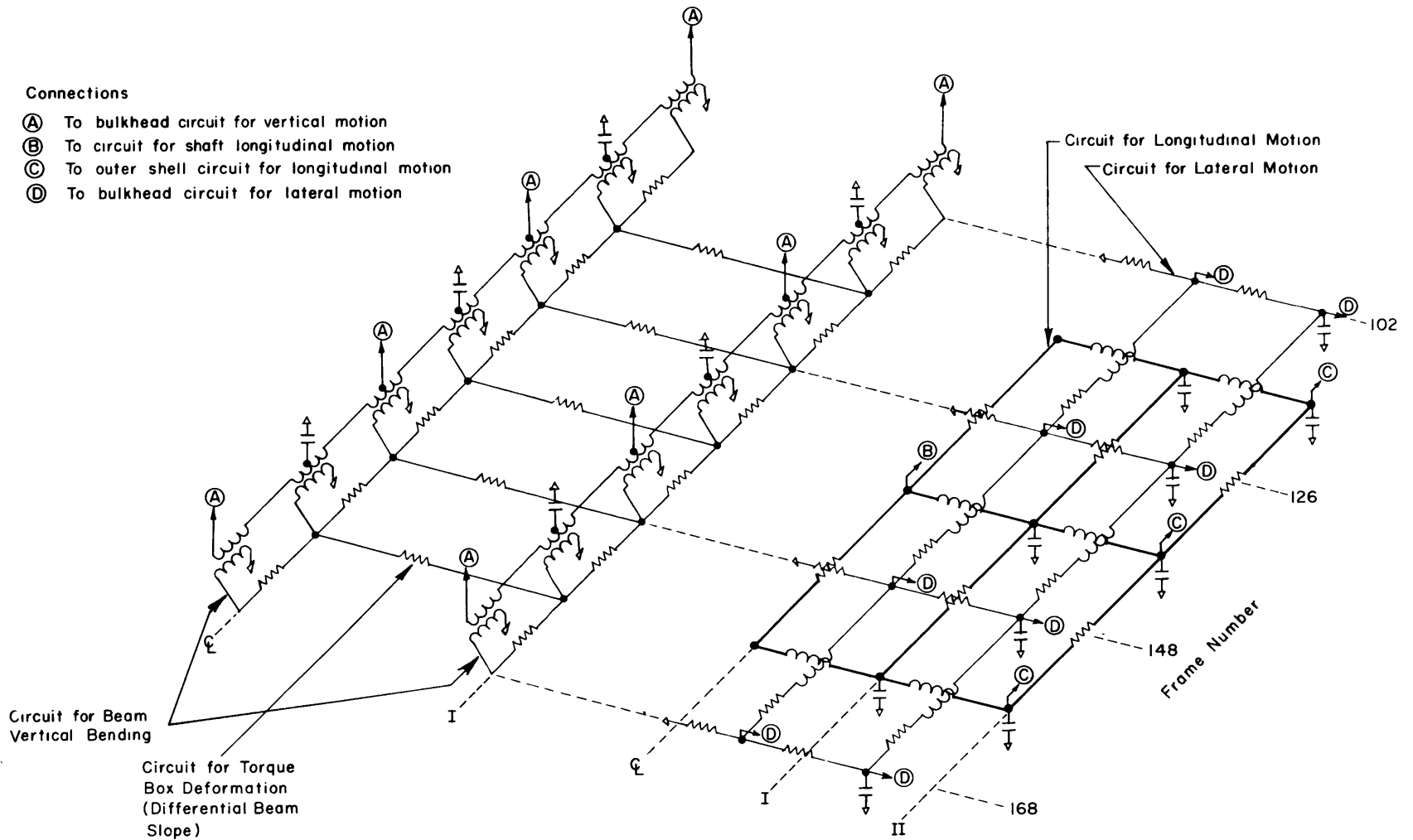


Figure 152a - Out-of-Plane Motion

Figure 152b - In-Plane Motion

Figure 152 - Circuits for Double Bottom

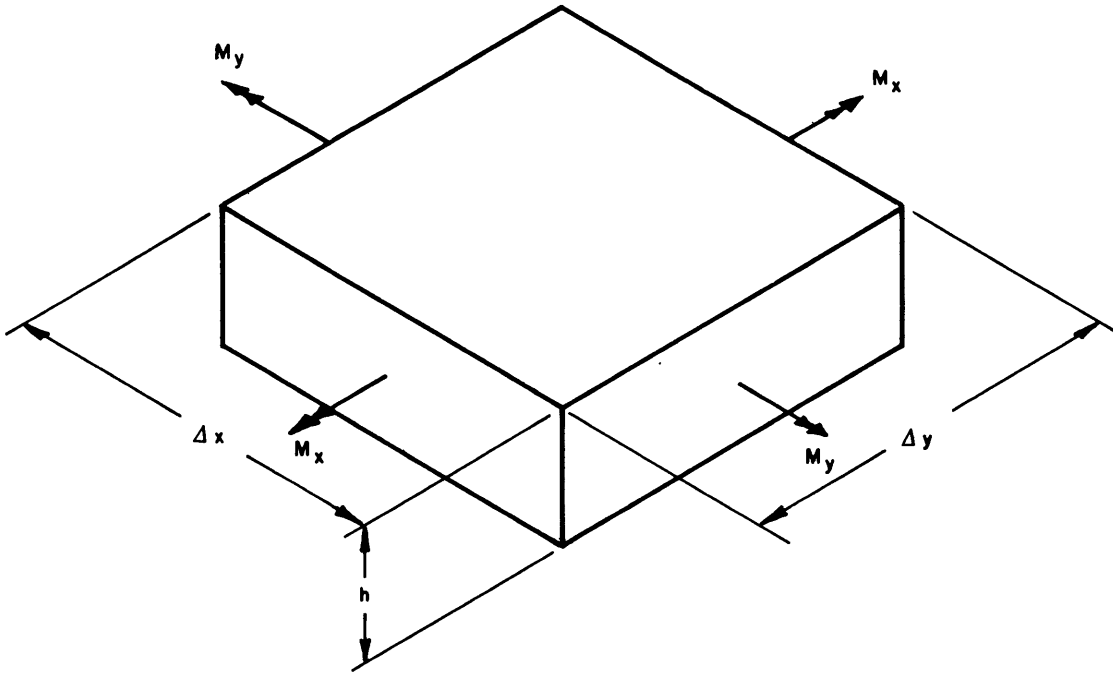


Figure 153a – Rectangular Torque Box

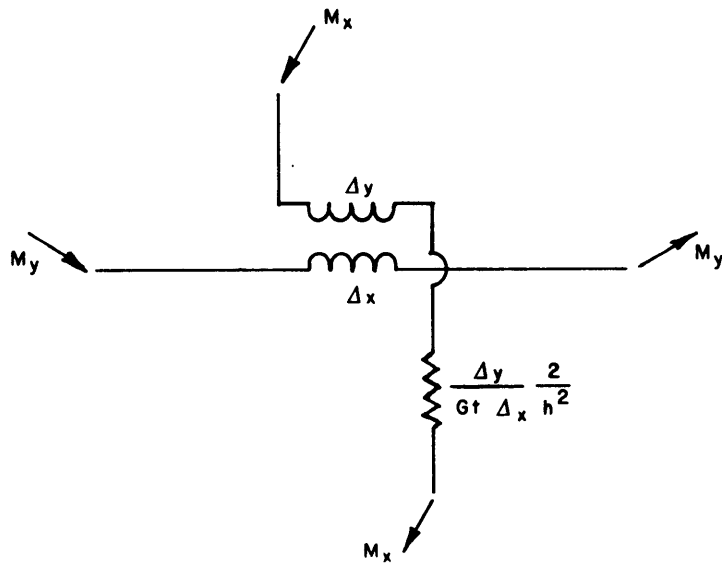


Figure 153b – Analogy for Rectangular Torque Box

Figure 153 - Rectangular Torque Box and Its Analog

REFERENCES

1. Leibowitz, R. C. and Kennard, E. H., "Theory of Freely Vibrating Nonuniform Beams, Including Methods of Solution and Application to Ships," David Taylor Model Basin Report 1317 (May 1961).
2. Leibowitz, R. C., "Effects of Damping on Modes of Vertical Vibration of Hull of USS THRESHER (SSN 593)", David Taylor Model Basin Report 1384 (Mar 1960).
3. MacNeal, R. H., "Electric Circuit Analogy for Elastic Structures," John Wiley and Sons, New York (1962).
4. Hill, J. H., "Vibration Analysis of NS SAVANNAH," Computer Engineering Associates (CEA Project: ES 195), Pasadena, California (31 Dec 1962).
5. Timoshenko, S. T. and Woinowsky-Krieger, S., "Theory of Plates and Shells," McGraw-Hill Book Co., Second Edition (1959).
6. Fung, Y. C., "An Introduction to the Theory of Aeroelasticity," John Wiley and Sons (1955).
7. MacNeal, R. H., "The Solution of Elastic Plate Problems by Electrical Analogies," Journal of Applied Mechanics, Trans American Society of Mechanical Engineers, Vol. 73, (1951), p. 59.
8. MacNeal, R. H., "Electrical Analogies for Stiffened Shells with Flexible Rings," National Advisory Committee of Aeronautics TN 3280 (Dec 1954).
9. Hill, J. H. and MacNeal, R. H., "Dynamic Analysis of a Hydrofoil Structure," Computer Engineering Associates Report ESD 154 (Aug 1959).

10. Kennard, E. H. and Leibowitz, R. C., "Theory for Rudder-Diving Plane-Ship Vibrations and Flutter, Including Methods of Solution," David Taylor Model Basin Report 1507 (Feb 1962).

BLANK

INITIAL DISTRIBUTION

| Copies | | Copies | |
|--------|--------------------------------|--------|---|
| 12 | CHBUSHIPS | 1 | NAVSHIPYD NORVA (Code 240) |
| 3 | Tech Lib (Code 210L) | 1 | NAVSHIPYD PHILA (Code 240) |
| 1 | Lab Mgt (Code 320) | 1 | NAVSHIPYD BSN (Code 240) |
| 1 | Applied Res (Code 340) | 2 | NAVSHIPYD NYK |
| 3 | Ship Silencing Br (Code 345) | 1 | Des Supt (Code 240) |
| 1 | Prelim Des Br (Code 420) | 1 | USNASL |
| 1 | Hull Des Br (Code 440) | 1 | CMDT, USCG |
| 1 | Sci & Res Sec (Code 442) | 1 | Secy, Ship Struc Comm |
| 1 | Hull Structure Sec (Code 443) | | |
| 3 | CHONR | | |
| 1 | Math Sci Div (Code 430) | | |
| 1 | Fluid Dyn Br (Code 438) | | |
| 1 | CHBUWEPS | 1 | DIR, Natl BuStand |
| 1 | CO & DIR, USNMEL | 1 | ADM, MARAD |
| 1 | CO & DIR, USNMDL | 2 | DIR, NASA |
| 1 | CDR, USNOL | 1 | Ship Struc Comm |
| 1 | CDR, USNOTS, China Lake | 20 | DDC |
| 1 | CDR, USNOTS, Pasadena | 1 | WHOI |
| 1 | DIR, USNRL | 5 | MIT |
| 1 | CO, USNROTC & NAVADMINU MIT | 1 | Dept of NAME |
| 1 | ADM WEBB INST | 2 | Fluid Dyn Res Grp |
| 1 | O in C, PGSCOL, Webb Inst | 1 | Mr. John Dugundsi |
| 1 | NAVSHIPYD LBEACH (Code 240) | 1 | Mr. Holt Ashley |
| 1 | NAVSHIPYD PEARL (Code 240) | 1 | Mr. J. D. Crisp, Aeroelastic & Struc Res Lab |
| 1 | NAVSHIPYD PUG (Code 240) | 1 | Prof. M. Landahl, Dept of Aero & Astro |
| 1 | NAVSHIPYD SFRAN (Code 240) | 2 | New York Univ |
| | | 1 | Dept of Meteorology |
| | | 1 | Fluid Mech Lab |
| | | 1 | Inst of Hydraul Res, Univ of Iowa |
| | | 1 | Sch of Engin & Arch, Catholic Univ |

Copies

- 2 Inst of Engin Res, Univ of California-
 - 1 Head, Dept of Nav Arch, Attn: Prof. Schade
- 3 Univ of Michigan
 - 1 Exper Naval Tank
 - 1 Dept of Engin Mech
 - 1 Dr. Finn Michelson, Dept of Nav Arch
- 1 Hudson Lab, Columbia Univ
- 1 Univ of Notre Dame
 - Attn: Prof. A. Strandhagen, Head
 - Dept of Eng Mech
- 1 APL, JHU
- 3 Dept of Applied Mech, SWRI
 - 1 Dr. H. Norman Abramson
 - 1 Mr. Wen-Hwa Chu
 - 1 Mr. Jack T. Irick
- 2 DIR, Davidson Lab, SIT
 - 1 Mr. Charles J. Henry
 - 1 Dr. John P. Breslin
- 1 St. Anthony Falls Hydraul Lab
- 1 NNSB & DD Co.
 - Attn: Mr. Montgomery
- 1 Gen Dyn, EB Div
- 1 SNAME
 - 1 Hull Struc Comm
- 2 Grumman Aircraft Eng Corp

Copies

- 2 Technical Research Group
 - 2 Aerial Way, Syosset, N.Y.
- 1 Engineering Index, New York
- 1 Dr. E.H. Kennard, 4057 Tenango Rd, Claremont, Calif
- 1 Dr. Theodore Theodorsen, Republic Aircraft Corp, Farmingdale, L.I., N.Y.
- 1 Mr. I.E. Garrick, Langley Res Ctr, NASA, Langley Field, Va.
- 1 Mr. Maurice Sevik, College of Engin & Arch, ORL, Penn State Univ
- 1 Mr. Alexander H. Flax, Cornell Aero Lab, Inc.
- 1 Mr. R.T. McGoldrick, Box 293, Sheffield, Mass.
- 1 MacNeal Schwendler Corp, 2556 Mission St., San Marino, Calif
- 2 Hydronautics Inc., Pindell School Rd., Laurel, Md.
- 1 Pres. Oceanics, Inc., 114 E 40 St., N.Y. 16
- 1 J.G. Eng Res Associates, 3831 Menlo Drive, Baltimore 15, Md.

David Taylor Model Basin. Report 1728.

THREE-DIMENSIONAL (BEAM-SHELL-SPRUNG BODY) VIBRATION ANALYSIS OF N.S. SAVANNAH, by Ralph C. Leibowitz and Robert G. Schwendler. Apr 1965. v, 132p. UNCLASSIFIED

The normal modes of coupled vertical, transverse, and longitudinal flexural vibrations and the steady-state damped response were calculated by means of a passive electrical-analog computer for surface ship NS SAVANNAH using a three-dimensional (beam shell-sprung body) analysis similar to that applied to aircraft. This ship was selected as a case study because of the many test results, data, and calculations available for this ship. Vertical flexural vibrations based upon beam theory were also computed by a digital computer. To demonstrate the techniques involved in making a three-dimensional analysis, the methods and data

1. Cargo ships (Nuclear)--Flexural vibration--Three-dimensional theory
2. Ship hulls--Flexural vibration--Three-dimensional theory
3. Ship hulls--Structural analysis--Three-dimensional theory
4. Ship hulls--Structural response--Three-dimensional theory
5. Beam-shell-sprung bodies--Vibration--Three-dimensional theory

David Taylor Model Basin. Report 1728.

THREE-DIMENSIONAL (BEAM-SHELL-SPRUNG BODY) VIBRATION ANALYSIS OF N.S. SAVANNAH, by Ralph C. Leibowitz and Robert G. Schwendler. Apr 1965. v, 132p. UNCLASSIFIED

The normal modes of coupled vertical, transverse, and longitudinal flexural vibrations and the steady-state damped response were calculated by means of a passive electrical-analog computer for surface ship NS SAVANNAH using a three-dimensional (beam shell-sprung body) analysis similar to that applied to aircraft. This ship was selected as a case study because of the many test results, data, and calculations available for this ship. Vertical flexural vibrations based upon beam theory were also computed by a digital computer. To demonstrate the techniques involved in making a three-dimensional analysis, the methods and data

1. Cargo ships (Nuclear)--Flexural vibration--Three-dimensional theory
2. Ship hulls--Flexural vibration--Three-dimensional theory
3. Ship hulls--Structural analysis--Three-dimensional theory
4. Ship hulls--Structural response--Three-dimensional theory
5. Beam-shell-sprung bodies--Vibration--Three-dimensional theory

David Taylor Model Basin. Report 1728.

THREE-DIMENSIONAL (BEAM-SHELL-SPRUNG BODY) VIBRATION ANALYSIS OF N.S. SAVANNAH, by Ralph C. Leibowitz and Robert G. Schwendler. Apr 1965. v, 132p. UNCLASSIFIED

The normal modes of coupled vertical, transverse, and longitudinal flexural vibrations and the steady-state damped response were calculated by means of a passive electrical-analog computer for surface ship NS SAVANNAH using a three-dimensional (beam shell-sprung body) analysis similar to that applied to aircraft. This ship was selected as a case study because of the many test results, data, and calculations available for this ship. Vertical flexural vibrations based upon beam theory were also computed by a digital computer. To demonstrate the techniques involved in making a three-dimensional analysis, the methods and data

1. Cargo ships (Nuclear)--Flexural vibration--Three-dimensional theory
2. Ship hulls--Flexural vibration--Three-dimensional theory
3. Ship hulls--Structural analysis--Three-dimensional theory
4. Ship hulls--Structural response--Three-dimensional theory
5. Beam-shell-sprung bodies--Vibration--Three-dimensional theory

David Taylor Model Basin. Report 1728.

THREE-DIMENSIONAL (BEAM-SHELL-SPRUNG BODY) VIBRATION ANALYSIS OF N.S. SAVANNAH, by Ralph C. Leibowitz and Robert G. Schwendler. Apr 1965. v, 132p. UNCLASSIFIED

The normal modes of coupled vertical, transverse, and longitudinal flexural vibrations and the steady-state damped response were calculated by means of a passive electrical-analog computer for surface ship NS SAVANNAH using a three-dimensional (beam shell-sprung body) analysis similar to that applied to aircraft. This ship was selected as a case study because of the many test results, data, and calculations available for this ship. Vertical flexural vibrations based upon beam theory were also computed by a digital computer. To demonstrate the techniques involved in making a three-dimensional analysis, the methods and data

1. Cargo ships (Nuclear)--Flexural vibration--Three-dimensional theory
2. Ship hulls--Flexural vibration--Three-dimensional theory
3. Ship hulls--Structural analysis--Three-dimensional theory
4. Ship hulls--Structural response--Three-dimensional theory
5. Beam-shell-sprung bodies--Vibration--Three-dimensional theory

used in the calculations and the results obtained are presented. Results show that significant reductions in vibration amplitudes can be achieved by such methods as damping or inertia coupling, which directly affect the sharpness of the structural resonance peaks.

6. Shafting--Vibration--Theory
7. Analog computers--Network analyzer--Applications
8. Digital computers--Applications
9. SAVANNAH (U.S. cargo ship, Nuclear)
 - I. Leibowitz, Ralph C
 - II. Schwendler, Robert G.

used in the calculations and the results obtained are presented. Results show that significant reductions in vibration amplitudes can be achieved by such methods as damping or inertia coupling, which directly affect the sharpness of the structural resonance peaks.

6. Shafting--Vibration--Theory
7. Analog computers--Network analyzer--Applications
8. Digital computers--Applications
9. SAVANNAH (U.S. cargo ship, Nuclear)
 - I. Leibowitz, Ralph C
 - II. Schwendler, Robert G.

used in the calculations and the results obtained are presented. Results show that significant reductions in vibration amplitudes can be achieved by such methods as damping or inertia coupling, which directly affect the sharpness of the structural resonance peaks.

6. Shafting--Vibration--Theory
7. Analog computers--Network analyzer--Applications
8. Digital computers--Applications
9. SAVANNAH (U.S. cargo ship, Nuclear)
 - I. Leibowitz, Ralph C
 - II. Schwendler, Robert G.

used in the calculations and the results obtained are presented. Results show that significant reductions in vibration amplitudes can be achieved by such methods as damping or inertia coupling, which directly affect the sharpness of the structural resonance peaks.

6. Shafting--Vibration--Theory
7. Analog computers--Network analyzer--Applications
8. Digital computers--Applications
9. SAVANNAH (U.S. cargo ship, Nuclear)
 - I. Leibowitz, Ralph C
 - II. Schwendler, Robert G.



David Taylor Model Basin. Report 1728.

THREE-DIMENSIONAL (BEAM-SHELL-SPRUNG BODY) VIBRATION ANALYSIS OF N.S. SAVANNAH, by Ralph C. Leibowitz and Robert G. Schwendler. Apr 1965. v, 132p. UNCLASSIFIED

The normal modes of coupled vertical, transverse, and longitudinal flexural vibrations and the steady-state damped response were calculated by means of a passive electrical-analog computer for surface ship NS SAVANNAH using a three-dimensional (beam shell-sprung body) analysis similar to that applied to aircraft. This ship was selected as a case study because of the many test results, data, and calculations available for this ship. Vertical flexural vibrations based upon beam theory were also computed by a digital computer. To demonstrate the techniques involved in making a three-dimensional analysis, the methods and data

1. Cargo ships (Nuclear)--Flexural vibration--Three-dimensional theory
2. Ship hulls--Flexural vibration--Three-dimensional theory
3. Ship hulls--Structural analysis--Three-dimensional theory
4. Ship hulls--Structural response--Three-dimensional theory
5. Beam-shell-sprung bodies--Vibration--Three-dimensional theory

David Taylor Model Basin. Report 1728.

THREE-DIMENSIONAL (BEAM-SHELL-SPRUNG BODY) VIBRATION ANALYSIS OF N.S. SAVANNAH, by Ralph C. Leibowitz and Robert G. Schwendler. Apr 1965. v, 132p. UNCLASSIFIED

The normal modes of coupled vertical, transverse, and longitudinal flexural vibrations and the steady-state damped response were calculated by means of a passive electrical-analog computer for surface ship NS SAVANNAH using a three-dimensional (beam shell-sprung body) analysis similar to that applied to aircraft. This ship was selected as a case study because of the many test results, data, and calculations available for this ship. Vertical flexural vibrations based upon beam theory were also computed by a digital computer. To demonstrate the techniques involved in making a three-dimensional analysis, the methods and data

1. Cargo ships (Nuclear)--Flexural vibration--Three-dimensional theory
2. Ship hulls--Flexural vibration--Three-dimensional theory
3. Ship hulls--Structural analysis--Three-dimensional theory
4. Ship hulls--Structural response--Three-dimensional theory
5. Beam-shell-sprung bodies--Vibration--Three-dimensional theory

David Taylor Model Basin. Report 1728.

THREE-DIMENSIONAL (BEAM-SHELL-SPRUNG BODY) VIBRATION ANALYSIS OF N.S. SAVANNAH, by Ralph C. Leibowitz and Robert G. Schwendler. Apr 1965. v, 132p. UNCLASSIFIED

The normal modes of coupled vertical, transverse, and longitudinal flexural vibrations and the steady-state damped response were calculated by means of a passive electrical-analog computer for surface ship NS SAVANNAH using a three-dimensional (beam shell-sprung body) analysis similar to that applied to aircraft. This ship was selected as a case study because of the many test results, data, and calculations available for this ship. Vertical flexural vibrations based upon beam theory were also computed by a digital computer. To demonstrate the techniques involved in making a three-dimensional analysis, the methods and data

1. Cargo ships (Nuclear)--Flexural vibration--Three-dimensional theory
2. Ship hulls--Flexural vibration--Three-dimensional theory
3. Ship hulls--Structural analysis--Three-dimensional theory
4. Ship hulls--Structural response--Three-dimensional theory
5. Beam-shell-sprung bodies--Vibration--Three-dimensional theory

David Taylor Model Basin. Report 1728.

THREE-DIMENSIONAL (BEAM-SHELL-SPRUNG BODY) VIBRATION ANALYSIS OF N.S. SAVANNAH, by Ralph C. Leibowitz and Robert G. Schwendler. Apr 1965. v, 132p. UNCLASSIFIED

The normal modes of coupled vertical, transverse, and longitudinal flexural vibrations and the steady-state damped response were calculated by means of a passive electrical-analog computer for surface ship NS SAVANNAH using a three-dimensional (beam shell-sprung body) analysis similar to that applied to aircraft. This ship was selected as a case study because of the many test results, data, and calculations available for this ship. Vertical flexural vibrations based upon beam theory were also computed by a digital computer. To demonstrate the techniques involved in making a three-dimensional analysis, the methods and data

1. Cargo ships (Nuclear)--Flexural vibration--Three-dimensional theory
2. Ship hulls--Flexural vibration--Three-dimensional theory
3. Ship hulls--Structural analysis--Three-dimensional theory
4. Ship hulls--Structural response--Three-dimensional theory
5. Beam-shell-sprung bodies--Vibration--Three-dimensional theory

used in the calculations and the results obtained are presented. Results show that significant reductions in vibration amplitudes can be achieved by such methods as damping or inertia coupling, which directly affect the sharpness of the structural resonance peaks.

6. Shafting--Vibration--Theory
7. Analog computers--Network analyzer--Applications
8. Digital computers--Applications
9. SAVANNAH (U.S. cargo ship, Nuclear)
 - I. Leibowitz, Ralph C
 - II. Schwendler, Robert G.

used in the calculations and the results obtained are presented. Results show that significant reductions in vibration amplitudes can be achieved by such methods as damping or inertia coupling, which directly affect the sharpness of the structural resonance peaks.

6. Shafting--Vibration--Theory
7. Analog computers--Network analyzer--Applications
8. Digital computers--Applications
9. SAVANNAH (U.S. cargo ship, Nuclear)
 - I. Leibowitz, Ralph C
 - II. Schwendler, Robert G.

used in the calculations and the results obtained are presented. Results show that significant reductions in vibration amplitudes can be achieved by such methods as damping or inertia coupling, which directly affect the sharpness of the structural resonance peaks.

6. Shafting--Vibration--Theory
7. Analog computers--Network analyzer--Applications
8. Digital computers--Applications
9. SAVANNAH (U.S. cargo ship, Nuclear)
 - I. Leibowitz, Ralph C
 - II. Schwendler, Robert G.

used in the calculations and the results obtained are presented. Results show that significant reductions in vibration amplitudes can be achieved by such methods as damping or inertia coupling, which directly affect the sharpness of the structural resonance peaks.

6. Shafting--Vibration--Theory
7. Analog computers--Network analyzer--Applications
8. Digital computers--Applications
9. SAVANNAH (U.S. cargo ship, Nuclear)
 - I. Leibowitz, Ralph C
 - II. Schwendler, Robert G.

.....

MIT LIBRARIES

DUPL



3 9080 02754 4532

MAR 21 1976

OCT 1 1982

NOV 2 1982